MECHANISTIC AND STRUCTURAL STUDIES OF PHENYLALANINE HYDROXYLASE FROM *CHROMOBACTERIUM VIOLACEUM*

A Dissertation

by

ARAM JOEL PANAY ESCOBAR

Submitted to the Office of Graduate Studies of
Texas A&M University
in partial fulfillment of the requirements for the degree of

DOCTOR OF PHILOSOPHY

August 2010

Major Subject: Biochemistry

Mechanistic and Structural Studies of

Phenylalanine Hydroxylase from *Chromobacterium*

violaceum

MECHANISTIC AND STRUCTURAL STUDIES OF PHENYLALANINE HYDROXYLASE FROM *CHROMOBACTERIUM VIOLACEUM*

A Dissertation

by

ARAM JOEL PANAY ESCOBAR

Submitted to the Office of Graduate Studies of
Texas A&M University
in partial fulfillment of the requirements for the degree of

DOCTOR OF PHILOSOPHY

Approved by:

Co-Chairs of Committee,	Paul F. Fitzpatrick
	Gregory D. Reinhart
Committee Members,	Marty J. Scholtz
	Gary Kunkel
Head of Department,	Gregory D. Reinhart

August 2010

Major Subject: Biochemistry

ABSTRACT

Mechanistic and Structural Studies of Phenylalanine Hydroxylase from

Chromobacterium violaceum. (August 2010)

Aram Joel Panay Escobar, B.S., Universidad del Valle, Cali, Colombia

Co-Chairs of Advisory Committee: Dr. Paul F. Fitzpatrick
Dr. Gregory D. Reinhart

The phenylalanine hydroxylase from *Chromobacterium violaceum* (CvPheH) is a non-heme iron monooxygenase that catalyzes the hydroxylation of phenylalanine. This study presents the use of kinetic isotope effects (KIE) as mechanistic probes to compare the reactivity of CvPheH and that of the eukaryotic aromatic amino acid hydroxylases. This study also describes the use of different spectroscopic and kinetic techniques to identify the hydroxylating intermediate for this enzyme and the assignment of the NMR backbone resonances of CvPheH.

Kinetic isotope effects on aromatic and benzylic hydroxylation were used to establish that bacterial and eukaryotic phenylalanine hydroxylases have similar reactivity. The observed KIE on aromatic hydroxylation of 1.4 was shown to be a combination of an inverse isotope effect on the hydroxylation of the amino acid and a normal isotope effect on a subsequent step in the reaction. An isotope effect on benzylic hydroxylation of 10 was found for CvPheH. This result establishes the similar reactivity for CvPheH and the eukaryotic aromatic amino acid hydroxylases and suggests the involvement of a common hydroxylating intermediate.

Kinetic isotope effects were used to study the hydroxylation of the aliphatic substrate cyclohexylalanine. The $^{D}k_{cat}$ value with [1,2,2,3,3,4,4,5,5,6,6-$^{2}H_{11}$]-cyclohexylalanine is unity with wild-type CvPheH, suggesting that chemistry is not rate-limiting with this substrate. The intramolecular isotope effect calculated using [1,2,3,4,5,6-$^{2}H_{6}$]-cyclohexylalanine yields a value of 14. This result is evidence for the involvement of a reactive iron species capable of abstracting a hydrogen atom from the aliphatic carbon in cyclohexylalanine.

Analysis of the CvPheH reaction using freeze-quench Mössbauer spectroscopy allowed the detection of an Fe(IV) species in the first turnover of the enzyme. Chemical quench and stopped-flow spectrophotometric methods were used to establish the kinetic competency of the Fe(IV) intermediate as the hydroxylating species.

The NMR amide backbone resonances in the HSQC spectrum of CvPheH were assigned to the corresponding amino acid residues using a suite of TROSY-based three-dimensional triple resonance experiments. We were able to assign 224 residues out of the 278 assignable residues in CvPheH, this constitutes 81 % of the assignable protein sequence.

DEDICATION

This work, which is a big part of my life, goes to Margarita for her endless love, encouragement, and for always believing in me.

ACKNOWLEDGEMENTS

I would like to thank my advisor, Dr. Paul Fitzpatrick, for believing in my capabilities and for his endless patience and guidance. Working in his laboratory has been a great experience. I would also like to thank the members of my committee, and in general the people in the department, who were always there for help or just to chat. Special thanks go to Dr. Donald Pettigrew for sharing his great wisdom unselfishly.

Thanks also go to all the past and present lab members who made research very enjoyable. Also, I would like to thank all the wonderful people that I met during the past six years. Especially, to the members of the C.A.G.A.T.E. They prove every day that smart people can be fun!

ABBREVIATIONS

PheH	Phenylalanine Hydroxylase
CvPheH	*Chromobacterium violaceum* Phenylalanine Hydroxylase
TyrH	Trosine Hydroxylase
TrpH	Tryptophan Hdroxylase
DHPR	Dihydropteridine Reductase
DOPA	Dihydroxyphenylalanine
BH_4	Tetrahydrobiopterin
6-MePH_4	6-Methyltetrahydropterin
$DMPH_4$	6,7-Dimethyltetrahydropterin
EDTA	Ethylenediaminetetraacetic Acid
NTA	Nitrilotriacetic Acid
RMSD	Root Mean Square Deviation
NMR	Nuclear Magnetic Resonance
NDA	Naphtalene-2-3-dicarboxaldehyde
DTT	Dithiothreitol
THF	Tetrahydrofuran
HPLC	High Performance Liquid Chromatography
HSQC	Heteronuclear Single Quantum Coherence

TABLE OF CONTENTS

CHAPTER Page

LIST OF FIGURES

FIGURE Page

FIGURE Page

LIST OF TABLES

CHAPTER I

INTRODUCTION

Phenylalanine hydroxylase (PheH) is a non-heme iron dependent enzyme that catalyzes the hydroxylation of the amino acid phenylalanine to tyrosine . In mammals PheH is present in the liver where it catalyzes the first and rate-limiting step in the metabolism of the phenylalanine acquired in the diet . More than 500 mutations in PheH have been associated with the metabolic disorder phenylketonuria (*1, 2*). In individuals suffering from phenylketonuria the activity of PheH is hindered. Thus, phenylalanine accumulates in the blood. When not diagnosed in time phenylketonuria leads to mental retardation. Despite the severity of the disease, the problem can be avoided with a diet low in phenylalanine. All babies born in the United States are tested for phenylketonuria after birth by measuring the level of phenylalanine in the blood (*3*).

Phenylalanine hydroxylase is a member of the family of aromatic amino acid hydroxylases, which also includes tyrosine hydroxylase (TyrH) and tryptophan hydroxylase (TrpH) (*4*). Figure 1.1 summarizes the reactions catalyzed by the aromatic amino acid hydroxylases. The product of the reaction catalyzed by TyrH, dihydroxyphenylalanine (DOPA), is the precursor of the neurotransmitters dopamine, norepinephrine and epinephrine (*5*). TrpH converts tryptophan to 5-hydroxytryptophan, which is further metabolized to the neurotransmitter serotonin (*6*).

This dissertation follows the style of *Biochemistry*.

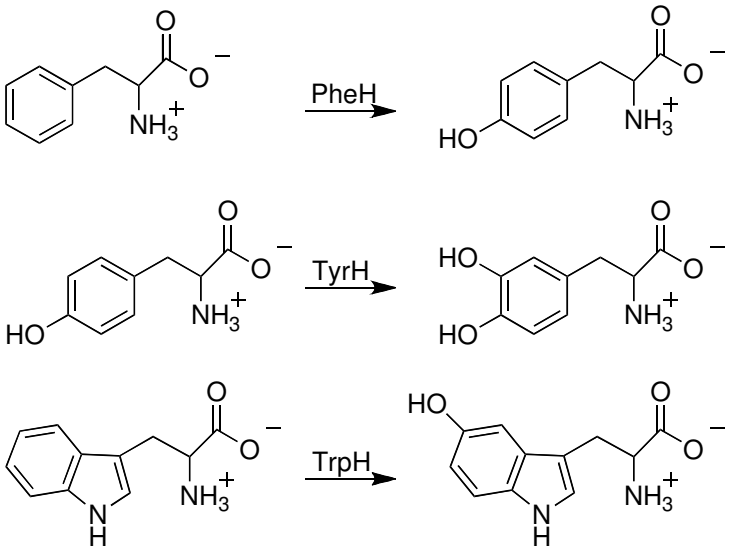

Figure 1.1: Reactions catalyzed by the aromatic amino acid hydroxylases phenylalanine hydroxylase (PheH), tyrosine hydroxylase (TyrH), and tryptophan hydroxylase (TrpH).

In addition to the amino acid substrate, all the aromatic amino acid hydroxylases require ferrous iron and a tetrahydropterin for catalysis. *In vivo*, the electrons from a tetrahydrobiopterin (BH_4) are used to activate ground-state (triplet) molecular oxygen to react, with the aromatic side chain of the substrate (*7, 8*). As the result of the reaction, one oxygen atom from molecular oxygen is incorporated into the aromatic ring of the amino acid and the other into the 4a-position of the biopterin. Once in solution the pterin-4a-carbinolamine dehydrates to quinonoid dihydrobiopterin. BH_4 is regenerated by dihydropteridine reductase (DHPR) using electrons from NAD(P)H (*9*) (Figure 1.2).

The kinetic mechanism has been determined for TyrH and CvPheH (*10-12*). In the case of the eukaryotic enzyme, Fitzpatrick (*10*) reported that 6-methyltetrahydropterin (6-$MePH_4$) bound first followed by oxygen and tyrosine. Two different results have been reported for CvPheH. Pember et al. (*11*) reported that oxygen bound first followed by random binding of 6,7-dimethyltetrahydropterin ($DMPH_4$) and phenylalanine. Volner et al. (*12*) reported an ordered binding in which $DMPH_4$ binds first followed by phenylalanine and oxygen. Regardless of the order, all the substrates must be bound in the active site before the reaction can take place.

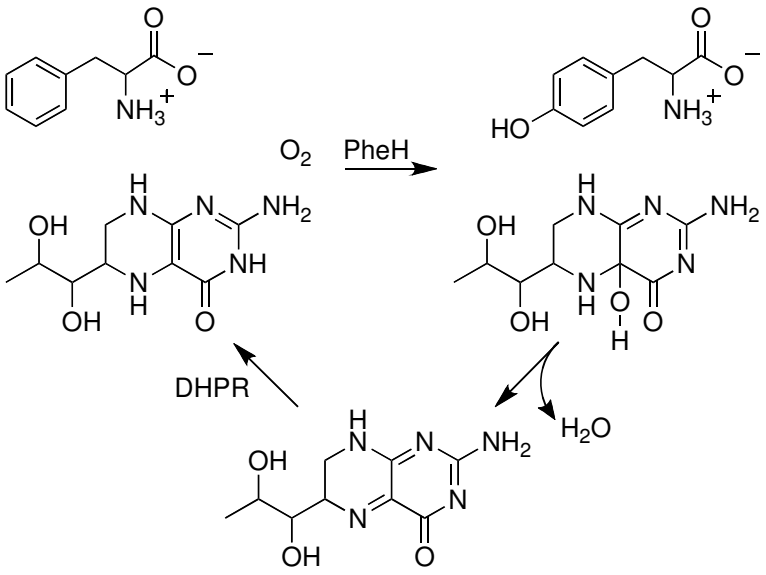

Figure 1.2: Hydroxylation of phenylalanine catalyzed by phenylalanine hydroxylase. The transformations of the pterin after the reaction are shown.

DHPR: Dihydropteridine reductase.

Studies using $^{18}O_2$ showed that molecular oxygen was the source of the oxygen atoms incorporated in the amino acid (*13*) and the 4a-hydroxypterin (*14*) products. This result argued against the role of the tetrahydropterin as a mere electron supplier and supported a model in which a peroxypterin was formed upon reaction of molecular oxygen and the tetrahydropterin. The viability of this structure as the hydroxylating species was supported by the resemblance of tetrahydropterin and flavin and the observation of a 4a-peroxyflavin in flavoprotein-catalyzed hydroxylation reactions (*15*). In addition, the production of hydrogen peroxide in the slow hydroxylation of tyrosine by PheH is consistent with the breakdown of a peroxypterin species (*16*).

The capability of a peroxypterin species as the hydroxylating intermediate in the aromatic amino acid hydroxylases is challenged by the fact that in the flavoenzymes the substrates must be activated before hydroxylation by the 4a-peroxyflavin (*17*). In contrast, unactivated benzylic and aliphatic carbons are readily hydroxylated by the aromatic hydroxylases (*4, 18, 19*), suggesting a much more reactive species than a peroxypterin. The iron requirement and the need for a more reactive species led to the proposal of an Fe(II) μ-peroxypterin as the hydroxylating species or an intermediate to its formation (*14*). The intermediacy of the Fe(II) would avoid the spin-forbidden direct interaction of oxygen with the tetrahydropterin. Moreover, computational studies were not able to find a mechanism for the reaction of oxygen and the tetrahydrobiopterin in the absence of the metal (*20*).

The experimental data supports the Fe(II) μ-peroxypterin as an intermediate rather than the hydroxylating species itself. Stoichiometric amounts of hydroxylated

amino acid and 4a-hydroxypterin are expected from the hydroxylation by such a species. However, when tyrosine is the substrate for PheH or TrpH the amount of DOPA formed is only a fraction of the tetrahydropterin that is oxidized (*16, 21*). Similar results were obtained using the S395A mutant of TyrH (*22*). These results are in disagreement with the concerted rupture of the peroxypterin OO bond and the hydroxylation of the amino acid substrate. On the contrary, they support a model in which the hydroxylating intermediate is formed from the heterolytic cleavage of the OO bond of Fe(II) μ-peroxypterin, generating the hydroxypterin product and an Fe(IV)O species (*23*). Computational and biomimetic studies have shown the ability of oxoferryl species to hydroxylate the wide range of carbons that the amino acid hydroxylases accept as substrates (*20, 24, 25*). An Fe(IV)O species has been identified as the hydroxylating intermediate in the α-ketoglutarate dependent taurine dioxygenase system (*26, 27*). In both the latter enzyme and the aromatic amino acid hydroxylases the Fe(II) is coordinated by a carboxylic group and two histidine residues. More recently, Eser et al. reported spectroscopic evidence for the existence of a kinetically competent Fe(IV)O species for TyrH (*28*).

A chemical mechanism for aromatic amino acid hydroxylation that is consistent with all the evidence gathered for all the hydroxylases is shown in Figure 1.3 (*23*). Once the three substrates are present in the active site, a peroxo bridge is formed between the tetrahydropterin and the ferrous iron. The first product, 4a-hydroxypterin, and the hydroxylating species Fe(IV)O are produced after the heterolytic cleavage of the oxygen-oxygen bond. Once formed the Fe(IV)O reacts with the aromatic side chain of

the amino acid, generating a carbocation that undergoes a 1,2 hydride transfer to form a dienone. Tautomerization of the dienone gives the final product, tyrosine.

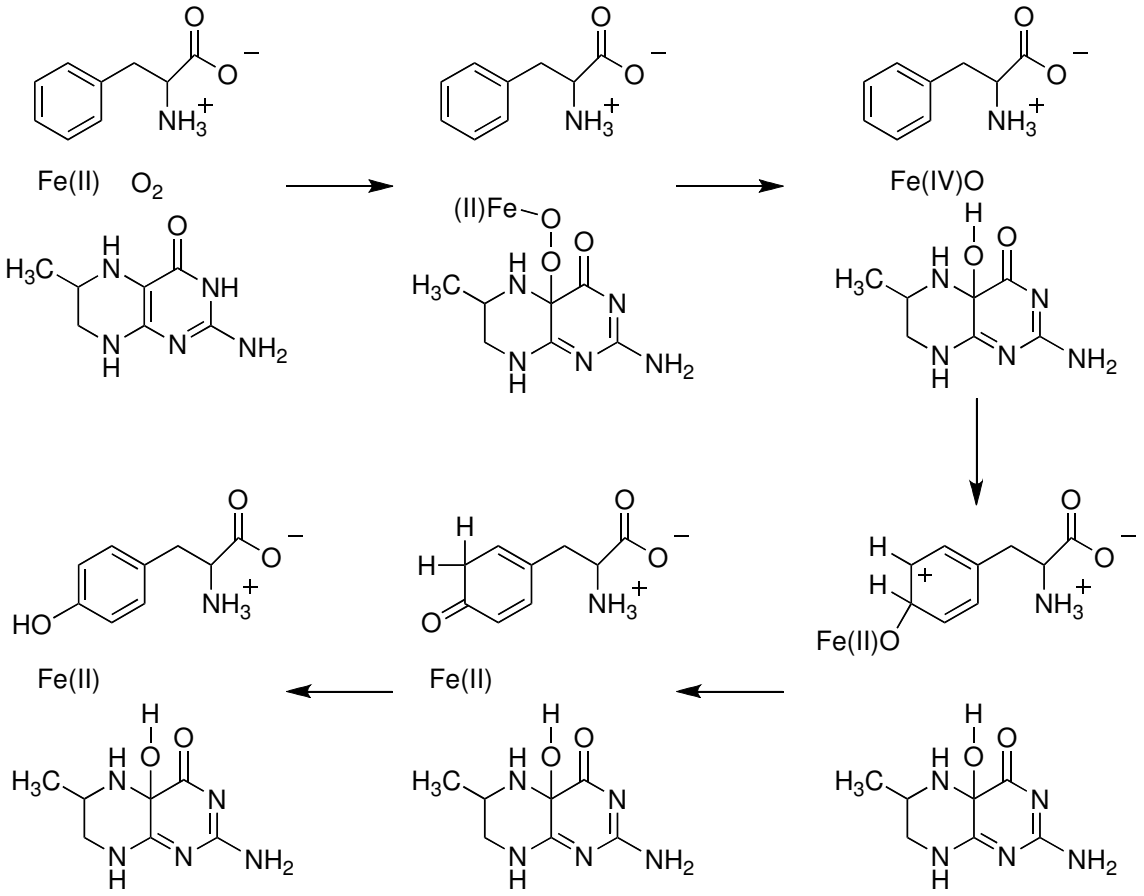

Figure 1.3: Proposed chemical mechanism of aromatic hydroxylation.

In spite of having a similar chemical mechanism the three aromatic amino acid hydroxylases differ in their reactivity and rate limiting steps. In TrpH the rate limiting step is the reaction of the hydroxylating intermediate with the indole side chain (*21*). Recently, Eser and Fitzpatrick (*29*) reported that for TyrH hydroxylation of tyrosine is about 26 fold faster than the release of the products. In the case of PheH multiple steps are partially rate limiting (*30*).

Most of the evidence for the proposed chemical mechanism comes from studies using ring-deuterated amino acids as substrates. When 5-^{2}H-tryptophan is used as substrate, TrpH shows an inverse deuterium isotope effect. This is consistent with a change in hybridization from sp^2 to sp^3 at the hydroxylated carbon (*21*). On the other hand, TyrH and PheH show no or small normal isotope effects, respectively, when deuterated substrates are used (*30, 31*). In both enzymes, the intrinsic isotope effect on hydroxylation was unmasked using mutant enzymes in which an alternate pathway for the decay of the hydroxylating intermediate was introduced (*30, 32*). These mutant enzymes show inverse isotope effects when the site of hydroxylation in the substrate is deuterated; this result is consistent with the formation of a carbocation after the electrophilic addition of the Fe(IV)O species (Figure 1.3). In addition, supporting evidence for the arenium cation intermediate comes from studies using para-substituted (X = F, Br, Cl, CH_3, OCH_3) phenylalanines as substrates for TyrH (*31*). The ρ value of about – 5 is in agreement with an electron deficient transition state. After the formation of the carbocation intermediate the subsequent step is a hydroxylation-induced migration, known as NIH shift, of the atom present at the site of hydroxylation to the

adjacent carbon (*33*). The evidence for this phenomenon in the aromatic amino acid hydroxylases comes from studies using tritiated phenylalanine and tryptophan (*34, 35*). Computational studies using hybrid density functional theory found the NIH shift to have a low energy barrier making it isotope insensitive (*20*). For PheH an intramolecular isotope effect of 5.1 was measured for the final tautomerization step (*30*).

Phenylalanine hydroxylase is also present in prokaryotes. A gene for phenylalanine hydroxylase has been reported in almost 200 bacterial genomes. The phenylalanine hydroxylase from *Chromobacterium violaceum* (CvPheH) is the only one that has been subject to biochemical study. CvPheH has been cloned and expressed in *Escherichia coli* (*36, 37*). The metal requirement of CvPheH has yielded contradictory results. Initially, CvPheH was reported to be a copper-requiring enzyme (*11*). Subsequently, the same group reported evidence for catalysis by metal-free CvPheH. Also, copper was reported to be an inhibitor of the metal-free CvPheH (*18, 38*). More recently, Chen and Frey (*36*) showed that iron was required for the hydroxylation of phenylalanine. In addition, the crystal structure of CvPheH showed an iron center identical to that found in the eukaryotic enzymes (*39*). Despite the structural evidence and the iron requirement for catalysis displayed by CvPheH, the fact that apo-CvPheH was able to catalyze the oxidation of $DMPH_4$ at 5 % the rate of the iron-containing enzyme raised the possibility of a metal independent mechanism of oxygen activation (*36*). This result stands in stark contrast to the complete iron dependence showed by TyrH to oxidize either the tetrahydropterin or the amino acid (*19*). The discrepant results between eukaryotic and prokaryotic hydroxylases could be explained by a more reactive

iron center present in the more evolved bacterial enzyme. Nevertheless, the residual $DMPH_4$ oxidation activity displayed by apo-CvPheH could arise from adventitious iron present in the buffers used for the assays. The latter possibility is supported by the low concentrations of enzyme used in steady-state assays and the fact that tetrahydropterins can reduce ferric iron to the catalytically active ferrous form. A re-examination of the metal independent oxidation of $DMPH_4$ under conditions where free metal ions are minimized, like in the presence of EDTA, could clarify the discrepancy between the findings reported for CvPheH and TyrH.

The aromatic amino acid hydroxylases can accept different amino acids as substrates. The range of reactions catalyzed by these enzymes includes aromatic hydroxylation of ring-substituted amino acids, benzylic hydroxylation, aliphatic hydroxylation, epoxidation and sulfoxidation (*4*). When presented with 4- CH_3-phenylalanine, hydroxylation occurs at the benzylic carbon and the aromatic ring (Figure 1.4). The ratio of the hydroxylated products varies depending on the enzyme (*40*). PheH produces roughly equal amounts of 4-$HOCH_2$-phenylalanine and 3-CH_3-4-HO-phenylalanine and just detectable amounts of 3-HO-4-CH_3-phenylalanine. In TyrH the main products are hydroxylated in the aromatic ring. TrpH behaves in a similar fashion to PheH but 3-HO-4-CH_3-phenylalanine constitutes 20 % of the products. When 4-C^2H_3-phenylalanine is used as a substrate, the partitioning of benzylic to aromatic products changes and the deuterium isotope effect on benzylic hydroxylation can be determined from that partitioning (*40, 41*). A large isotope effect of about 13 was found for all the eukaryotic enzymes. The similar effect of temperature on the isotope effect was

interpreted as evidence of a similar chemical mechanism and comparable reactivity among the eukaryotic amino acid hydroxylases.

Few isotopic studies have been carried out using CvPheH. The only reported attempt to use deuterated substrates with this enzyme used a metal free enzyme (*18*). No isotope effect was found when fully deuterated or para-deuterated phenylalanine was used. These results highlight the need for a more comprehensive characterization of the bacterial phenylalanine hydroxylase.

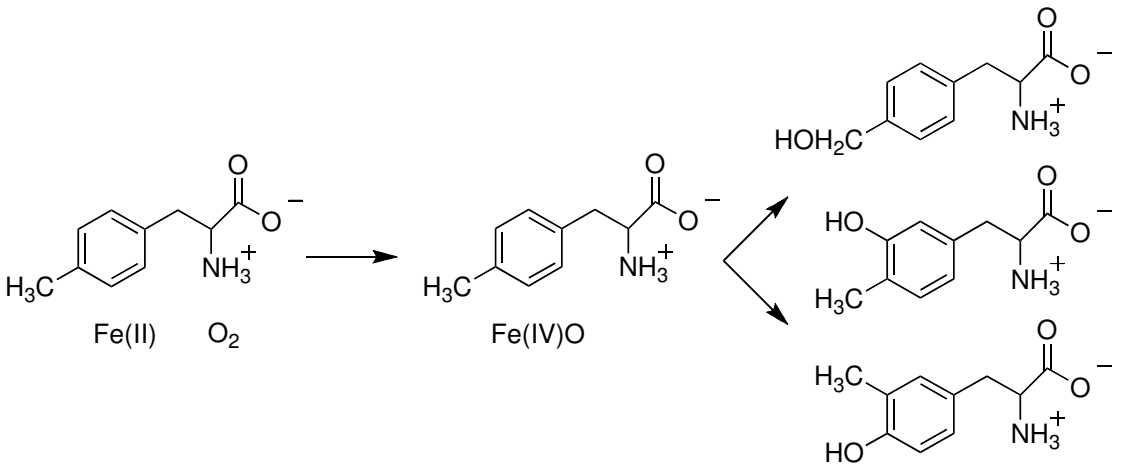

Figure 1.4: Benzylic hydroxylation by the aromatic amino acid hydroxylases. The mixture of products varies depending on the enzyme.

The eukaryotic amino acid hydroxylases form homotetramers in solution. Each monomer can be divided into three domains, an N-terminal regulatory domain, a catalytic core and a C-terminal domain responsible for tetramerization (*23*). The N-

terminal regulatory domain, which spans on average the first 130 residues, contains different serine residues that can be phosphorylated (*4*). The effect of phosphorylation varies for each of the enzymes, and accordingly the similarity of the regulatory domains is less than 14 % (*23*). Only in the case of PheH has a crystal structure been reported that includes the regulatory domain (*42*). This structure shows that in the absence of the substrates the regulatory domain blocks the active site. The catalytic domain, of about 280 amino acids, contains all the residues necessary for catalysis and substrate recognition (*43-47*). Among the eukaryotic enzymes the catalytic domains share about 52 % identity, and the crystal structures of the three enzymes show a similar protein fold for this domain (*48-50*). The bacterial CvPheH is a monomer comprising only the catalytic domain. The crystal structure of the 32 kDa CvPheH can be superimposed on that of the catalytic domain of human PheH with an RMSD of 1.2 Å (*39*) , confirming the homology across the species. Finally, for the eukaryotic enzymes the last 40-50 residues make up the tetramerization domain (*45*). The crystal structure of TyrH shows the helix of approximately 25 residues that interacts in the coil-coil structure that holds the tetramers together (*50*).

Crystal structures of the catalytic domains of all three eukaryotic enzymes and of CvPheH are available (*39, 48-50*). In all of these structures the iron binding site is located about 12 Å deep in a cleft formed by the protein. The iron ligands are two histidines, a glutamate and, in the resting state of the enzyme, three water molecules that coordinate the iron in an octahedral fashion. The structure of CvPheH with BH_2 shows a bidentate glutamate, whereas the glutamate is a monodentate ligand in the structure of

the human enzyme (*39*). The changes in the coordination of the glutamate as well as the displacement of two water molecules, triggered by the presence of the substrates, leave a five-coordinated iron that is ready for oxygen activation (*51*). The tetrahydropterin binding site is close to the iron. The structure of human PheH with BH_4 shows a loop comprising residues 247 to 251 interacting directly with BH_4 (*48*). Most of these interactions involve the protein backbone instead of the amino acid side chains. Only the hydroxyl group of Ser251 hydrogen bonds to the dihydroxypropyl group of biopterin. This interaction is not crucial for the proper binding of the tetrahydropterin, since a variety of 6 and 7 substituted tetrahydropterins are accepted as electron donors for hydroxylation (*4*). The crystal structure of this binary complex can be superimposed over the free enzyme with an RMSD of 0.21 Å. Only when both the pterin and the amino acid are present do significant changes take place in the protein structure. No structure of a hydroxylase with only the amino acid is available. However, human PheH was crystallized with both tetrahydrobiopterin and 3(2-thienyl)-L-alanine. This structure shows the amino acid being held in place by an electrostatic interaction between the carboxylate of the substrate and Arg270. Hydrogen bonding between the substrate amino group and the side chain hydroxyl of Thr278 also contributes to positioning the amino acid. A group of mainly aromatic residues including Trp326, Phe331, and Pro281 form a hydrophobic pocket that holds the aromatic side chain of the substrate in place. Additionally, the substrate aromatic ring π-stacks with the side chain of the metal ligand His285. The crystal structure of this ternary complex shows an RMSD of 2.2 Å when compared to the free enzyme (*48*). When both substrates are present, the

tetrahydrobiopterin moves 2.6 Å closer to the metal center and a loop containing residues 131-155 moves almost 10 Å towards the iron center with Tyr138 packing against the residues that make up the hydrophobic pocket around the active site. This structure is believed to resemble the catalytically active enzyme. No other aromatic amino acid hydroxylase has been crystallized with both an amino acid and a pterin substrate. However, fluorescence anisotropy studies with TyrH show that the region corresponding to Tyr138 changes upon binding of the substrates (*52*). The crystallographic and fluorescence data provide evidence that PheH and TyrH are flexible enzymes that fluctuate between conformations during catalysis. More information on this has been recently obtained using hydrogen/deuterium exchange experiments on these two enzymes. For TyrH, phosphorylation at Ser40 displaces the equilibrium from a closed, dopamine-bound conformation, to a catalytically active open conformation (*53*). Similar studies on PheH provide direct evidence for an autoregulatory role for the N-terminal sequence of the protein (*54*). In the presence of the activator phenylalanine peptides that lie in the interface regions of the regulatory and catalytic domain show increased deuterium incorporation. This result is consistent with a more open structure in which the regulatory domain moves away from the active site when phenylalanine is present. The results from the isotope exchange studies support the use of a more specific technique like nuclear magnetic resonance to study the aromatic amino acid hydroxylases. NMR studies could provide detailed information on the dynamic changes that take place in regulation and catalysis by this family of enzymes.

CHAPTER II

KINETIC ISOTOPE EFFECTS ON AROMATIC AND BENZYLIC HYDROXYLATION BY *CHROMOBACTERIUM VIOLACEUM* PHENYLALANINE HYDROXYLASE AS PROBES OF THE CHEMICAL MECHANISM AND REACTIVITY

Phenylalanine hydroxylase (PheH) is a non-heme iron monooxygenase that catalyzes the hydroxylation of phenylalanine by oxygen to form tyrosine (*55*). After the three substrates, oxygen, phenylalanine and a tetrahydropterin are bound in the active site, the electrons from the tetrahydropterin are used to activate molecular oxygen. One oxygen atom is incorporated into the aromatic ring of phenylalanine and the other is reduced to the level of water (*4*). While *in vivo* the source of electrons for the reaction is tetrahydrobiopterin (BH_4), *in vitro* 6-methyltetrahydropterin (6-$MePH_4$) and 6,7-dimethyltetrahydropterin ($DMPH_4$) are able to sustain the reaction (Figure 2.1).

PheH is found in different organisms ranging from prokaryotes to eukaryotes. In humans, mutations in PheH are linked to the metabolic disorder phenylketonuria, which is associated with mental retardation (*1*). To date almost 200 bacterial genomes have been reported to include a gene for PheH. The phenylalanine hydroxylase from *Chromobacterium violaceum* (CvPheH) was previously cloned and expressed in *Escherichia coli* (*36*) . The sequence of CvPheH shows about 35% identity with the corresponding residues of human PheH, and the X-ray crystal structures can be superimposed with an RMSD of 1.2 Å (*39*). The active site is well conserved; both

proteins share the same triad of metal ligands, 2 histidine residues and a glutamate residue, and show complete dependence on iron for activity (*4, 36*). The homology between bacterial and eukaryotic PheH extends to the other two aromatic amino acid hydroxylases, tyrosine hydroxylase and tryptophan hydroxylase. Their relationship is confirmed by the similar folds of the catalytic domains (*39*). Recently, it was shown that despite different substrate specificities and catalytic properties, all three eukaryotic amino acid hydroxylases use the same chemical mechanism for catalysis, and the reactivities of the metal centers are comparable (*30, 40*). Figure 2.2 shows the proposed mechanism of aromatic amino acid hydroxylation using the PheH reaction as a model (*23*). After the three substrates are in the active site, molecular oxygen forms a bridge between the 4a position of the tetrahydropterin and the iron. The oxygen-oxygen bond cleaves to form the hydroxylating species Fe(IV)O and a 4a-hydroxy-pterin. Direct evidence for the existence of the Fe(IV)O hydroxylating intermediate has recently been obtained for tyrosine hydroxylase (*28*). Once formed the Fe(IV)O reacts with the side chain of the amino acid, generating a carbocation that undergoes a 1,2-hydride transfer to form a dienone. Tautomerization of the latter gives the final tyrosine product.

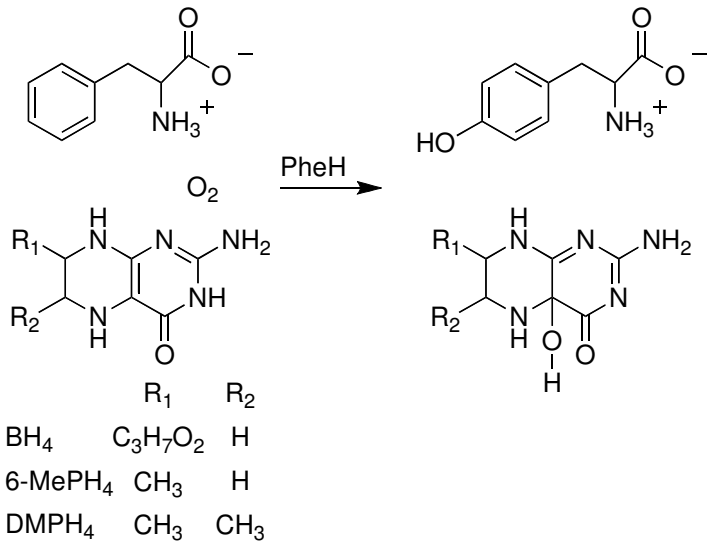

Figure 2.1: Chemical reaction catalyzed by phenylalanine hydroxylase.

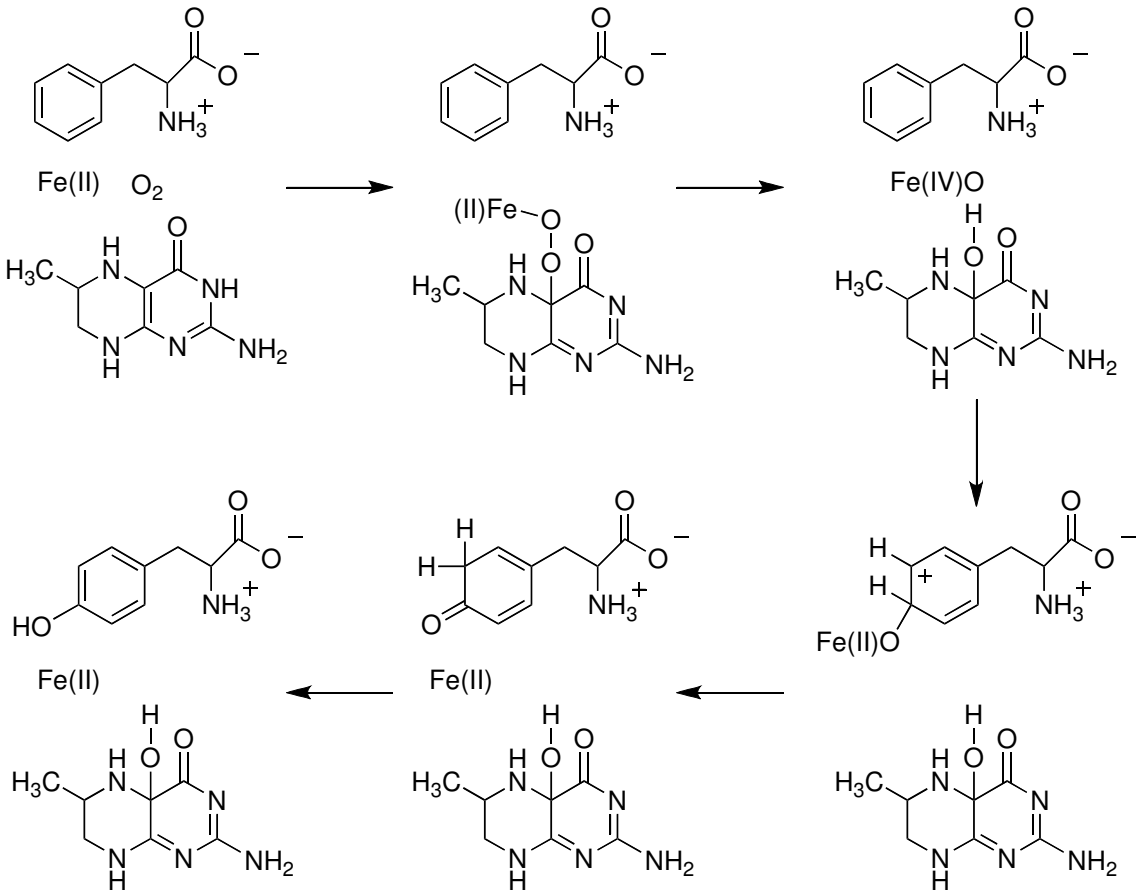

Figure 2.2: Proposed chemical mechanism of phenylalanine hydroxylase.

The affinity of CvPheH for various metals, including iron, led to controversy in the literature regarding the iron requirement of this enzyme (*18, 38, 56*). More recently, Chen and Frey (*36*) showed that CvPheH required ferrous iron to hydroxylate phenylalanine. In addition, the crystal structure of CvPheH showed an arrangement of iron ligands essentially identical to that of the eukaryotic enzymes (*39*). These results suggest that for prokaryotic and eukaryotic hydroxylases an Fe(IV)O is the common hydroxylating intermediate (*23, 36, 57*). However, the latter species could arise from direct interaction of oxygen with the ferrous iron or initial electron donation from the tetrahydropterin. Chen and Frey (*36*) reported that iron-free CvPheH could catalyze the oxidation of $DMPH_4$ at about 5% the rate of the iron containing enzyme suggesting that iron is not necessary for oxygen activation. In stark contrast, the eukaryotic tyrosine hydroxylase showed a complete dependence for iron to catalyze the oxidation of the tetrahydropterin or the hydroxylation of the amino acid (*19*). This discrepancy could arise from a more reactive iron center in CvPheH.

The goal of the work reported here was to use kinetic isotope effects as probes of transition state structures for hydroxylation reactions catalyzed by CvPheH to allow comparison with the reactivities of the eukaryotic enzymes. In addition to aromatic hydroxylation, the bacterial and eukaryotic PheHs are capable of hydroxylating benzylic carbons (*18, 58*). In the case of the eukaryotic enzymes, the deuterium kinetic isotope effect on benzylic hydroxylation is consistent with a mechanism involving hydrogen atom abstraction from the methyl group (*40*); this reaction was used to compare the reactivities of the Fe(IV)O intermediates in the three eukaryotic enzymes (*40*).

EXPERIMENTAL PROCEDURES

Materials. Oligonucleotides were purchased from Integrated DNA Technologies (Coralville, IA). Plasmid pET21b was from Novagen (San Diego, CA). Restriction and DNA modification enzymes were purchased from New England Biolabs (Ipswich, MA) and Promega (Madison, WI). Plasmids were purified using Wizard mini-prep kits from Promega. Catalase was from Roche (Indianapolis, IN). DEAE-Sephacel was from Amersham Pharmacia Biotech (Uppsala, Sweden). The *E. coli* strain BL21(DE3), used for protein expression, was from Novagen, and the strain Mach1, used for subcloning, was from Invitrogen (Carlsbad, CA). 6-MePH_4 and DMPH_4 were from B. Schircks Laboratories (Jona, Switzerland). L-Tyrosine, L-phenylalanine, L-tryptophan, D,L-phenylalanine, dihydropteridine reductase, sodium cyanide, boric acid and 5-hydroxytryptophan were from Sigma-Aldrich Chemical Co. (Milwaukee, WI). Napthalene-2,3-dicarboxaldehyde (NDA) was from Invitrogen. L-$^2H_5$-Phenylalanine was from Cambridge Isotope Laboratories (Andover, MA). Dithiotreitol (DTT) was from Inalc (Milan, Italy). The synthesis of D,L-[4-^{2}H]-phenylalanine and D,L-[3,5-$^2H_2$]-phenylalanine was previously described (*59*). All other reagents were of the highest purity commercially available.

Construction of vectors, enzyme expression and purification. A vector containing the cDNA for *C. violaceum* phenylalanine hydroxylase was obtained from Dr. Perry Frey (University of Wisconsin). The cDNA was amplified by PCR and subcloned into the pET21b vector using the restriction sites 5' *NdeI* and 3' *Hind III* to generate the plasmid pET21b-CvPheH. The plasmid was sequenced by the Gene Technology Laboratory of the Biology Department of Texas A&M University. We found discrepancies with the published sequences of CvPheH (*36, 39*). Specifically, methionine 64 is a leucine in the X-ray structure of CvPheH (*39*). Sequence alignments using all the available bacterial phenylalanine hydroxylase sequences revealed a conserved leucine residue at position 64. Consequently, we introduced the mutation M64L into pET21b-CvPheH using the QuikChange protocol (Stratagene).

Purification of CvPheH was carried out with modifications of previously reported procedures (*37, 39*). The *E. coli* strain BL21(DE3) was transformed with the plasmid pET21b-CvPheH. A single colony was used to inoculate 50 mL of LB broth (100 μg/mL of ampicillin) and allowed to grow at 37 °C for 16 hours. Ten mL of the overnight culture were used to inoculate 1 L of fresh LB broth (100 μg/mL of ampicillin). When the A_{600} reached a value between 0.8 and 1.0 the cells were induced with isopropyl-β-thiogalactoside at a final concentration of 120 mg/L. After 5 hours at 37 °C the cells were harvested by centrifugation for 30 minutes at 2620 x g. The cell pellet was suspended in an 8-fold excess (with respect to the initial weight of the cells) of 50 mM Hepes buffer (pH 7.2), 1 mM DTT and 100 μg/mL phenylmethanesulfonyl fluoride (dissolved in acetone). Cells were disrupted using 100 mg/mL lysozyme and

sonication for 5 cycles of 3 min. The suspension was centrifuged at 17640 x g for 30 minutes. The supernatant was made 600 μM in $FeSO_4$ and stirred for 30 min at 4 °C. The solution was brought to 2% streptomycin sulfate, stirred for 15 min and centrifuged for 30 min at 17640 x g. The resulting solution was made 50% saturated in ammonium sulfate, stirred for 15 min and centrifuged for 30 min at 17640 x g. The resulting protein pellet was dissolved in a minimal amount of 50 mM Hepes (pH 7.2), 20 mM NaCl, and dialyzed for four hours against a 100-fold excess of the same buffer solution with two buffer changes. The dialyzed solution was loaded onto a DEAE-Sephacel column equilibrated with 50 mM Hepes (pH 7.2) and 20 mM NaCl. The protein was eluted with a linear gradient formed with 500 mL of 50 mM Hepes buffer at pH 7.2 containing 20 mM NaCl and 500 mL of the same buffer containing 500 mM NaCl. The fractions were analyzed using A_{280} and SDS-PAGE gel electrophoresis. Fractions containing the purest and most active enzyme were pooled. This method usually gave 100 mg of more than 95% pure CvPheH per liter of LB.

The metal-depleted CvPheH was made by incubating the enzyme with 5 mM EDTA and 5 mM NTA on ice for 2 hours followed by dialysis against 50 mM Hepes (pH 7.2) and 20 mM NaCl. For the $DMPH_4$ oxidation studies, gel filtration chromatography using Micro Bio-Spin columns from Bio-Rad (Hercules, CA) was carried out after incubation with EDTA. The metal content of the protein was measured as previously described (*60*) using a Perkin-Elmer Model 2380 atomic absorption spectrophotometer equipped with a graphite furnace. The $DMPH_4$ oxidation studies by the apo-CvPheH were performed as previously described (*36, 38*).

Enzyme assays. All spectroscopic assays were carried out in a Hewlett-Packard Model 8453 diode array spectrophotometer equipped with a thermostatically controlled cuvette holder. Tyrosine formation was measured by monitoring the change in absorbance at 275 nm; an ε_{275} value of 1.34 mM^{-1} cm^{-1} was used to calculate the rate of product formation (*43, 61*). The assays were performed at 25 °C in 50 mM Hepes (pH 7.2), 5 mM DTT, 10 μM ferrous ammonium sulfate, 50 μg/ml catalase, 0.1-0.3 μM CvPheH, 150 μM 6-MePH_4 or 250 μM $DMPH_4$, and varying concentrations of phenylalanine. The steady-state kinetic parameters for the hydroxylation of tryptophan or cyclohexylalanine were measured using a coupled assay in which the oxidation of NADH by DHPR was followed (*62*).

The coupling between amino acid oxidation and the tetrahydropterin oxidation was measured using an HPLC-based assay (*62*). The conditions were 500 μM phenylalanine, 10 μM ferrous ammonium sulfate, 1 μM CvPheH and 25-100 μM tetrahydropterin. The reactions were carried out for 5 min in 400 μL of 10 mM sodium phosphate buffer (pH 7.0). The reaction was quenched with 100 μL of 100 mM sodium borate (pH 9.0). To this, 50 μL of 50 mM sodium cyanide and 100 μL of 50 mM naphthalene-2,3-dicarboxaldehyde were added. The fluorescent derivatives were separated using a Nova-Pack C 18 column and a gradient of 30-40% acetonitrile in 70-60% 10 mM sodium phosphate with 1% THF (pH 7.0). The fluorescent molecules were detected using a Waters 2475 detector. The excitation and emission wavelengths were 420 and 490 nm, respectively. The amount of tyrosine was quantified using a standard curve generated using the same reaction conditions but with omission of the protein.

The samples sent for mass spectrometry for the determination of the isotope effect on the tautomerization were prepared following the same protocol, except that 1 mM 6-MePH_4 or $DMPH_4$, 1 μM CvPheH and 500 μM D,L-[4-^{2}H]-phenylalanine or D,L-[3,5-$^2H_2$]-phenylalanine were used. The reactions were incubated at 25 °C for 30 min. The peak corresponding to tyrosine was collected and analyzed by negative ion electrospray time-of-flight mass spectrometry at the Laboratory of Biological Mass Spectrometry at Texas A&M University. The data were corrected for ^{13}C contributions and used in the calculation of the isotope effects.

The benzylic and aromatic hydroxylation products from the reaction of CvPheH with 4-CH_3-phenylalanine were detected and quantified using an HPLC-based assay as previously reported for tyrosine and phenylalanine hydroxylase (*40, 41*). The conditions for the reaction were 500 μM 4-CH_3-phenylalanine or 4-C^2H_3-phenylalanine, 10 μM ferrous ammonium sulfate, 1 μM CvPheH and 250 μM tetrahydropterin. The reactions were carried out for 2 min in 300 μL of 10 mM sodium phosphate buffer (pH 7.0) and quenched and analyzed by HPLC as described above.

Data analysis. Initial rates obtained as a function of the concentration of a single substrate were fit to the Michaelis-Menten equation to obtain k_{cat}, k_{cat}/K_M, and K_M values using the program KaleidaGraph (Synergy Software, Reading, PA). When substrate inhibition was observed, the data were fit to equation 2.1 in which K_i is the substrate inhibition constant. When the DTT concentration was varied, the data were fit to equation 2.2. Here v_0 and v_∞ are the rates when DTT is absent and saturating, respectively. Steady-state kinetic isotope effects were determined using Igor Pro (WaveMetrics, Lake Oswego, OR) to fit the data to equation 2.3 which assumes an isotope effect on k_{cat} only. Here, v is the initial rate, F_i is the fraction of deuterium in the substrate and E_v is the isotope effect on k_{cat}.

$$v = k_{cat} [S] / [K_M + S + (S^2/ K_i)] \quad (2.1)$$

$$v = v_\infty [A] / (K_A + A) + v_0 \quad (2.2)$$

$$v = k_{cat} [S] / [K_M + S*(1+F_i*(E_v -1))] \quad (2.3)$$

RESULTS

Metal requirement for hydroxylation. Because of contradictory reports in the literature, we re-examined the metal content and kinetics of CvPheH. In our hands the recombinant enzyme expressed in *E.coli* contained significant amounts of copper, zinc and iron when isolated. The activity of this enzyme was only 30% of the reported value (*36, 39*) and it correlated with the amount of iron present in the enzyme. Fully active, 100% iron-containing enzyme could be obtained by addition of $FeSO_4$ to the cell extract. However, we observed a decrease in activity of the enzyme purified in this fashion after prolonged periods at –80 °C. The activity of the protein could be restored after treatment with 2 mM EDTA and subsequent addition of ferrous ammonium sulfate after dialysis, suggesting a slow inhibition by other metals during the storage period (Table 2.1).

Table 2.1: Effect of storage conditions on the activity of *C. violaceum* phenylalanine hydroxylase*

Enzyme condition	K_{Phe} (μM)	k_{cat} (s^{-1})
Recently purified	69 ± 7	11 ± 1
After 1 month at -80 °C	105 ± 8	7.9 ± 0.2
After 1 month at - 80°C treated with 2 mM EDTA	68 ± 11	12 ± 1

*The solution contained 50 mM HEPES (pH 7.2), 5 mM DTT, 10 μM ferrous ammonium sulfate, 50 μg/ml catalase, 150 μM 6-$MePH_4$, 0.1-0.3 μM CvPheH.

It was previously reported that CvPheH required DTT to couple tetrahydropterin oxidation to the hydroxylation of phenylalanine and that no tyrosine could be formed without the addition of a thiol (*36*). However, we found that in the absence of DTT the activity of recently purified CvPheH is 50% of that achieved when DTT is present. Maximal activity was reached at 2 mM DTT (Figure 2.3). Fitting the data to equation 2.2 yielded a value of 0.6 ± 0.2 mM for the concentration of DTT giving half-maximal activation. The activity of the EDTA-treated CvPheH is independent of the presence of DTT, relating the activation by DTT to its ability to remove inhibitory metals, like copper, from CvPheH (*38, 56*).

The steady-state parameters for the fully active enzyme (Table 2.2) are consistent with previous reports (*18, 63*). The hydroxylation of phenylalanine was completely coupled to the oxidation of the tetrahydropterin for all the tetrahydropterin co-substrates used here. Substrate inhibition was observed with phenylalanine when BH_4 was the co-substrate but not for $DMPH_4$ or 6-$MePH_4$ (Figure 2.4). CvPheH could hydroxylate tryptophan at about 20% the rate at which it does phenylalanine (Table 2.2), in contrast to previous reports of very low activity with this amino acid (*63*). On the other hand, no DOPA was detected by HPLC with tyrosine up to 2 mM.

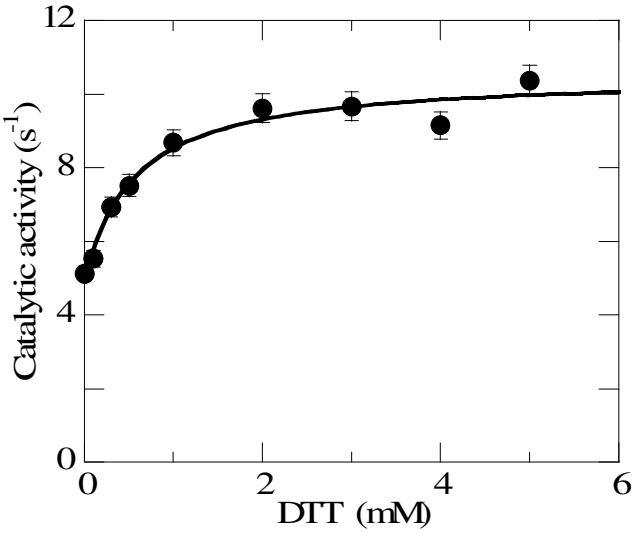

Figure 2.3: Initial rate of tyrosine formation by phenylalanine hydroxylase as a function of DTT concentration. The *line* is from the fit of the data to Equation 2.2.

Table 2.2: Steady-state kinetic parameters for *C. violaceum* phenylalanine hydroxylase

Substrate pair		K_{Phe} (μM)	K_{MPH4} (μM)	k_{cat}/K_{Phe} (s^{-1} μM^{-1})	k_{cat}/K_{MPH4} (s^{-1} μM^{-1})	k_{cat} (s^{-1})
Phe*	6-$MePH_4$	68 ± 11	18 ± 5	0.18 ± 0.02	0.61 ± 0.05	12 ± 1
Phe*	$DMPH_4$	137 ± 23	44 ± 6	0.33 ± 0.07	0.73 ± 0.07	35 ± 2
Phe*	BH_4	61 ± 10	43 ± 4	0.15 ± 0.05	0.23 ± 0.06	10 ± 1
Cha[§†]	6-$MePH_4$	60 ± 10	49 ± 9	0.045 ± 0.006	0.054 ± 0.008	2.8 ± 0.1
Trp[§†]	6-$MePH_4$	800 ± 80	ND	0.003 ± 0.001	ND	2.2 ± 0.2

*The solution contained 50 mM HEPES (pH 7.2), 5 mM DTT, 10 μM ferrous ammonium sulfate, 50 μg/ml catalase, 0.1-0.3 μM CvPheH.

[§] Determined using the coupled assay.

[†]The solution contained 50 mM HEPES (pH 7.2), 50 μg/ml catalase, 250 μM NADH, 0.3 Units of DHPR, 10 μM ferrous ammonium sulfate, 0.1-0.3 μM CvPheH.

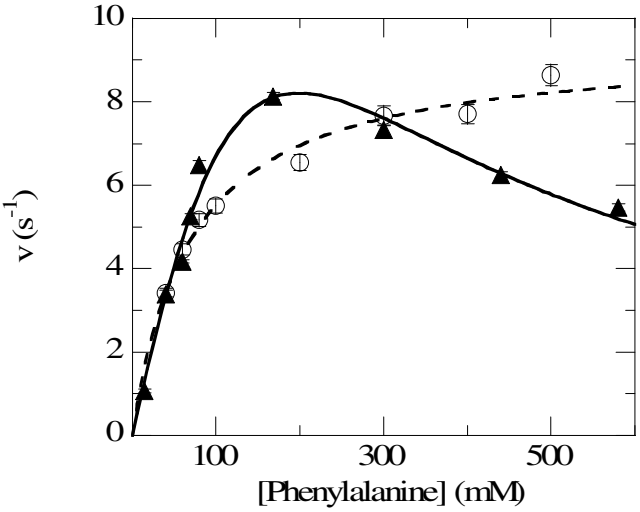

Figure 2.4: Initial rate of tyrosine formation by phenylalanine hydroxylase as a function of phenylalanine concentration. 150 μM 6-MePH_4 (circles); 150 μM BH_4 (triangles). The *lines* are from fits of the data to the Michaelis-Menten equation for 6-MePH_4 and to Equation 2.1 for BH_4.

Isotope effects on aromatic hydroxylation. The mechanism shown in Figure 2.2 predicts that multiple steps will be affected by deuterium substitution at the site of hydroxylation. In order to identify those steps we used phenylalanine in which deuterium was incorporated at the site of hydroxylation, the adjacent carbons or the whole ring. The best fit of the data was to Equation 2.3 which assumes an isotope effect only on k_{cat}. The observed kinetic isotope effect was normal with both $6MePH_4$ and $DMPH_4$ (Table 2.3). A similar result has been reported for rat PheH. With that enzyme the normal isotope effect was shown to be a combination of two isotope-sensitive steps, the initial reaction of the hydroxylating intermediate with the aromatic ring of phenylalanine and the final tautomerization required to form tyrosine (*30, 64*).

Table 2.3: Kinetic isotope effects on k_{cat} for *C. violaceum* phenylalanine hydroxylase with deuterated phenylalanine*

Enzyme	6-$MePH_4$	$DMPH_4$
Wild-type	1.24 ± 0.04	1.43 ± 0.07
I234D	1.00 ± 0.01	0.90 ± 0.03

*The solution contained 50 mM HEPES (pH 7.2), 5 mM DTT, 10 μM ferrous ammonium sulfate, 50 μg/ml catalase, 0.1-0.3 μM CvPheH.

With eukaryotic TyrH and PheH the intrinsic isotope effect on the initial formation of the CO bond could be obtained using mutant enzymes in which an alternative pathway for the decay of the hydroxylating intermediate was introduced (*30, 32*). In the case of rat PheH, the single V379D mutation was sufficient to unmask the intrinsic isotope effect on hydroxylation. Consequently, we introduced the corresponding mutation, I234D, into CvPheH. The hydroxylation of phenylalanine by CvPheH I234D was only 60 and 30% coupled to the oxidation of 6-MePH_4 and $DMPH_4$, respectively. Moreover, the isotope effect observed with $DMPH_4$ was inverse with the mutant enzyme, and the isotope effect observed with the more-coupled 6-MePH_4 was clearly less normal than for the wild-type enzyme (Table 2.3). The value of 0.90 obtained with the mutant protein and $DMPH_4$ is within error of the intrinsic kinetic isotope effect for addition of oxygen to the aromatic ring of the amino acid substrate by both TyrH (*32*) and rat PheH (*30*). It is thus likely to be the intrinsic isotope effect for that step with CvPheH also.

In order to measure the isotope effect on the subsequent tautomerization of the dienone to tyrosine (Figure 2.2), the deuterium content of tyrosine produced from [4-^{2}H]- or 3,5-$^2H_2$-phenylalanine was determined using mass spectrometry. While hydrogen is preferentially lost in all cases, there is slightly more deuterium in the tyrosine from [4-^{2}H]-phenylalanine, independent of the identity of the pterin (Table 2.4). The kinetic isotope effect on the tautomerization can be determined from the data of Table 2.4 using the minimal mechanism in Figure 2.5 (*30*). After the 1,2-hydride shift, both atoms are on the carbon adjacent to the site of hydroxylation. To form tyrosine H_a can be lost with

rate constant k_a or H_b with rate constant k_b. When [4-^{2}H]-phenylalanine is the substrate k_a is subject to a primary deuterium isotope effect. Likewise, k_b is subject to an isotope effect when 3,5-$^2H_2$-phenylalanine is the substrate. The isotope effects on k_a and k_b are related to the deuterium content of the tyrosine products from [4-^{2}H]- and [3,5-$^2H_2$]phenylalanine by equations 2.4 and 2.5, respectively. Here, P_D and P_H (equation 2.4) are the relative amounts of tyrosine retaining one or zero deuterium atoms in the reaction with [4-^{2}H]-phenylalanine, while P_{D2} and P_D in equation 2.5 are the relative amounts of tyrosine containing two or one deuterium atoms in the reaction with [3,5-$^2H_2$]phenylalanine. If k_a and k_b are affected in the same way by deuterium substitution, then the geometric mean of the ratios reported in Table 2.4 gives the isotope effect for the tautomerization (*65*). This value is 5.1 ± 1.0 for the reactions with both 6-MePH_4 and $DMPH_4$.

$$P_D/P_H = R_1 = {}^Dk_a(k_b/k_a) \quad (2.4)$$

$$P_{D2}/P_D = R_2 = {}^Dk_b(k_a/k_b) \quad (2.5)$$

Table 2.4: Ratio of deuterium to protium in the tyrosine produced by *C. violaceum* phenylalanine hydroxylase*

Tetrahydropterin	Phenylalanine	
	4-^{2}H-Phe	3,5-$^{2}H_2$-Phe
6-MePH_4	6.3 ± 0.5	4.1 ± 0.2
$DMPH_4$	5.7 ± 0.3	4.4 ± 0.3

*Conditions: 10 mM phosphate buffer (pH 7.0), 10 μM ferrous ammonium sulfate, 1 μM CvPheH, 400 μM phenylalanine and 3 mM $DMPH_4$ or 6-MePH_4. After 30 min the reaction was stopped, the amino acids products were purified by HPLC and their deuterium content was determined using ESI mass spectrometry.

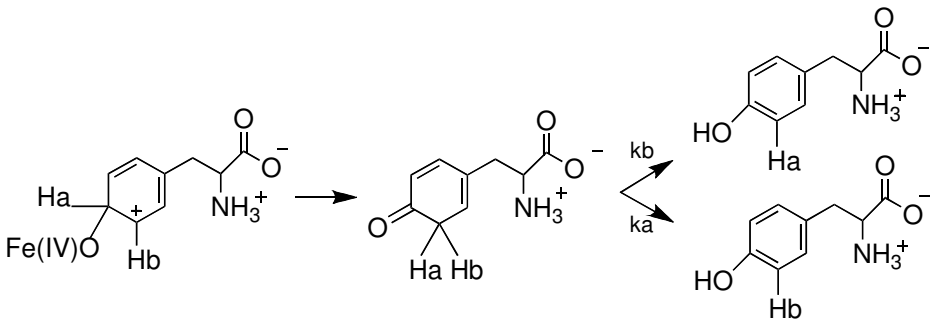

Figure 2.5: Final step in the hydroxylation of phenylalanine to tyrosine.

Isotope effects on benzylic hydroxylation. The eukaryotic and prokaryotic hydroxylases will catalyze hydroxylation on the benzylic carbon as well as on the aromatic ring of 4-methylphenylalanine (Figure 2.6) (*18, 40, 41*). In the case of CvPheH we found that 89% of the product is 4-$HOCH_2$-phenylalanine and 11% 4-HO-3-CH_3-phenylalanine. However, when 4-C^2H_3-phenylalanine is the substrate a metabolic switch takes place and 45% of the product comes from benzylic hydroxylation and 55% from aromatic hydroxylation. The intrinsic isotope effect on benzylic hydroxylation, $^{D}k_{Benz}$, is related to the isotope effect on the fraction of 4-$HOCH_2$-phenylalanine produced through equation 2.6 (*40, 41*). Here k_1 and k_2 are the net rate constants for the reaction of the hydroxylating intermediate with the non-deuterated substrate for benzylic and aromatic hydroxylation, respectively (Figure 2.6). Application of equation 2.6 to the data for CvPheH yields an intrinsic isotope effect on benzylic hydroxylation of 10 ± 1 at at 25 °C. This large isotope effect suggests a contribution of hydrogen tunneling to catalysis. In order to test this possibility we measured the temperature dependence of the isotope effect on benzylic hydroxylation (Figure 2.7). The isotope effects at different temperatures were fit to equation 2.7 (*66*) to obtain the isotope effect on the Arrhenius prefactor (A_H/A_D) of 0.29 ± 0.03 and the difference in activation energy (ΔE_a) for hydrogen and deuterium of 2.1 ± 0.4. These results show a moderate contribution of tunneling to the benzylic hydroxylation reaction catalyzed by CvPheH (*67*).

$$^{D}(\%\ \text{Benz OH}) = {}^{D}k_{Benz} + k_1/k_2\ /\ (1 + k_1/k_2) \qquad (2.6)$$

$$\ln(k_H/k_D) = \ln(A_H/A_D) + [E_a(D) - E_a(H)]/RT \qquad (2.7)$$

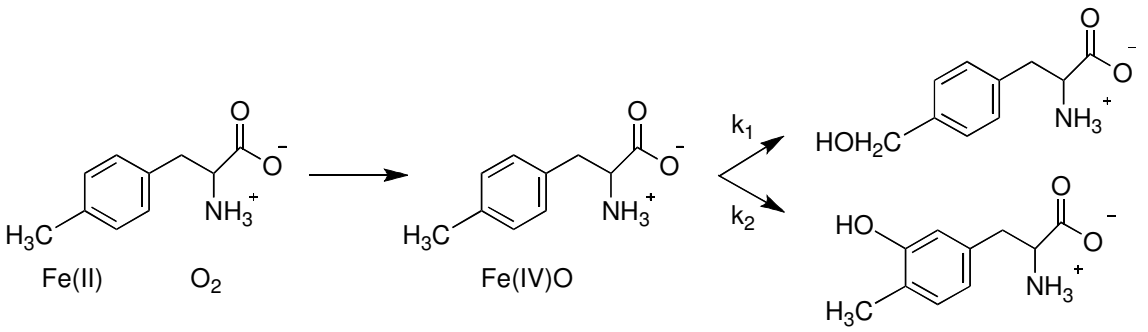

Figure 2.6: Benzylic hydroxylation carried out by phenylalanine hydroxylase.

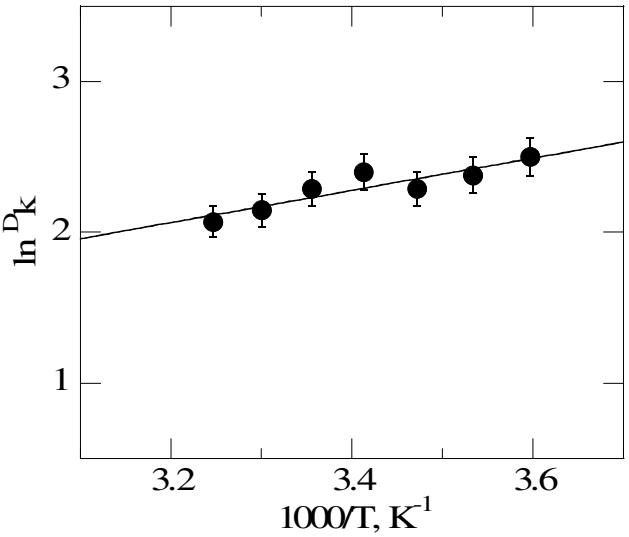

Figure 2.7: Temperature dependence of the isotope effect on the benzylic hydroxylation reaction catalyzed by *C. violaceum* phenylalanine hydroxylase.

Uncoupled $DMPH_4$ oxidase activity of CvPheH. Chen and Frey (*36*) reported that metal-free CvPheH is able to catalyze the phenylalanine-dependent oxidation of $DMPH_4$ at about 5% the rate of the metal containing enzyme. This result was interpreted as support of a model in which the initial interaction of molecular oxygen is with the tetrahydropterin with no need for the iron. To confirm this result we used EDTA to remove all the bound metal from the enzyme. After dialysis to remove the chelating agent, analysis of the metal content of this apo-CvPheH showed that iron was present at less than 1 mol %. In the absence of added iron in the assay, the EDTA-treated CvPheH still exhibited 3.5 % the phenylalanine hydroxylation activity of the metal-containing enzyme, consistent with the results of Chen and Frey (*36*). However, in our hands tyrosine formation and $DMPH_4$ oxidation were completely coupled and increasing amounts of enzyme yielded decreasing k_{cat} values, suggesting that the residual activity was due to a very low concentration of iron in the dialysis buffers or assay. To avoid exposure of the apoenzyme to adventitious iron during dialysis and to remove excess EDTA, the chelator was removed by gel filtration. In addition, we included 10 μM EDTA in the assays to scavenge any free metal. When CvPheH was treated in this fashion, the formation of tyrosine was reduced below the detection limit of 8 nM, and the rate of $DMPH_4$ oxidation was unaffected by the presence of the enzyme (Table 2.5).

Table 2.5: Effect of *C. violaceum* phenylalanine hydroxylase on the rate of $DMPH_4$ oxidation*

CvPheH	Rate (nmol s^{-1})
No CvPheH	0.034 ± 0.002
EDTA-treated CvPheH (0.1 μM)	0.030 ± 0.002
EDTA-treated CvPheH (0.1 μM) + Fe(II) (15 μM)	1.2 ± 0.01

*Conditions: 100 mM HEPES (pH 7.2), 3 mM phenylalanine and 150 μM $DMPH_4$, 10 μM EDTA. The rate was determined from the change in A_{437} with time using an ε_{437} value of 3600 M^{-1} cm^{-1}.

DISCUSSION

Several authors (*47, 68*) have proposed that the eukaryotic amino acid hydroxylases evolved from a common ancient hydroxylase that resembled the bacterial phenylalanine hydroxylase. Consistent with such a model, bacterial and eukaryotic phenylalanine hydroxylases share 35 % sequence identity and similar structures for their catalytic domains (*39, 49, 50, 69*). While this makes the bacterial enzyme an attractive and simpler model for study of the mechanism of aromatic amino acid hydroxylation, structural differences and the different metal binding ability of the bacterial enzyme raise the possibility that there are substantive differences in the reactivities of the bacterial and eukaryotic enzymes. Comparison of the intrinsic isotope effects for the bacterial enzyme with previously reported values for the eukaryotic enzyme provides a test of this hypothesis, in that the intrinsic isotope effects reflect the transition state structures for the individual reactions and thus of the reactivity of the Fe(IV)O intermediate in the different enzymes.

The physiological reaction catalyzed by CvPheH, the hydroxylation of phenylalanine to form tyrosine, exhibits a deuterium kinetic isotope effect greater than one with both 6-MePH4 and DMPH4. The value with DMPH4 is similar to that for the catalytic domain of rat PheH (*30*), while that with 6-MePH4 is somewhat smaller. Neither value is the intrinsic isotope effect for the reaction of the Fe(IV)O intermediate with the aromatic ring of the substrate. Rather, the observed isotope effects are combinations of the isotope effect on this step and the isotope effect on the subsequent tautomerization to form phenylalanine. For the three eukaryotic enzymes, the isotope

effects on the initial hydroxylation are all 0.90 ± 0.03 (*21, 30, 32*). With both rat PheH and rat TyrH, this isotope effect is masked by other slower steps and could only be measured in mutant proteins in which an unproductive side path was introduced. This same strategy was effective with CvPhe, in that the I234D enzyme exhibits a $^{D}k_{cat}$ value identical to the intrinsic isotope effects for the eukaryotic enzymes when the less-coupled DMPH4 is used as substrate. This agreement of the isotope effects and the fact that homologous mutations in CvPheH and rat PheH unmask it are consistent with similar transition states for hydroxylation by both enzymes. The isotope effects for the subsequent tautomerization step are also identical for rat and CvPheH at 5.1, suggesting that this step is also identical in the two enzymes. The much smaller values for the observed isotope effects are consistent with hydroxylation or an isotope-insensitive step being about 9-fold slower than tautomerization. Tautomerization is expected to be much more favorable in the absence of a catalyst than formation of the Fe(IV)O species or the hydroxylation step, raising the possibility that there is no need for the enzyme to actively catalyze this step, so that it occurs after product release. However, with CvPheH there is a 20% preference for loss of the hydrogen initially present at the 3-position of the aromatic ring. In the case of rat PheH there is a slight (34%) preference for loss of the other hydrogen (*30*). These results are most consistent with this step occurring in the active site of both enzymes and with the small differences in the structures seen in the X-ray structures.

The magnitude of the isotope effect on benzylic hydroxylation is a far more sensitive probe of the reactivities of the Fe(IV)O intermediate in the prokaryotic and

eukaryotic enzymes due to its much greater magnitude. The relative amount of benzylic hydroxylation of 4-methylphenylalanine is greater with CvPheH (89%) than with the rat enzyme (55%) (*40*), further establishing that the active sites are very similar but not identical. The isotope effect for benzylic hydroxylation of 10 ± 1 is slightly smaller than the value for the catalytic domain of the rat enzyme, 12 ± 1, but this is probably not significant. Importantly, benzylic hydroxylation by CvPheH also involves moderate tunneling of the substrate hydrogen atom. Of the two parameters derived from the temperature dependence of the isotope effect on this reaction, the effect of deuteration on the activation energy, ΔE_a can be measured with greater confidence that the effect on the Arrhenius prefactor, in that the latter involves extrapolation to infinite temperature. The former value for CvPheH is within error of the value for rat PheH. The interpretation of the temperature dependence of kinetic isotope effects is a matter of intense investigation at present, and no final consensus has been reached. While temperature-dependent isotope effects such as those described here for benzylic hydroxylation by CvPheH can be rationalized using a simple correction to the transition state such that hydrogen tunnels through the barrier at a lower energy than deuterium (*70*), the temperature dependence of the isotope effects for a growing number of enzymes cannot be explained by such a simple model. Instead, more sophisticated models are required in which the temperature dependence reflects the extent of preorganization of the active site and/or the involvement of protein motion in the reaction coordinate (*71, 72*). In these models, the significant temperature dependence of the isotope effect for benzylic hydroxylation would reflect an active site that is not

optimized for the reaction. Such a model is certainly reasonable in that PheH and the other aromatic amino acid hydroxylases have not been designed by evolution for this reaction. More importantly, the similar effects of temperature on the isotope effects for CvPheH and the eukaryotic enzymes indicate similar active site environments for hydroxylation in all.

Chen and Frey (*36*) reported that iron-free CvPheH was able to catalyze the oxidation of DMPH4 without the formation of tyrosine. However, the results on Table 2.5 show that this activity is lost when metal-free CvPheH is used. These two results can be reconciled if the residual tetrahydropterin oxidation activity reported previously was conferred by a metal other than iron. A precedent for this is the H336Q mutant of tyrosine hydroxylase, which in the presence of Co(II) catalyzes the oxidation of tetrahydropterin without hydroxylation of tyrosine (*73*).

The isotope effects reported here for hydroxylation of phenylalanine and 4-methylphenylalanine by CvPheH, the temperature dependence of the latter, and the iron requirement for catalysis of tetrahydropterin oxidation by CvPheH all demonstrate that the reactivity of the hydroxylating intermediate in this bacterial amino acid hydroxylase is indistinguishable from that of the eukaryotic enzyme. Thus, for mechanistic if not regulatory studies, the bacterial enzyme is a valid model for the eukaryotic enzymes.

CHAPTER III

MEASUREMENT OF THE INTRAMOLECULAR ISOTOPE EFFECT ON ALIPHATIC HYDROXYLATION BY *CHROMOBACTERIUM VIOLACEUM* PHENYLALANINE HYDROXYLASE

Phenylalanine hydroxylase (PheH) is a non-heme iron dependent monooxygenase that catalyzes the hydroxylation of the amino acid phenylalanine to yield tyrosine (Figure 3.1) (*4*). PheH is found in organisms ranging from bacteria to humans. In mammals, the enzyme is responsible for catabolism of dietary phenylalanine, and mutations in PheH are linked to the disorder phenylketonuria (*1*). Among the bacterial enzymes, that from *Chromobacterium violaceum* (CvPheH) is the most studied (*36, 37, 74*). PheH is a member of the family of aromatic amino acid hydroxylases, along with tyrosine hydroxylase (TyrH) and tryptophan hydroxylase (*75*). Each of these enzymes catalyzes the hydroxylation of the corresponding aromatic amino acid using molecular oxygen and the electrons from a tetrahydropterin. In addition to aromatic hydroxylation, the aromatic amino acid hydroxylases can catalyze the hydroxylation of benzylic and aliphatic substrates (*18, 58*). Previously, the isotope effect on benzylic hydroxylation was used to compare the reactivity of the eukaryotic enzymes and that of CvPheH (*40, 41, 74*). These studies showed a similar reactivity for all the enzymes and suggested a common hydroxylating intermediate for all the family members.

Crystal structures of the three eukaryotic enzymes and CvPheH reveal a common fold for the catalytic domain (*39, 49, 50*). The active sites are characterized by a ferrous

iron coordinated on one face by two histidines and a glutamate. Three water molecules complete an octahedral geometry. When a tetrahydropterin and an amino acid substrate are present the geometry around the iron changes from six to five coordinate, presumably opening a site for oxygen to directly coordinate the iron (*48, 51, 76*). The proposed hydroxylating intermediate is an Fe(IV)O species; direct evidence for such an intermediate has been obtained for TyrH (*28*) and CvPheH (Chapter IV). Such a reactive intermediate could explain the rich chemistry displayed by these enzymes. Here we report the use of an intramolecular kinetic isotope effect as a probe of the chemical mechanism of aliphatic hydroxylation by CvPheH. The results presented here shed light on the reactivity of the hydroxylating intermediate for the family of aromatic amino acid hydroxylases.

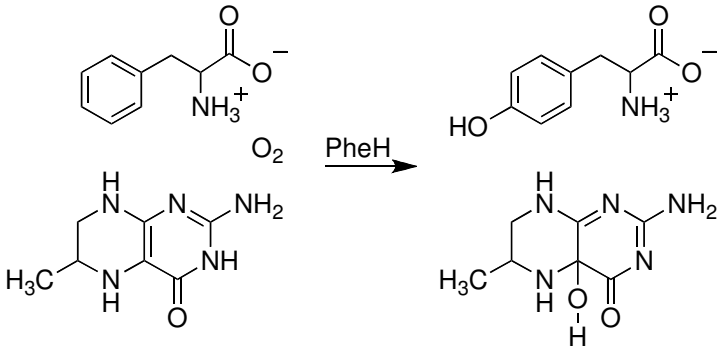

Figure 3.1: Reaction catalyzed by phenylalanine hydroxylase.

EXPERIMENTAL PROCEDURES

Materials. Catalase was from F. Hoffmann-La Roche Ltd (Indianapolis, IN). DEAE-Sephacel was from Amersham Pharmacia Biotech (Uppsala, Sweden). The *E. coli* strain BL21(DE3), used for protein expression, was from Novagen. 6-Methyltetrahydropterin (6-MePH_4), and 6,7-dimethyltetrahydropterin ($DMPH_4$) were from B. Schircks Laboratories (Jona, Switzerland). L-Tyrosine, L-phenylalanine, dihydropteridine reductase, sodium cyanide, boric acid and platinum oxide were from Sigma-Aldrich Chemical Co. (Milwaukee, WI). Napthalene-2,3-dicarboxaldehyde was from Invitrogen. L-[Ring-$^2H_5$]-phenylalanine was from Cambridge Isotope Laboratories (Andover, MA). Dithiothreitol was from Inalc (Milan, Italy).

Cyclohexylalanine was synthesized by reduction of L-phenylalanine with H_2 over 100 mg of platinum oxide (*18*). L-3-[$^2H_{11}$-Cyclohexyl]-alanine was prepared by reducing L-[ring-$^2H_5$]-phenylalanine with D_2 in DCl. L-3-[1,2,3,4,5,6-$^2H_6$-Cyclohexyl]-alanine was synthesized following the same protocol, starting from L-phenylalanine or L-[ring-$^2H_5$]-phenylalanine, using DCl and D_2 or HCl and H_2, respectively. Complete reduction of the starting material was confirmed by HPLC and ^{1}H NMR. The purities of the products were confirmed using HPLC. 4-Hydroxycyclohexylalanine was similarly obtained from the reduction of tyrosine with H_2 (*18*). All other reagents were of the highest purity commercially available.

Enzyme purification and enzymatic assays. CvPheH was expressed and purified as previously described (*74*). The steady-state kinetic parameters for the hydroxylation of cyclohexylalanine and of 3-[$^2H_{11}$-cyclohexyl]-alanine were measured using a coupled assay in which the oxidation of NADH by dihydropteridine reductase was followed (*43*). The assays were performed at 25 °C in a solution containing 50 mM HEPES (pH 7.2), 50 μg/ml catalase, 250 μM NADH, 0.3 units of dihydropteridine reductase, 10 μM ferrous ammonium sulfate, 0.1 - 0.3 μM CvPheH, 150 μM 6-MePH_4 or 250 μM $DMPH_4$, and varying concentrations of cyclohexylalanine or 3-[$^2H_{11}$-cyclohexyl]-alanine.

The hydroxylation of cyclohexylalanine was monitored by HPLC (*41, 59*). The reaction conditions were 500 μM cyclohexylalanine or 3-[$^2H_{11}$-cyclohexyl]-alanine, 10 μM ferrous ammonium sulfate, 1 μM CvPheH and 1 mM 6-MePH_4 or $DMPH_4$. Reactions were carried out for 1 min in 300 μL of 10 mM sodium phosphate buffer (pH 7.0) and then quenched with 100 μL of 100 mM sodium borate (pH 9.0). To this, 50 μL of 50 mM sodium cyanide and 100 μL of 50 mM naphthalene-2,3-dicarboxaldehyde were added. The fluorescent derivatives were separated using a Nova-Pack C 18 column and a gradient of 30-40% acetonitrile in 70-60% 10 mM sodium phosphate with 1% tetrahydrofuran (pH 7.0).

The fluorescent molecules were detected using a Waters 2475 detector, with excitation and emission wavelengths of 420 and 490 nm, respectively. The amount of product was quantified using a standard curve generated using known amounts of the product 4-HO-cyclohexylalanine.

In order to determine the amount of deuterium retained in the hydroxylated cyclohexylalnine after the reaction with CvPheH the samples were isolated by HPLC following the protocol described above. For the determination of the deuterium content of 4-HO-cyclohexylalanine, 1 mM $DMPH_4$ and 500 μM 3-[$^2H_6$-cyclohexyl]-alanine were used. The reactions were carried at 25 °C for 30 min. The peak corresponding to 4-HO-cyclohexylalanine was collected and analyzed by negative ion electrospray time-of-flight mass spectrometry at the Laboratory of Biological Mass Spectrometry at Texas A&M University. The data were corrected for ^{13}C contributions and used in the calculation of the isotope effect.

RESULTS AND DISCUSSION

The hydroxylation of cyclohexylalanine by prokaryotic or eukaryotic PheH yields 4-HO-cyclohexylalanine as the only amino acid product (*18*). With 6-$MePH_4$ the k_{cat} and k_{cat}/K_m values for cyclohexylalanine as substrate for CvPheH are 2.8 ± 0.1 s^{-1} and 45 ± 6 $mM^{-1}s^{-1}$, respectively, and amino acid hydroxylation is fully coupled to tetrahydropterin oxidation (*18*). In order to gain insight into the chemical mechanism of this reaction we measured the deuterium kinetic isotope effect using 3-[$^2H_{11}$-cyclohexyl]-alanine. Isotope effects within error of one were obtained for both k_{cat} and k_{cat}/K_M with either 6$MePH_4$ or $DMPH_4$. (Table 3.1) This result suggests that a step that does not involve hydrogen atom abstraction is rate-limiting with this substrate.

As an alternative approach, the isotope effect on the hydroxylation of cyclohexylalanine was analyzed as an intramolecular isotope effect. Such an approach can avoid the problem of slow, non-chemical steps (*65, 77*). To do so, 3-[1,2,3,4,5,6-$^2H_6$-cyclohexyl]-alanine was used as the substrate, so that the carbon of interest contained one deuterium and one hydrogen. The amount of deuterium in the 4-HO-cyclohexylalanine formed from 3-[1,2,3,4,5,6-$^2H_6$-cyclohexyl]-alanine was then determined by mass spectrometry of the isolated product. The ratio of product with six deuteriums to that with five was 2.5 ± 0.1. When similar experiments were carried out with 3-[2,3,4,5,6-$^2H_5$-cyclohexyl]-alanine obtained by reduction of L-[ring-$^2H_5$]-phenylalanine with H_2 the ratio of products was 3.03 ± 0.1. The average of the two values was used in the calculation of the isotope effect.

Table 3.1: Kinetic isotope effects on k_{cat} and k_{cat}/K_M for *C. violaceum* phenylalanine hydroxylase with 3-[$^2H_{11}$-cyclohexyl]-alanine*

Parameter	6-MePH_4	$DMPH_4$
$^Dk_{cat}$	1.03 ± 0.1	0.99 ± 0.1
$^Dk_{cat}/K_M$	1.35 ± 0.5	1.24 ± 0.5

*The solution contained 50 mM HEPES (pH 7.2), 50 μg/ml catalase, 250 μM NADH, 0.3 Units of DHPR, 10 μM ferrous ammonium sulfate, 0.1-0.3 μM CvPheH.

The isotope effect for CH bond cleavage can be obtained from the partitioning between H and D abstraction if one makes two reasonable assumptions: 1) CH bond cleavage is irreversible, and 2) the cyclohexyl ring cannot flip in the active site more rapidly than CO bond formation occurs. The first assumption is reasonable for a hydroxylation reaction. The second is supported by the structure of human PheH with bound amino acid (*48*) and by the stoichiometric coupling of tetrahydropterin oxidation to amino acid hydroxylation with cyclohexylalanine as a substrate for CvPheH. The position of the hydroxyl group in the product is the result of the partitioning between hydroxylation of C4 at the axial position and hydroxylation at the equatorial position (Figure 3.2). The ratio of the two products (P_a/P_e) is then described by equation 3.1. The monodeuterated substrate can be bound with deuterium in the axial or the equatorial position. If deuterium is in the axial position, the rate constant for cleavage of the axial CH bond, k_a, will be subject to the primary kinetic isotope effect ^{D}k and the rate constant for cleavage of the equatorial CH bond, k_e, will be subject to the secondary isotope effect $^{\alpha D}k$. In this case the ratio of the product that has lost deuterium, P_H, to that which retains deuterium, P_D, is given by equation 3.2. If deuterium is in the equatorial position the isotope effects are on the opposite steps (Figure 3.2), and the ratio of products is given by equation 3.3. No preference is anticipated for binding the substrate with deuterium in the equatorial versus the axial position. Thus, the isotopic content of the product will be the average of the contents from the two binding orientations (Equation 3.4).

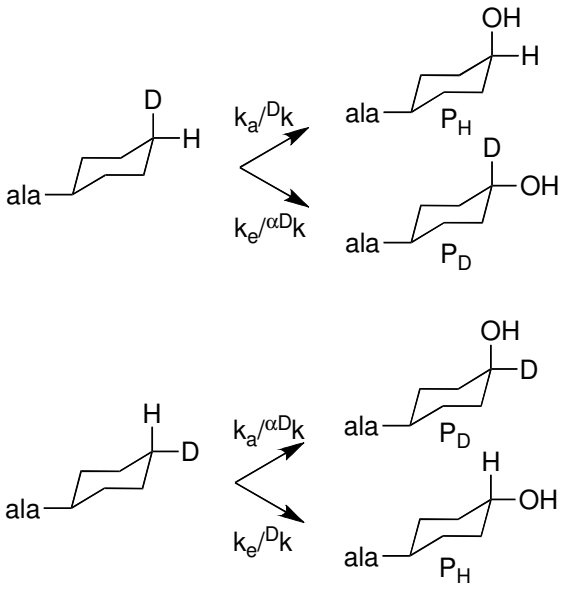

Figure 3.2: Possible outcomes of the hydroxylation of cyclohexylalanine by phenylalanine hydroxylase.

Previously Carr et al. (*18*) reported that 90% of the hydroxylation occurred at the axial position with cyclohexylalanine, so that $k_a/k_e = 9$. Combining this value with the value of 0.37 ± 0.02 for P_H/P_D reported here yields a value for ${}^{D}k/{}^{\alpha D}k$ of 12.3 ± 1. If an upper limit of 1.2 is used for the secondary isotope effect (*40*), ${}^{D}k$ has an upper limit of 14.7 ± 1.2.

$$P_a/P_e = k_a/k_e \quad (3.1)$$

$$P_H/P_D = (k_a/k_e)({}^{\alpha D}k/{}^{D}k) \quad (3.2)$$

$$P_H/P_D = (k_e/k_a)({}^{\alpha D}k/{}^{D}k) \quad (3.3)$$

$$P_H/P_D = 0.5({}^{\alpha D}k/{}^{D}k)[(k_a/k_e) + (k_e/k_a)] \quad (3.4)$$

The isotope effect on hydroxylation of cyclohexylalanine by CvPheH is slightly larger than that on benzylic hydroxylation by the enzyme of 10 ± 1 (*74*). Given its magnitude, the intermolecular isotope effect of 12.3-14.7 is likely to be the intrinsic one. This value is comparable to those reported for aliphatic hydroxylation by cytochrome P450 (*78-80*), but smaller than values obtained from rapid reaction studies of the α-ketoglutarate-dependent non-heme enzymes TauD (${}^{D}k = 16$) (*26*) and prolyl-4-hydroxylase (${}^{D}k = 60$) (*81*), which utilize a Fe(IV)O center similar to that in PheH (*27*). The magnitude of the value with CvPheH is consistent with a mechanism involving hydrogen atom abstraction by the Fe(IV)O center followed by rebound of the hydroxyl radical, a mechanism also suggested for the other enzymes (Figure 3.3) (*26, 27, 81*). The large isotope effect also suggests the involvement of tunneling in this reaction, although not as much as occurs when TauD or prolyl-4-hydroxylase react with their normal substrates. Evidence of tunneling was also observed for the hydroxylation of benzylic

carbons by all the aromatic amino acid hydroxylases (*40, 41, 74*). The lack of an isotope effect on the k_{cat} value with 3-[$^{2}H_{11}$-cyclohexyl]-alanine establishes that hydrogen atom abstraction is much faster than other steps in turnover, even though this enzyme is not evolved to carry out this reaction.

The results presented here are consistent with the involvement of a highly reactive Fe(IV)O as the hydrogen atom abstracting species for the aliphatic hydroxylation carried out by CvPheH. The magnitude of the isotope effect on aliphatic hydroxylation reported here is comparable to that found for benzylic hydroxylation by CvPheH and all the eukaryotic enzymes (*40, 41, 74*). Thus, for both reactions a similar mechanism of hydrogen atom abstraction followed by radical rebound can be proposed . Based on the similar iron centers shared by all the members of the family, these results suggest that an Fe(IV)O species is the general hydroxylating intermediate for the family of aromatic amino acid hydroxylases. Further spectroscopic investigations using CvPheH and the aliphatic substrate cyclohexylalanine could help better characterize the hydroxylating intermediate utilized by this family of enzymes.

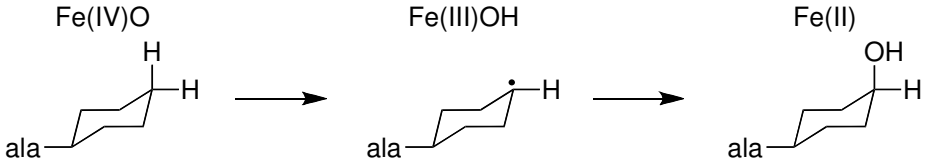

Figure 3.3: Proposed chemical mechanism of aliphatic hydroxylation by phenylalanine hydroxylase.

CHAPTER IV

SPECTROSCOPIC EVIDENCE FOR A HIGH SPIN Fe(IV)O SPECIES IN THE CATALYTIC CYCLE OF *CHROMOBACTERIUM VIOLACEUM* PHENYLALANINE HYDROXYLASE

Phenylalanine hydroxylase (PheH) is a non-heme iron-dependent monooxygenase that catalyzes the hydroxylation of the aromatic amino acid phenylalanine to yield tyrosine. PheH belongs to the family of aromatic amino acid hydroxylases, along with tyrosine hydroxylase (TyrH) and tryptophan hydroxylase. PheH is found in organisms ranging from eukaryotes to prokaryotes. In mammals PheH is present in the liver where it catalyzes the first and rate-limiting step in the metabolism of the phenylalanine acquired in the diet (*82*). TyrH and tryptophan hydroxylase catalyze the hydroxylation of the corresponding amino acids and they play key roles in the metabolism and synthesis of neurotransmitters (*5, 6, 82*). Mutations that hamper the function of PheH have been linked to the disease phenylketonuria (*83*). Individuals suffering from this disease have elevated levels of L-Phe in the blood and suffer from mental retardation (*1*). The reaction catalyzed by PheH is depicted in Figure 4.1. Once the three substrates are present in the ferrous active site, the electrons from tetrahydrobiopterin are used to activate molecular oxygen to react with the aromatic side chain of the substrate (*7, 8*). As the result of the reaction, one oxygen atom from molecular oxygen is incorporated into the aromatic ring of the amino acid and the other into the 4a-position of the biopterin.

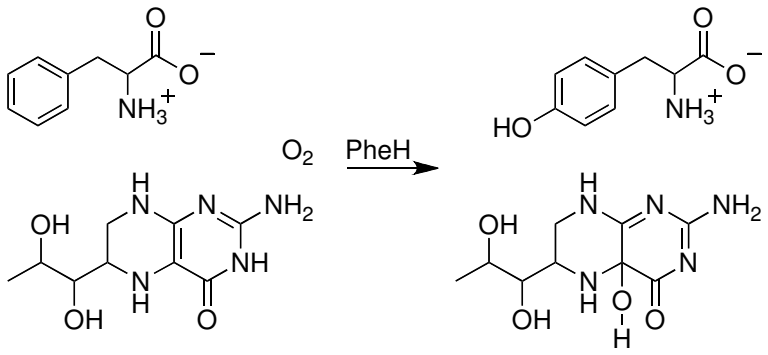

Figure 4.1: Hydroxylation of phenylalanine by phenylalanine hydroxylase.

The crystal structures of the catalytic domains of the eukaryotic and prokaryotic aromatic amino acid hydroxylases reveal a common fold around the active site (*39, 49, 50*). In the case of the human PheH, the crystal structures of the resting enzyme and that of the binary complex with a tetrahydropterin show the iron atom coordinated in an octahedral fashion by two histidine residues, a glutamate, and three water molecules. In the crystal structure of the ternary complex of PheH with 3-(2-thienyl)-L-alanine and tetrahydrobiopterin, the iron atom is coordinated by two histidine residues, a bidentate glutamate, and a water molecule. Thus, binding of the three substrates would open a site for oxygen to directly coordinate to the iron. This model is supported by spectroscopic evidence for PheH and tyrosine hydroxylase (*51, 76*). X-Ray absorption spectroscopy shows that only when both tetrahydropterin and amino acid substrate are present does the coordination around the iron change from six-coordinate to five-coordinate. The change in iron coordination is a prerequisite for catalysis since it modulates the reactivity of the iron center towards oxygen. The reaction of oxygen and tetrahydropterin is accelerated by two orders of magnitude in the five-coordinated enzyme.

A chemical mechanism for aromatic amino acid hydroxylation that is consistent with all the evidence gathered for all the hydroxylases is shown in Figure 4.2 (*23*). Initially, the three substrates are recruited to the six-coordinate ferrous iron active site. A change in the iron coordination from six to five-coordinate opens a site for oxygen to coordinate the iron and form a peroxo bridge between the tetrahydropterin and the ferrous iron. The hydroxylating species, an Fe(IV)O, and the first product, 4a-hydroxypterin, are produced after the heterolytic cleavage of the oxygen-oxygen bond.

Direct spectroscopic evidence for the existence of a kinetically competent Fe(IV)O species was reported by Eser et al. (*28*) for the reaction of TyrH with its natural substrate. Once formed the Fe(IV)O reacts with the aromatic side chain of the amino acid, generating a carbocation that undergoes a 1,2 hydride transfer to form a dienone (*31*). Tautomerization of the dienone gives the final product, tyrosine.

The iron center in the aromatic amino acid hydroxylases is capable of accepting a wide range of amino acids as substrates (*4*). Besides the aromatic hydroxylation of ring-substituted substrates, the aromatic hydroxylases can perform benzylic, and aliphatic hydroxylation (*18, 58*). The isotope effect on benzylic hydroxylation has been used to compare the reactivity of the eukaryotic enzymes (*40*) and that of CvPheH (Chapter II). These studies showed a similar reactivity for all the enzymes and suggested a common hydroxylating intermediate for all the family members. The large isotope effect of about 13 calculated for benzylic hydroxylation for all the enzymes was interpreted as evidence for a chemical mechanism involving hydrogen atom abstraction by the Fe(IV)O followed by recombination of the hydroxyl and benzylic radicals. Recently, an intramolecular isotope effect of similar magnitude has been determined for the hydroxylation of the aliphatic cyclohexylalanine by CvPheH (Chapter III). These results are consistent with the involvement of a highly reactive Fe(IV)O species capable of hydrogen atom abstraction from the relatively less activated carbon atoms of the benzylic and aliphatic substrates.

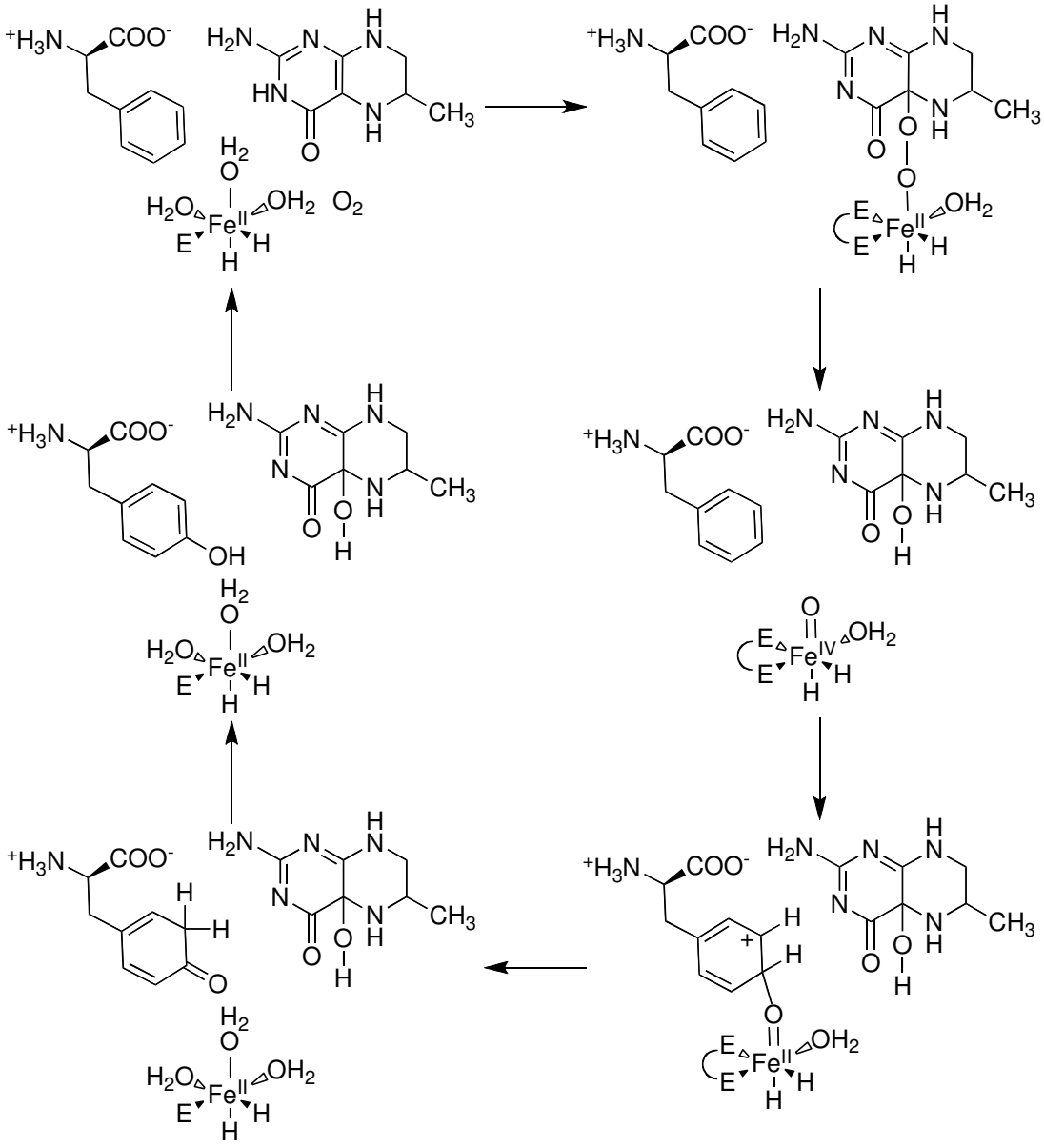

Figure 4.2: Chemical mechanism of aromatic amino acid hydroxylation.

The only direct spectroscopic evidence for the existence of an Fe(IV)O species in the catalytic cycle of any of the aromatic amino acid hydroxylases comes from freeze quench Mössbauer spectroscopy of TyrH (*28*). When a complex of TyrH, tyrosine, and 6-$MePH_4$ is exposed to oxygen, an iron intermediate with characteristics similar to those observed for high-spin Fe(IV) intermediates in other mononuclear non-heme enzymes (*27, 28, 81*) is seen at 20 ms . Cryoreduction of the 20 ms sample gives rise to an EPR signal consistent with a high-spin Fe(III) complex, as expected for one-electron reduction of a high-spin Fe(IV). A similar strategy was used to characterize the iron intermediate in the α-ketoglutarate dependent taurine dioxygenase (TauD) (*27*). Both TyrH and TauD share an iron center in which the iron is coordinated by two histidine residues and a carboxylate, and the spectroscopic evidence suggests that both use similar Fe(IV)O hydroxylating intermediates.

Here we report the use of Mössbauer spectroscopy to monitor the early stages of the catalytic cycle of CvPheH. The results provide direct spectroscopic evidence for the formation of an Fe(IV) species during the hydroxylation of phenylalanine by CvPheH. Rapid chemical quench experiments were also used to establish the kinetic competency of the Fe(IV) intermediate as the hydroxylating species.

EXPERIMENTAL PROCEDURES

Materials. The *E. coli* strain BL21(DE3), used for protein expression, was from Novagen. 6-Methyltetrahydropterin (6-$MePH_4$) was from B. Schircks Laboratories (Jona, Switzerland). L-Phenylalanine, Hepes, and ferrous ammonium sulftate were from Sigma-Aldrich Chemical Co. (Milwaukee, WI). Dithiothreitol was from Inalc (Milan, Italy). L-Cyclohexylalanine and L-3-[$^2H_{11}$-Cyclohexyl]-alanine were prepared as described in chapter III. All other reagents were of the highest purity commercially available.

Enzyme expression and purification. CvPheH was expressed in *E. coli* and purified as previously described (*74*). The enzyme was made apo by incubating with 5 mM EDTA and 5 mM NTA on ice for 2 hours followed by dialysis against 50 mM Hepes (pH 7.2) containing 50 mM NaCl.

Rapid chemical quench analyses. A solution of 100 mM Hepes buffer (pH 7.2) containing 1.6 mM apo-CvPheH, 50 mM NaCl, and 5 mM phenylalanine was made anaerobic in a tonometer through 20 argon-vacuum cycles over a period of 1 hour. Ferrous ammonium sulfate (1.5 mM) was added to the tonometer under argon. An aliquot from a stock solution of 6-$MePH_4$ sufficient for a final concentration of 5 mM after mixing was placed in one arm of the tonometer. Additional argon-vacuum cycles were performed before mixing the 6-$MePH_4$ with the CvPheH:Fe(II):Phe complex in the main body of the tonometer. A solution of 1.9 mM O_2 was generated by bubbling oxygen into a cold solution of 100 mM Hepes (pH 7.2) and 50 mM NaCl. Both oxygenated buffer and anaerobic enzyme solutions were loaded onto a SFM-400/Q

rapid-mixing instrument from Bio-Logic (Claix, France). The specifications in the manufacturer's manual were followed to achieve reactions of the desired time. The reactions were performed at 5 °C and quenched with 5 M HCl. The collected samples were chilled on ice until further analysis.

The precipitated protein was removed by centrifugation for 5 min at 13,700g. An aliquot of the sample was diluted in water and injected onto a Waters HPLC equipped with a Model 2475 fluorescence detector. Phenylalanine and tyrosine were separated using a Phenomenex C18 column using 10 mM sodium phosphate with 1% THF (pH 7.0) as the mobile phase. The intrinsic fluorescence of the amino acids was used for their detection with an excitation wavelength of 270 nm and an emission wavelength of 310 nm. The amount of tyrosine in each reaction was determined by comparing the area under the curve to that of a tyrosine standard curve. Oxygen contamination during the sample preparation was taken into account by analyzing the tyrosine present in reactions made by mixing the CvPheH:Fe(II):Phe:6-MePH_4 complex with anaerobic buffer. The amount of tyrosine found in the anaerobic control was subtracted from the amounts in samples generated using oxygenated buffer.

Rapid freeze quench Mössbauer spectroscopy. Mössbauer experiments were performed in the laboratories of Drs. J. Martin Bollinger and Carsten Krebs at the Pennsylvania State University. A solution of 100 mM Hepes buffer (pH 7.2) containing 1.6 mM apo-CvPheH, 50 mM NaCl, and 5 mM phenylalanine was made anaerobic in a round bottom flask through 30 argon-vacuum cycles over a period of 1 h. This solution was placed in an MBraun anoxic chamber with a nitrogen atmosphere (Peabody, MA)

where it was made 5 mM in 6-$MePH_4$ by the addition of an aliquot from a stock solution prepared by dissolving the solid compound in anaerobic 100 mM Hepes buffer (pH 7.2) and 50 mM NaCl. A 50 mM stock solution of $^{57}Fe(II)$ was made by dissolving $^{57}Fe(0)$ in anaerobic 1M H_2SO_4. In order to avoid precipitating the enzyme, the stock solution of $^{57}Fe(II)$ was mixed with 0.5 volume equivalents of anaerobic 1 M Tris·HCl (pH 7.6) before its addition to the CvPheH:Phe:6-$MePH_4$ complex at a final concentration of 1.5 mM. A 0 ms time point sample was prepared by taking an aliquot of the CvPheH:$^{57}Fe(II)$:Phe:6-$MePH_4$ complex and transferring it to a Mössbauer cell. The cell was sealed in a plastic vial, removed from the glovebox, frozen in liquid nitrogen, removed from the vial, and stored in liquid nitrogen.

The procedure for the preparation of freeze-quench Mössbauer samples has been described before (*80*). The CvPheH:$^{57}Fe(II)$:Phe:6-$MePH_4$ complex was transferred to a rapid-quench syringe in the glovebox. The syringe was removed from the glovebox and attached to the rapid quench instrument. A second syringe filled with oxygen saturated buffer (1.9 mM O_2) was also attached to the instrument. These two solutions were mixed in a 1:1 ratio at 5 °C and allowed to flow through an aging line before quenching by direct injection into 2-methylbutane at -150 °C. The total reaction time was calculated by adding 10 ms to the time of transit through the aging line (*84*).

Mössbauer spectra were recorded on spectrometers from WEB Research (Edina, MN) operating in the constant acceleration mode in a transmission geometry. The samples were kept at 4.2 K during the acquisition of the spectra. The samples were

inside 12VST dewars (Janis) equipped with a superconducting magnet that allowed the application of magnetic fields ranging from 0 to 8 T parallel to the γ-beam.

Stopped-Flow spectrophotometry. Stopped-flow experiments were performed in the laboratories of Drs. J. Martin Bollinger and Carsten Krebs at the Pennsylvania State University. The reactions were carried out at 5 °C in an Applied Photophysics (Surrey, U.K.) SX.18MV machine equipped with a photo diode array detector and mounted in the MBraun anoxic chamber. The anaerobic reactant complex of CvPheH was made as described above for the Mössbauer spectroscopy using 400 μM apo-CvPheH, 1 mM phenylalanine, 1.5 mM 6-MePH_4 and 360 μM Fe(II). The enzyme complex solution was loaded into one of the syringes of the stopped-flow instrument. The second syringe was loaded with 100 mM Hepes buffer containing 50 mM NaCl and 1.9 mM O_2.

Data analyses. The kinetics of tyrosine formation under pre-steady state conditions was analyzed by fitting the data to Equation 4.1 using the program KaleidaGraph (Synergy Software, Reading, PA). In Equation 4.1 $(Tyr/CvPheH)_0$ is the amplitude of the burst, k_{burst} is the rate constant for the burst phase, and k_{linear} is the rate constant for the linear phase. Global analyses of the kinetic data were performed using the program KinTek Explorer Pro (KinTek Corp., Austin, TX) (*85*). Error analysis was conducted using the FitSpace Explorer (*86*) option of KinTek Explorer using a value of 1.2 for the sum square error (SSE). All the Mössbauer data analysis was carried out by Dr. Carsten Krebs using the program WMOSS (WEB Research). The details of the analysis have been described previously for the iron center of TauD (*27*).

$$(Tyr/CvPheH)_t = (Tyr/CvPheH)_0 (1-e^{(-k_{burst}t)}) + k_{linear}\, t \qquad (4.1)$$

RESULTS

Rapid chemical quench studies with phenylalanine. Mössbauer spectroscopy studies require high concentrations of enzyme in order to generate detectable transient metal intermediates. In the past, attempts to perform such studies using eukaryotic PheH were hampered by the inactivation of the enzyme, presumably by aggregation at the millimolar concentrations used (Pavon and Fitzpatrick, personal communication). The bacterial CvPheH showed no signs of aggregation at concentrations up to 1 mM as judged by light scattering and gel filtration chromatography. We performed chemical quench experiments using conditions similar to those necessary for rapid freeze quench Mössbauer spectroscopy. When a complex of CvPheH:Fe(II):Phe:6-MePH_4 was mixed in a 1:1 ratio with O_2 (1.9 mM) containing buffer, tyrosine was produced up to almost 700 μM (Figure 4.3) This result shows that CvPheH is active under conditions similar to those required for Mössbauer experiments. Similar experiments performed using 200 μM CvPheH showed multiple turnovers and evidence of burst kinetics (Figure 4.4). Fitting of the data to Equation 4.1 gives a rate constant for the formation of tyrosine during the first turnover (k_{burst}) of 7.0 ± 2 and a rate for the subsequent turnovers (k_{linear}) of 3 ± 0.5. This result is consistent with hydroxylation being faster than the release of the products from the active site.

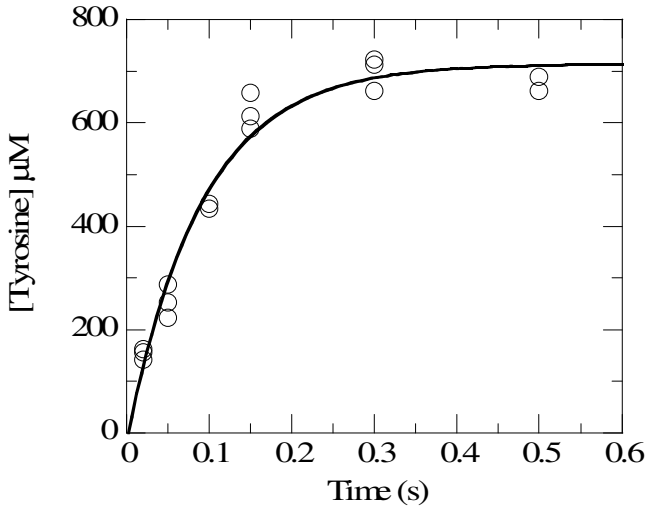

Figure 4.3: Time course at 5 °C for the formation of tyrosine from the reaction of CvPheH (1.6 mM):Fe(II) (1.5 mM):6-MePH_4 (5 mM):Phe (5 mM): with an equal volume of O_2 saturated buffer (1.9 mM). The line was calculated from the mechanism in Figure 4.7 using the rate constants listed in Table 4.1.

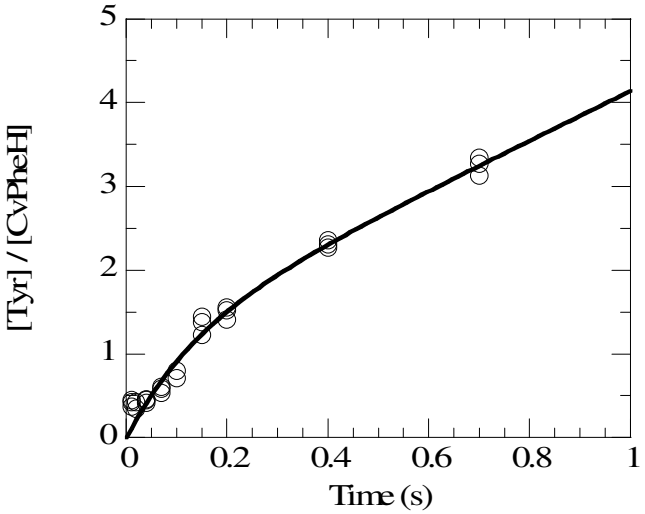

Figure 4.4: Time course at 5 °C for the formation of tyrosine from the reaction of CvPheH (200 μM):Fe(II) (500 μM):6-$MePH_4$ (5 mM):Phe (5 mM): with an equal volume of O_2 saturated buffer (1.9 mM). The line was calculated from the mechanism in Figure 4.7 using the rate constants listed in Table 4.1.

Rapid chemical quench studies with cyclohexylalanine. Phenylalanine hydroxylase hydroxylates cyclohexylalanine producing only 4-HO-cyclohexylalanine (*18*). We performed rapid chemical quench experiments with CvPheH and cyclohexylalanine. However, we found that the amount of 4-HO-cyclohexylalanine produced did not increase consistently with increasing reaction times. Instead, the amount of product fluctuated randomly in the samples. Presumably, the high concentration of HCl used to quench the enzyme dehydrates the alcohol product. We tried using THF and methanol as quenchers but they failed to stop the reaction fast enough.

Rapid freeze quench Mössbauer spectroscopy. The anaerobic complex of CvPheH:^{57}Fe(II):Phe:6-MePH_4 was reacted with O_2 enriched buffer and quenched by rapid-freeze. Mössbauer spectra for the reactions at 0, 20 and 100 ms are shown in Figure 4.4. The spectrum of the anaerobic complex shows a broad quadrupole doublet with parameters typical of a high-spin Fe(II) (*27*). The asymmetry of the doublet suggests the presence of at least two different Fe(II) complexes that possibly arise from the conversion of a six-coordinate Fe(II) to a five-coordinate square-pyramidal Fe(II) site.

The Mössbauer spectra of samples in which the reactant complex was exposed to oxygen for 20 and 100 ms exhibit a prominent peak at 0.9 mm/s in addition to the contribution from the high-spin Fe(II) (Figure 4.5). This peak is not seen in the spectrum of a sample reacted for 400 ms (not shown) as expected for a reaction intermediate. The signal centered at 0.9 mm/s is associated with an iron intermediate that exhibits a quadrupole doublet. The low energy line of this quadrupole overlaps with the low energy line of the Fe(II) site in the reactant complex. The spectra of the 20 and 100 ms samples can be analyzed as superpositions of the contributions from high-spin Fe(II) and the newly formed iron intermediate (*27*). Deconvolution of the spectra reveals that the new iron species contributes 17 % of the absorption at 20 ms and 14 % at 100 ms.

The possibility of increasing the life time of the iron intermediate was addressed using cyclohexylalanine and L-3-[$^{2}H_{11}$-cyclohexyl]-alanine as substrates in a similar experiment. Unfortunately no signal for an Fe(IV) species was detected using either of these two substrates.

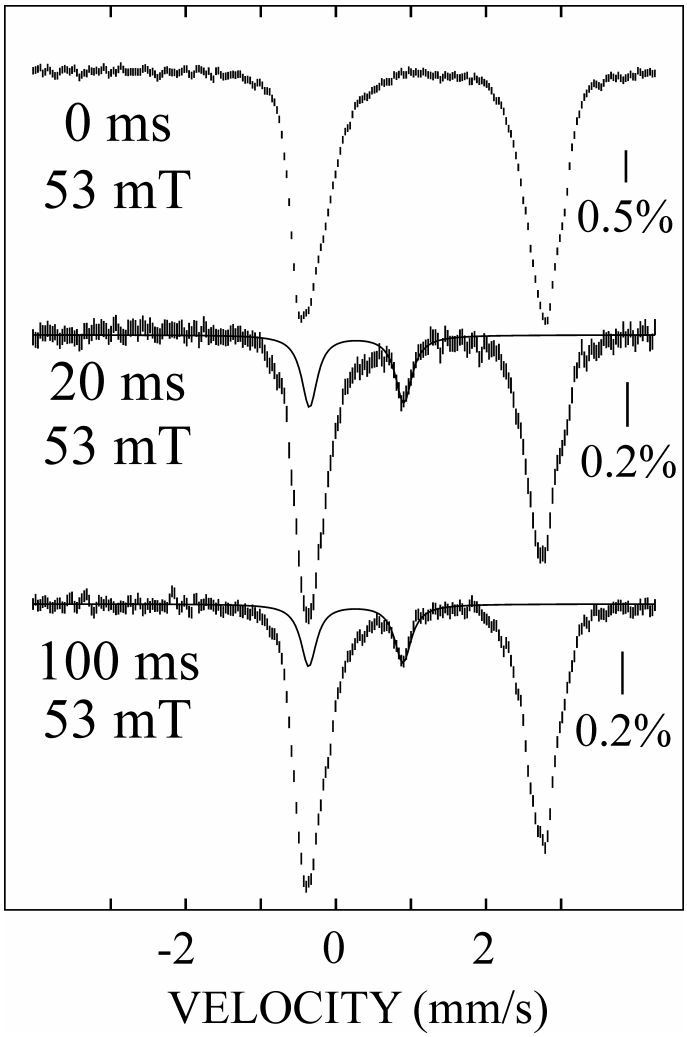

Figure 4.5: Mössbauer spectra at 4.2-K of the reactions at 5 °C of the CvPheH:^{57}Fe(II):Phe:6-MePH_4 complex. (1.6 mM CvPheH, 1.5 mM Fe(II), 5 mM 6-MePH_4, 5 mM Phe in 100 mM Hepes (pH 7.2), 50 mM NaCl with 1.9 mM oxygen-containing buffer). The reaction times and magnetic field strengths are indicated. The hashed marks are the Mössbauer spectra. The solid lines are quadrupole doublet simulations of the spectra of the Fe(IV) intermediate.

Stopped-Flow spectrophotometry. As an additional approach, we used stopped-flow absorbance spectroscopy to monitor the pterin during the hydroxylation of phenylalanine by CvPheH. Figure 4.6 shows the resulting absorbance traces at 246 nm. The absorbance at 246 nm reports mainly on the formation of the 4a-hydroxypterin product (*21*).

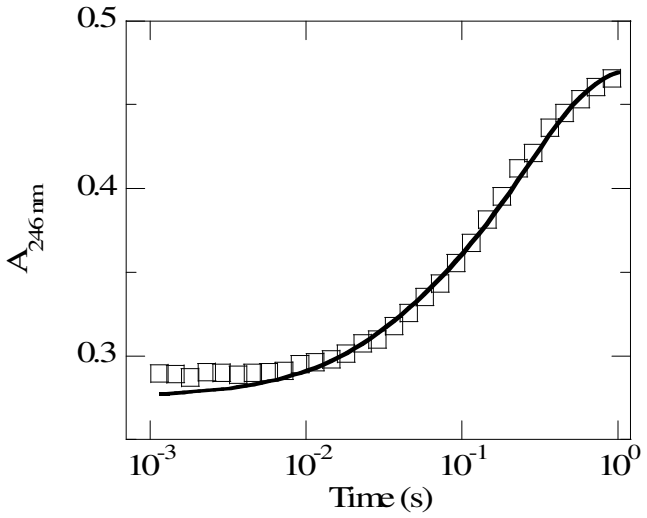

Figure 4.6: Stopped-flow absorbance traces at 246 nm for the reaction of *C. violaceum* phenylalanine hydroxylase with phenylalanine. The line was calculated from the mechanism in Figure 4.7 using the rate constants listed in Table 4.1.

DISCUSSION

The ability of PheH to perform aromatic, benzylic, and aliphatic hydroxylation reactions can be explained by the capability of the iron center to form a highly reactive Fe(IV)O species. The Mössbauer spectrum of the reaction of CvPheH with phenylalanine at 20 ms showed the maximal accumulation of an iron intermediate with an isomer shift (δ) and quadrupole splitting (ΔE_Q) of 0.277 mm/s and 1.255 mm/s respectively. These parameters are similar to those reported for the Fe(IV) intermediate observed in TauD (*27*) and TyrH (*28*). Both the aromatic amino acid hydroxylases and the α-ketoglutarate dependent enzyme utilize a non-heme Fe(II) center in which the catalytic iron is coordinated facially by two histidines and a carboxylate. The finding of an iron intermediate in PheH that is best described as Fe(IV) adds to the growing evidence suggesting that the 2-his 1-carboxylate motif serves as a platform for the formation of reactive Fe(IV)O species.

The different kinetic experiments described herein report on the concentration dependence of the chemical species formed during the reaction of CvPheH with time. Analysis of the individual experiments can provide rate constants for the life-time of intermediates and the formation of the products. However, a more powerful approach is to perform a global fitting of the different kinetic experiments to a single kinetic mechanism. The robustness of this strategy is that the values for the kinetic constants are based on more than one experimental approach. A logical starting point to finding a kinetic mechanism that can accommodate the experimental data is to divide the mechanism into steps that account for the formation of the chemical species that are

monitored in each of the different experiments. The hydroxylation of phenylalanine by CvPheH can be described with the minimal mechanism shown in Figure 4.7. Here, we excluded an initial oxygen binding step since all the experiments were done at a single saturating concentration of oxygen. Instead, the first step is the reaction of the ternary complex of CvPheH:Phe:6MePH$_4$ with O_2 to form the Fe(IV) and the first enzyme bound product 4a-HO-6MePH$_3$ with rate constant k_1. The rate constant k_2 is for the hydroxylation of phenylalanine, and k_3 is the rate constant for the release of the products from the active site. The last rate constant was included based on the burst kinetics observed in the chemical quench experiment shown in Figure 4.4.

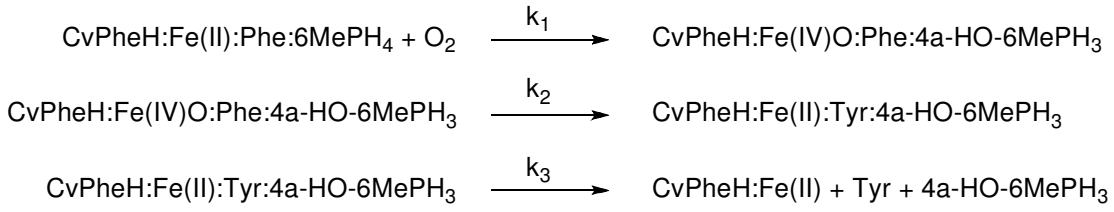

Figure 4.7: Minimal mechanism for the hydroxylation of phenylalanine by PheH.

The data from the rapid chemical and freeze quench experiments were used to perform a global fitting of the different kinetic experiments to the mechanism shown in Figure 4.7. The values for the rate constants and their confidence intervals as determined using the FitSpace option of the KinTek software are listed in Table 4.1.

Table 4.1: Values of the rate constants and their confidence intervals obtained from global fitting of the rapid chemical quench and Mössbauer data for the reaction of *C. violaceum* phenylalanine hydroxylase to the mechanism shown in Figure 4.7.

Rate constant	Best-fit value	Lower bound	Upper bound
k_1	30 ± 2 mM^{-1} s^{-1}	28 mM^{-1} s^{-1}	32 mM^{-1} s^{-1}
k_2	36 ± 4 s^{-1}	31 s^{-1}	42 s^{-1}
k_3	5.5 ± 0.3 s^{-1}	5.3 s^{-1}	5.8 s^{-1}

The rate constant k_1 corresponds to the formation of the Fe(IV) intermediate. Even though the Mössbauer data is a direct measure of the Fe(IV)O species, the data in the first 30 ms do not allow a reliable estimation of k_1. Nevertheless, the data places critical constraints on the rate constants for its formation and decay. The constant k_2 corresponds to the hydroxylation of the amino acid and the decay of the Fe(IV)O. The value of k_2 is more reliable since it is based on both the rapid freeze quench and the chemical quench data. Both k_1 and k_2 agree well with the experimental data. To illustrate the agreement, the rate constants in Table 4.1 were used to generate the lines in Figures 4.3 and 4.8.

The burst kinetics observed in the chemical quench experiment shown in Figure 4.4 predicts that a physical step rather than a chemical step is the slowest step in the reaction pathway. The rate constant k_3 in the mechanism in Figure 4.7 accounts for the release of the products from the active site. The magnitude of k_3 obtained in the global fitting lies within error of the value for k_{linear} obtained by fitting the chemical quench data shown in Figure 4.4 to Equation 4.1 and the steady-state k_{cat} at this temperature (6.0 ± 1). The rate constants in Table 4.1 can be used to simulate the kinetics of tyrosine formation observed during the first few turnovers of the CvPheH reaction (Figure 4.4). Altogether, these results suggest that the step that determines the k_{cat} value for CvPheH is the release of the products from the active site.

The chemical mechanism for the hydroxylation of phenylalanine is shown in Figure 4.2. This mechanism predicts the concomitant decay of the Fe(IV) and the formation of tyrosine. Comparison of the amount of Fe(IV) observed in the freeze

quench experiments to that of the tyrosine made in a similar chemical quench experiment shows the expected correlation for the decay of the Fe(IV) intermediate and the formation of tyrosine as expected for the hydroxylating species (Figure 4.8).

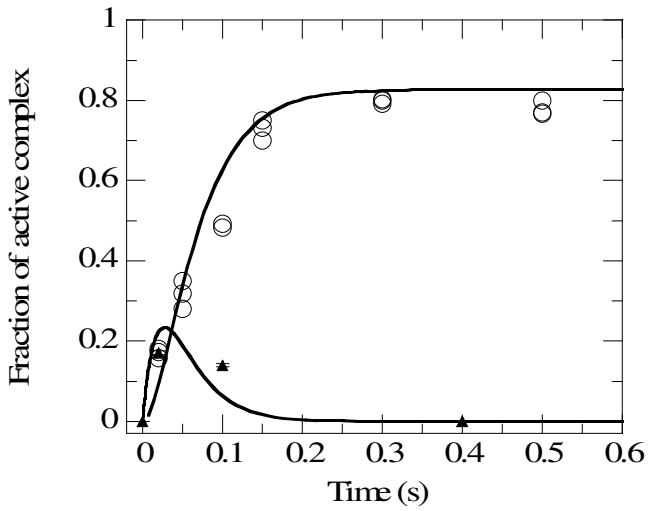

Figure 4.8: Comparison of the time courses for tyrosine formation (circles) and for formation and decay of the Fe(IV) (triangles). The lines were calculated from the mechanism of Figure 4.7 with the rate constants in Table 4.1.

During the turnover of CvPheH, $6MePH_4$ undergoes several transformations (Figure 4.2). The different reduced and oxidized forms of pterin have distinct absorbance spectra at 200-450 nm (*21*). Specifically, formation of the first product, 4a-HO-$6MePH_3$, is characterized by an increase in the absorbance at 246 nm. We included the stopped-flow absorbance data at 246 nm in the global analysis of the kinetic mechanism of Figure 4.7. The first step in the mechanism corresponds to an increase in absorbance at 246 nm as expected for the formation of 4a-HO-$6MePH_3$ in that step. The rate constants reported in Table 4.1 were used to generate the line in Figure 4.6. The agreement between the simulations and the experimental data points shows that the proposed kinetic mechanism can account for the concomitant formation of the Fe(IV) and the first enzyme bound product 4a-HO-$6MePH_3$, as predicted by the chemical mechanism shown in Figure 4.2.

The demonstration that the minimal mechanism in Figure 4.7 can account for the kinetics of the Fe(IV) intermediate and the formation of the products tyrosine and 4a-HO-$6MePH_3$ determined in different experiments indicates that it reflects important features of the CvPheH reaction. Nevertheless, it also contains untested assumptions and simplifications. First, it presumes the bimolecular nature of the first step, but this kinetic characteristic has not been tested by variation of reactant concentrations. Second, it considers the three steps to be irreversible. The latter assumption is based on the chemical nature of the transformations that take place in each step. Clearly, breakdown of the O-O bond, the decay of the Fe(IV) species, and the release of the products from the active site are all expected to be irreversible.

The other aromatic amino acid hydroxylase for which an Fe(IV) intermediate has been detected is TyrH (*28*). In the case of TyrH the hydroxylation of tyrosine was better described with a four-step mechanism (*29*) instead of the three steps used in this report to describe the reaction of CvPheH. The difference in the mechanisms is a reversible oxygen binding step for TyrH. In the mechanism in Figure 4.7, the second order rate constant k_1 groups the rate constants for O_2 binding and formation of the Fe(IV) intermediate. The magnitude of k_1 (30 $mM^{-1}s^{-1}$) is comparable to that of the corresponding net rate constant in the TyrH system (61 $mM^{-1}s^{-1}$). Also, the rate constant for the decay of the Fe(IV) species in TyrH (22 s^{-1}) and k_2 in Table 4.1 are of comparable magnitude. This observation is not surprising based on the very similar iron centers shared by PheH and TyrH (*23*). For both enzymes the rate limiting step is the release of the products from the active site. However, the rate constant for product release for TyrH is ~10-fold slower than that in CvPheH. The slower product release in TyrH might arise from the presence of dynamic protein loops that regulate the entrance of substrates to the active site in TyrH (*52, 53*).

Previously, kinetic isotope effects (KIEs) were used to study the reaction of CvPheH with phenylalanine (Chapter II). The observed normal isotope effect of 1.4 was determined to be a combination of an inverse isotope effect on C-O bond formation and a normal isotope effect on the final tautomerization step. Also, it was concluded that formation of the C-O bond or an isotope-insensitive step was ~9-fold slower than tautomerization. In the present analysis, the individual rate constants for C-O bond formation and tautomerization were not determined individually instead they are

grouped into the rate constant for tyrosine formation k_2 in Figure 4.7. Nevertheless, analysis of the rate constants reported in Table 4.1 shows that the rate constant for product release (k_3) is ~7-fold slower than the rate constant for tyrosine formation (k_2) consistent with an isotope-insensitive step being rate-limiting for the reaction. This result is in agreement with the prediction made by previous KIEs studies and establishes that product release is the isotope-insensitive step that masks the intrinsic isotope effects in the reaction of CvPheH.

This study provides spectroscopic evidence for the accumulation of an iron intermediate in the catalytic cycle of CvPheH. The intermediate is better described as an Fe(IV) species with characteristics similar to those observed in other enzymes using a 2-his 1-carboxylate triad motif (*27, 28*). Different experimental data using rapid quench experiments and stopped-flow spectroscopy present evidence for the kinetic competency of the Fe(IV) species as the hydroxylating intermediate for phenylalanine hydroxylase.

CHAPTER V

NMR BACKBONE RESONANCE ASSIGNMENT OF *CHROMOBACTERIUM VIOLACEUM* PHENYLALANINE HYDROXYLASE AND PERTURBATION MAP OF THE BACKBONE SIGNALS UPON LIGAND BINDING

Phenylalanine hydroxylase (PheH) catalyzes the hydroxylation of the aromatic amino acid phenylalanine to yield tyrosine (*75*). PheH is found in organisms ranging from eukaryotes to prokaryotes. PheH, tyrosine hydroxylase (TyrH) and tryptophan hydroxylase (TrpH) form the family of aromatic amino acid hydroxylases (*4*). Each enzyme catalyzes the hydroxylation of the corresponding amino acid. In mammals they play key roles in metabolism and synthesis of neurotransmitters (*5, 6, 82*). Mutations that hamper the function of PheH have been linked to the disease phenylketonuria (*1*). Individuals suffering from this disease have elevated levels of L-Phe in the blood and suffer from mental retardation. More than 500 mutations are associated with the disease; most of them occur in the catalytic domain of the enzyme (*2*).

The eukaryotic aromatic amino acid hydroxylases form tetramers in solution. The individual monomers can be divided into three domains, an N-terminal regulatory domain, a catalytic core containing an iron atom coordinated by two histidines and a glutamate, and a C-terminal domain involved in tetramerization (*23*). In contrast, PheH from *Chromobacterium violaceum* (CvPheH) is a monomer containing only the catalytic domain (*39*). Among the eukaryotic family members the catalytic domains share about

50% identity (*23*); the structures of CvPheH and the human counterpart can be superimposed with an RMSD of 1.2 Å (*39*).

Consistent with the similar fold around the active site, the eukaryotic and prokaryotic aromatic amino acid hydroxylases have similar reactivities and a common mechanism of hydroxylation (*30, 40, 74*). All the enzymes require ferrous iron for catalysis and use a tetrahydropterin as source of electrons to activate molecular oxygen (*36, 44, 57, 87*). The current model for the mechanism of hydroxylation is illustrated in Figure 1.3. Before oxygen activation can take place, both the tetrahydropterin and the amino acid must be present in the active site of the enzyme (*10, 12, 51*). After the three substrates are bound, a reactive Fe(IV)O species is formed (*23, 28*). An electrophilic reaction of the Fe(IV)O with the aromatic side chain of the amino acid leads to the formation of the hydroxylated product and a 4a-hydroxy-pterin (*23*).

Crystal structures have been described of the catalytic domains of all three eukaryotic enzymes and of CvPheH (*39, 48-50*). The iron is buried in a 12 Å deep pocket surrounded by protein loops. Crystal structures of the binary complex of the human PheH with dihydrobiopterin can be superimposed over the non-liganded enzyme with an RMSD for the main-chain atoms of 0.21 Å. In contrast, a comparison of the crystal structure of the human PheH ternary complex with tetrahydrobiopterin and 3-(2-thienyl)-L-alanine (THA) with that of the non-liganded enzyme shows an RMSD for main-chain atoms of 2.2 Å (*48*). The ternary complex is a more compact structure with the tetrahydropterin showing a displacement of 2.6 Å towards the metal center. The most dramatic changes take place in the loop containing residues 131-155, with Tyr138

moving almost 10 Å. In the free and tetrahydropterin-bound enzymes Tyr138 is near the surface and points towards the solvent. In the ternary complex the hydroxyl group of the tyrosine has moved into the active site. The crystallographic data with PheH supports a model in which the binding of the substrates triggers the conformational changes required for oxygen activation. This mechanism would ensure that the reactive Fe(IV)O is formed only in the presence of its intended substrate. Whether a similar mechanism is present in the other members of the family is not clear. Unfortunately, there are no crystal structures with both substrates for any of the other hydroxylases.

In contrast to the results of the crystallographic studies with PheH, fluorescence anisotropy studies with tyrosine hydroxylase show that the region of the protein that corresponds to Tyr138 becomes less mobile upon tetrahydropterin binding but not upon binding of the amino acid (*52*). This discrepancy in response might reflect the functional differences between PheH and TyrH. PheH is an allosteric enzyme with phenylalanine and tetrahydropterin having antagonistic roles, whereas TyrH is not an allosteric enzyme (*88, 89*). Also plausible is that the changes observed in the crystal structure of PheH do not accurately reflect the conformational changes that take place in solution. This discrepancy calls for more dynamic studies to be carried out with PheH and TyrH.

Growing lines of evidence link protein motions to catalysis, indicating that not only active site residues but also residues located throughout the protein are involved in the catalytic process (*90-92*). The ability to monitor specific amino acids in precise time and spatial resolution makes nuclear magnetic resonance (NMR) the perfect technique to study the dynamic changes that accompany catalysis in enzymes (*93, 94*). In the specific case of the aromatic amino acid hydroxylases, considering the size limitations of NMR and the size of the eukaryotic enzymes, the 32 kDa bacterial phenylalanine hydroxylase represents the best candidate for those studies. Here we report the NMR backbone resonance assignments of CvPheH and the chemical shift perturbation map generated upon binding of L-phenylalanine, 6-methyl-5-deazapterin or both. The similar tertiary structure and catalytic properties of bacterial and eukaryotic hydroxylases validate the extrapolation of the structural results presented here to the other members of the family.

EXPERIMENTAL PROCEDURES

Materials. DEAE-Sephacel was from Amersham Pharmacia Biotech (Uppsala, Sweden). *E. coli* strain BL21(DE3), used for protein expression, was from Novagen. 6-Methyltrahydropterin (6-MePH_4) was from B. Schircks Laboratories (Jona, Switzerland). Catalase was from Roche (Indianapolis, IN). The redox inactive 6-methyl-5-deazatetrahydropterin was synthesized essentially as described by Moad et al. (*95*). $^{15}NH_4Cl$ (98 %) was from Sigma-Aldrich Chemical Co. (Milwaukee, WI). D_2O (99.9 %), [$^{13}C_6$]-D-glucose (99 %), ^{15}N-leucine, ^{15}N-phenylalanine, 2-^{15}N-Lysine and ^{15}N-tyrosine were from Cambridge Isotope Laboratories (Andover, MA). All other commercial reagents were of the highest purity available and were used without further purification.

Enzyme expression and purification. Different growth conditions were used to generate ^{15}N-labeled and ^{2}H,^{13}C,^{15}N-labeled phenylalanine hydroxylase (*96*). ^{15}N-Labeled CvPheH was prepared by transforming *E. coli* BL21(DE3) cells with the expression plasmid pET21b-CvPheH (Chapter II). A single colony was used to inoculate 50 mL of LB broth (100 μg/mL ampicillin); this was allowed to grow at 37 °C for 16 h. Ten milliliters of the overnight culture were centrifuged for 30 min at 2600g and resuspended in the same volume of M9 minimal media (*96*). The resuspended cells were centrifuged again and the supernatant was discarded. The cell pellet was resuspended in 1 L M9 minimal media containing $^{15}NH_4Cl$ (1g/L), thiamin (1 mg/L), and ampicillin (100 mg/L). The cells were allowed to grow until the A_{600} reached a value between 0.9 and 1.0. Protein expression was induced by the addition of isopropyl β-thiogalactoside

(IPTG) at a final concentration of 120 mg/mL. After 6 h at 37 °C the cells were harvested by centrifugation for 30 min at 2600g. The cell pellet was kept at -80 °C until purification. Selectively labeled samples were prepared following a similar protocol but using media containing unlabeled NH_4Cl and unlabeled amino acids, except for ^{15}N-leucine, ^{15}N-phenylalanine, 2-^{15}N-Lysine or ^{15}N-tyrosine, using the concentrations described by Davis et al. (*97*).

^{2}H,^{13}C,^{15}N-Labeled CvPheH was prepared by inoculating 1 L of fresh LB with 10 mL of overnight culture. When the A_{600} reached a value of 0.7 the cells were centrifuged for 30 min at 2600g. The cell pellet was carefully resuspended in 1 L of M9 salts (*96*) without any carbon or nitrogen source, and the cells were centrifuged for 30 min at 2600g. After the wash, the cell pellet was resuspended in 500 mL of M9 minimal media containing 75% D_2O, thiamin (1 mg/L), $^{15}NH_4Cl$ (1 g/L), and [$^{13}C_6$]-D-glucose (4 g/L). The culture was allowed to grow for an additional 1 h after which expression was induced with IPTG (1.2 g/L). After 6 h the cells were harvested by centrifugation and the cell pellet stored at -80 °C.

The purification of labeled CvPheH was carried out as described in Chapter II. Protein yield was about 50 mg of more than 95% pure protein per liter of minimal media. In order to remove metals, the enzyme was incubated 2 hours on ice with 5 mM EDTA and 5 mM NTA. The chelators were removed by dialysis against a 100-fold excess of 50 mM Hepes buffer (pH 6.5) containing 100 mM NaCl with buffer changes every 4 h and a total of 5 buffer changes. The purified protein was concentrated to 400 – 500 μM using a 10,000 molecular weight cutoff centrifugal filter (Millipore, Billerica,

MA) and then dialyzed against 20 mM sodium phosphate buffer (pH 6.5) and 50 mM NaCl. For protein concentrations above 500 μM, 100 mM arginine was included in the final buffer to increase the stability of the protein at the higher concentrations (*98, 99*). The enzyme activity was measured using a spectrophotometric assay as previously described (*43, 61*).

NMR spectroscopy. The backbone resonance assignments of CvPheH were obtained using a suite of TROSY-based three-dimensional triple resonance experiments applied to samples of ^{13}C-^{15}N-CvPheH grown in 75 % D_2O. ^{1}H-^{15}N HSQC (*100*), HNCACB, and HN(CO)CACB experiments (*101, 102*) were performed at the University of Houston using a Bruker 800 MHz spectrometer equipped with a cryogenically cooled probe. HNCO, HN(CA)CO, HNCA, HN(CO)CA, HN(CA)CB, and HN(COCA)CB experiments (*101, 102*) were performed at the University of Texas Health Science Center (San Antonio, Texas) using a Bruker 600 or 700 MHz spectrophotometer equipped with either a cryogenically cooled (600 MHz) or a conventional (700 MHz) 5 mm ^{1}H probe with a ^{13}C and ^{15}N decoupler and pulsed field gradient coils.

Data analysis. Backbone resonance assignments of CvPheH were obtained by collecting and analyzing data from TROSY-based HNCA, HN(CO)CA, HNCACB, HN(CO)CACB, HNCO, HN(CA)CO, HN(CA)CB, and HN(COCA)CB experiments as applied to a deuterated, ^{13}C-^{15}N-labeled protein (*101, 102*). All spectra were processed using NMRPipe (*103*) and analyzed using the program Sparky (*104*). Initial rates obtained as a function of phenylalanine concentration were fit to the Michaelis-Menten

equation to obtain values for k_{cat}, k_{cat}/K_M, and K_M using KaleidaGraph (Synergy Software, Reading, PA).

Ligand Titrations of CvPheH. The ligands were added to a solution of 380 μM ^{15}N-labeled CvPheH and a series of ^{1}H-^{15}N HSQC spectra were recorded at concentrations of phenylalanine or 6-methyl-5-deazaptetrahydropterin ranging from 0 to 1200 μM. The perturbations of backbone amide hydrogen and nitrogen chemical shifts were monitored as a function of increasing ligand concentration, and the weighted average chemical shift change, Δ_{avg} (ppm), was calculated using Equation 5.1 (*105*). The calculated weighted average chemical shift change was normalized by $\Delta_{avg}/\Delta_{max} = 1.0$, where Δ_{max} is the maximum shift change at the final ligand concentration.

$$\Delta_{avg} = ((\Delta\delta^2_{HN} + (\Delta\delta^2_{N}/25))/2)^{1/2} \quad (5.1)$$

RESULTS

NMR assignments. In order to assign the amide backbone resonances of CvPheH, a heteronuclear single quantum coherence (HSQC) spectrum of the ^{1}H-^{15}N labeled sample was analyzed. The HSQC showed a combination of well dispersed peaks, as expected for a structurally order protein, in addition to regions of overlapping peaks (Figure 5.1).

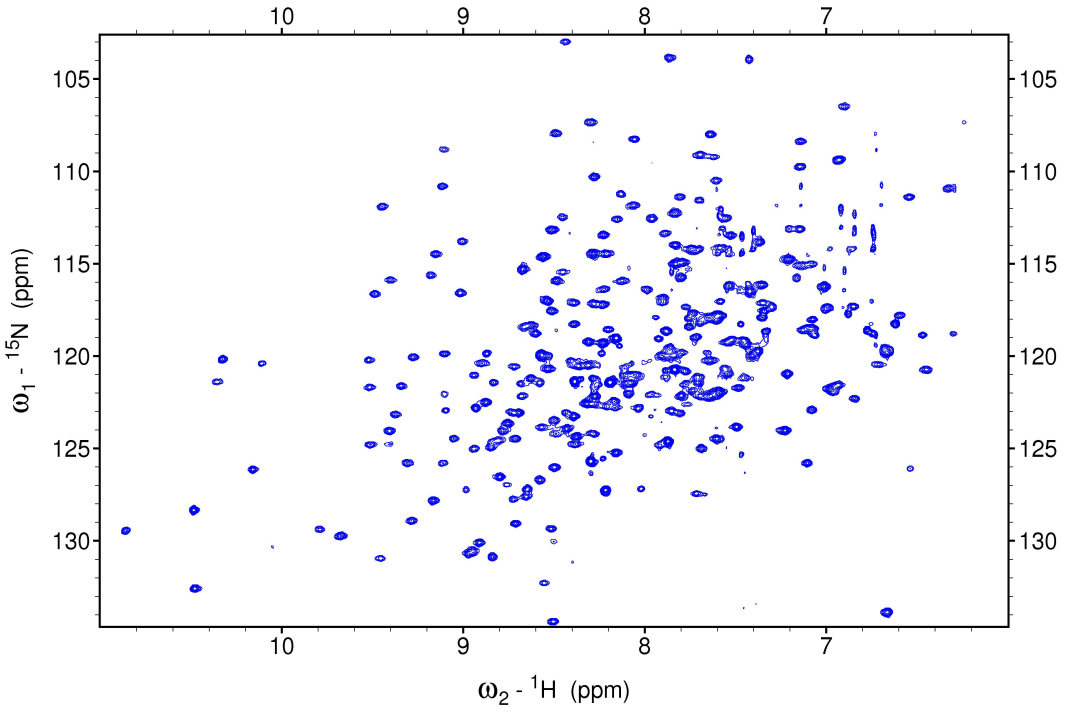

Figure 5.1: Two-dimensional ^{1}H-^{15}N HSQC spectrum of 0.3 mM ^{15}N-labeled CvPheH. The sample was in 20 mM phosphate buffer (pH 6.5) with 50 mM NaCl. Data were collected at 27 °C with a Varian 800 MHz spectrometer.

Due to the size of the protein we constantly found more than one residue resonating in the same ^{1}H-^{15}N plane. In order to identify carbon signals in heavily overlapped N-H planes, HSQC spectra of selectively labeled ^{15}N-leucine (Figure 5.2), ^{15}N-tyrosine (Figure 5.3), ^{15}N-phenylalanine (Figure 5.4), and 2-^{15}N-lysine (Figure 5.5) were collected. The HSQC spectrum of the ^{15}N-leucine-CvPheH showed 29 signals out of the expected 32 from the protein sequence. From the 29 pairs of N-H signals we were able to assign 22 to leucine residues. The unassigned signals correspond to leucine residues with carbon signals in heavily overlapped regions of the HNCACB spectrum likely to come from residues in the core of the protein. The spectra of both ^{15}N-tyrosine-CvPheH and ^{15}N-phenylalanine-CvPheH showed the expected number of signals, and we were able to assign all to the corresponding amino acids in the sequence. Finally, the spectrum of 2-^{15}N-lysine-CvPheH showed 10 signals out of the expected 11, and we assigned 8 of them to the corresponding lysine residues. The HSQC spectra of the selectively labeled samples were also used to confirm the assignments made using the triple resonance experiments.

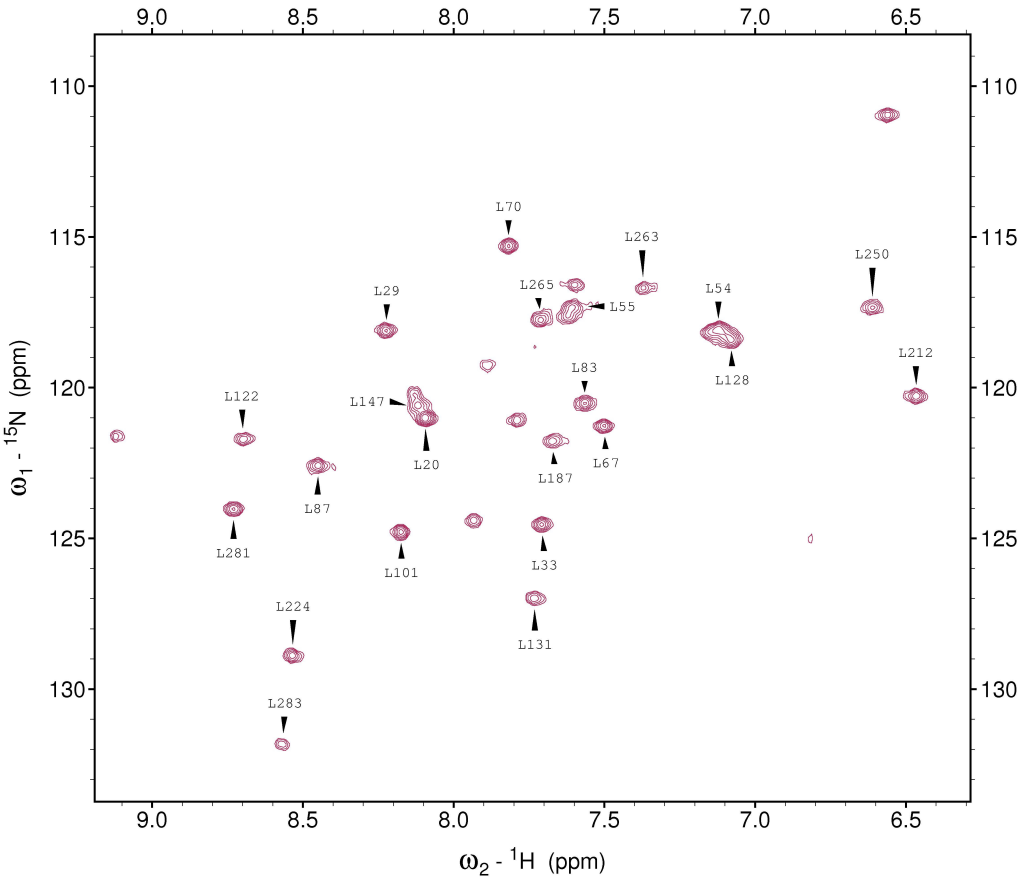

Figure 5.2: Two-dimensional ^{1}H-^{15}N HSQC spectrum of 0.3 mM ^{15}N-leucine labeled CvPheH. The sample was in 20 mM phosphate buffer (pH 6.5) with 50 mM NaCl. Data were collected at 27 °C with a Bruker 700 MHz spectrometer.

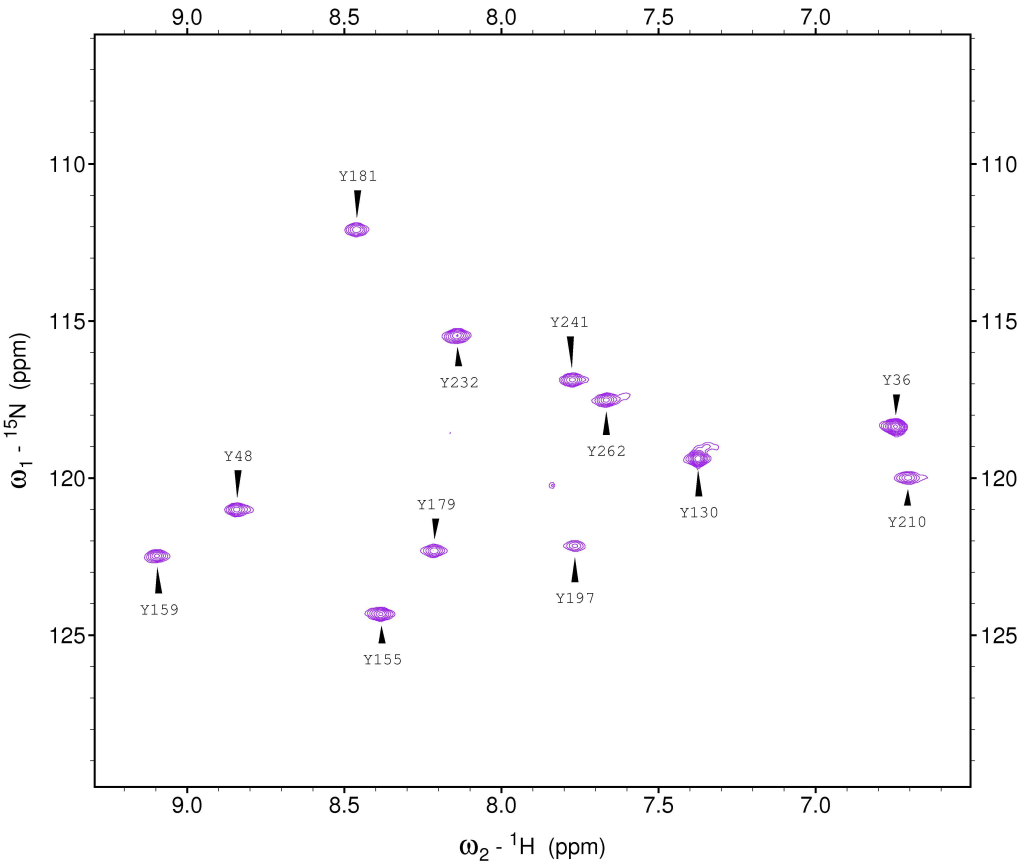

Figure 5.3: Two-dimensional ^{1}H-^{15}N HSQC spectrum of 0.3 mM ^{15}N-tyrosine labeled CvPheH. The sample was in 20 mM phosphate buffer (pH 6.5) with 50 mM NaCl. Data were collected at 27 °C with a Bruker 700 MHz spectrometer.

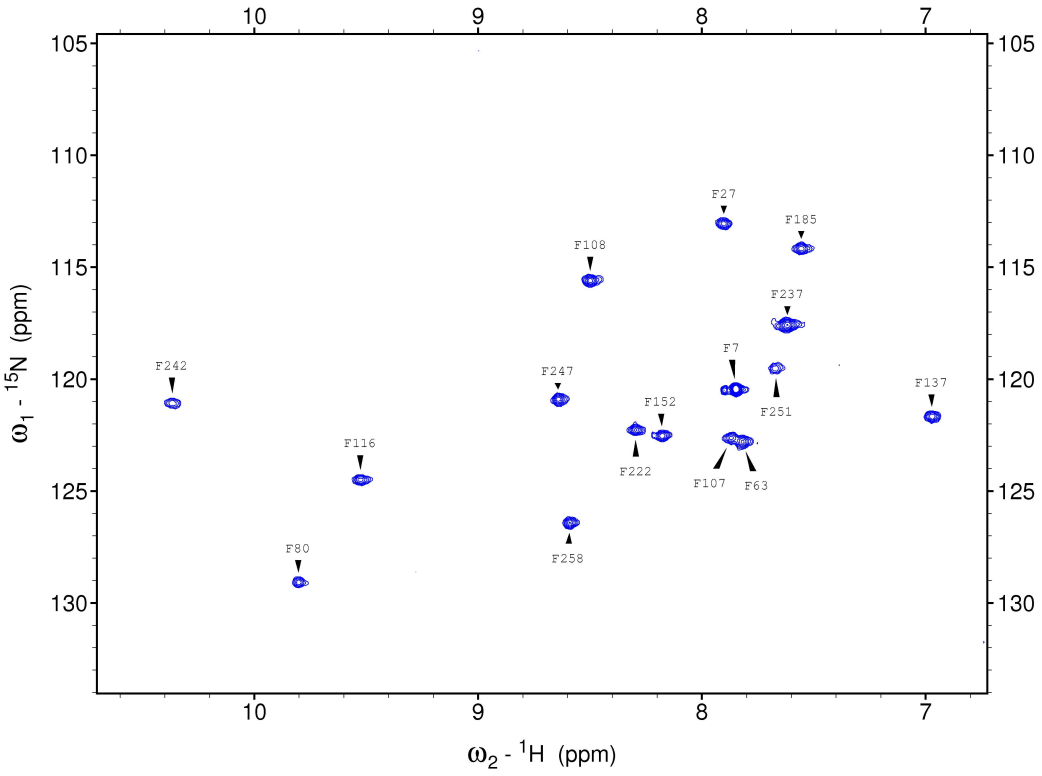

Figure 5.4: Two-dimensional ^{1}H-^{15}N HSQC spectrum of 0.3 mM ^{15}N-phenylalanine labeled CvPheH. The sample was in 20 mM phosphate buffer (pH 6.5) with 50 mM NaCl. Data were collected at 27 °C with a Bruker 700 MHz spectrometer.

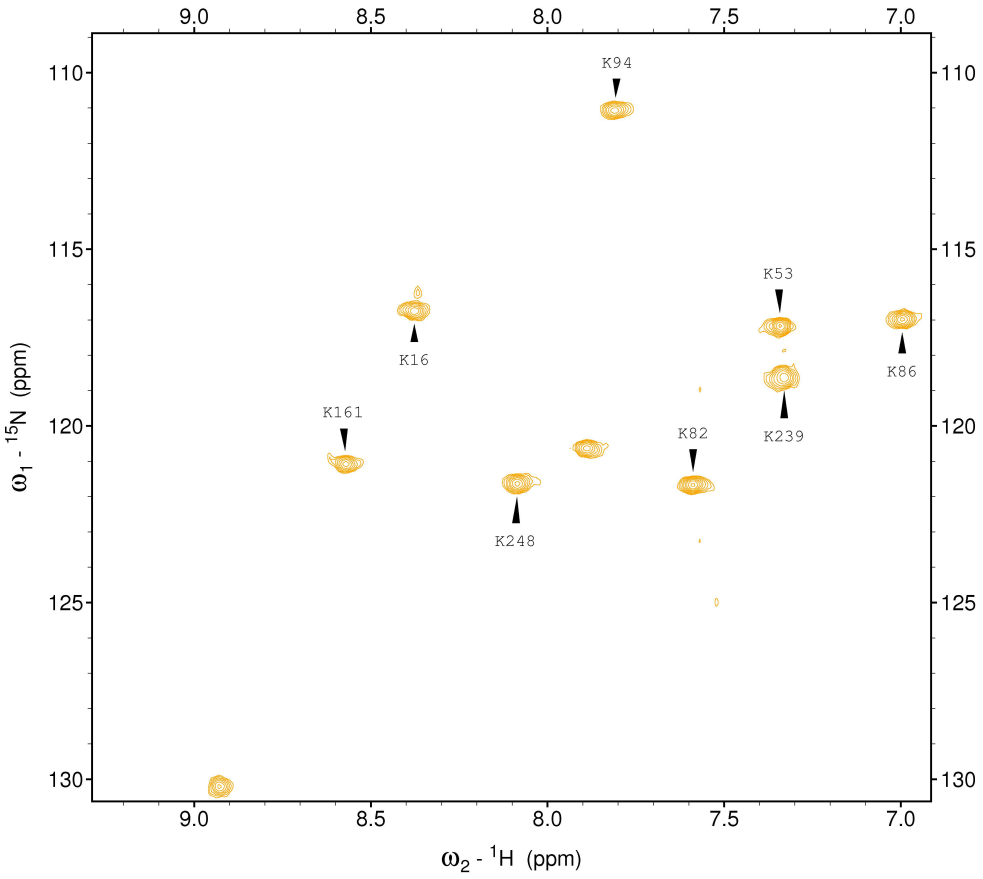

Figure 5.5: Two-dimensional ^{1}H-^{15}N HSQC spectrum of 0.3 mM ^{15}N-lysine labeled CvPheH. The sample was in 20 mM phosphate buffer (pH 6.5) with 50 mM NaCl. Data were collected at 27 °C with a Bruker 700 MHz spectrometer.

Excluding proline residues CvPheH contains a total of 278 assignable residues. However, the HSQC spectrum of CvPheH contains 291 signals. The extra signals come from the side chains of asparagine and glutamine residues as well as the aromatic protons of tryptophan and histidine. Combining all the available NMR data, we were able to assign 224 signals in the HSQC spectrum to their corresponding amino acid residues in the CvPheH sequence. The assigned residues constitute 81 % of the assignable CvPheH protein sequence (Appendix-A).

Titrations of CvPheH with phenylalanine. The residues of CvPheH affected by binding of phenylalanine were identified by titrating the enzyme with increasing amounts of the amino acid and monitoring the perturbation of the protein backbone amide nitrogen and amide hydrogen chemical shifts. Consistent with the specific interaction with a small molecule we observed a subset of residues showing chemical shift changes in addition to the total disappearance of multiple signals with increasing amounts of phenylalanine. Figure 5.6 shows an example of the characteristic responses observed. The HSQC signals of residues Asp245 and Val77 shift progressively during the titration, indicating fast exchange, while the signal of residue Asp26 remained unvaried at all the phenylalanine concentrations and the signal of Asp252 was lost after the addition of 25 μM phenylalanine, consistent with a line broadening effect most likely due to a strong direct interaction with the ligand or a conformational change. In Figure 5.7 the changes in chemical shifts are displayed through the use of the normalized weighted chemical shift average Δ_{avg} between the free CvPheH and its complex with

phenylalanine. Gly162 showed the maximum chemical shift perturbation and was used to normalize the perturbations of the other amino acids.

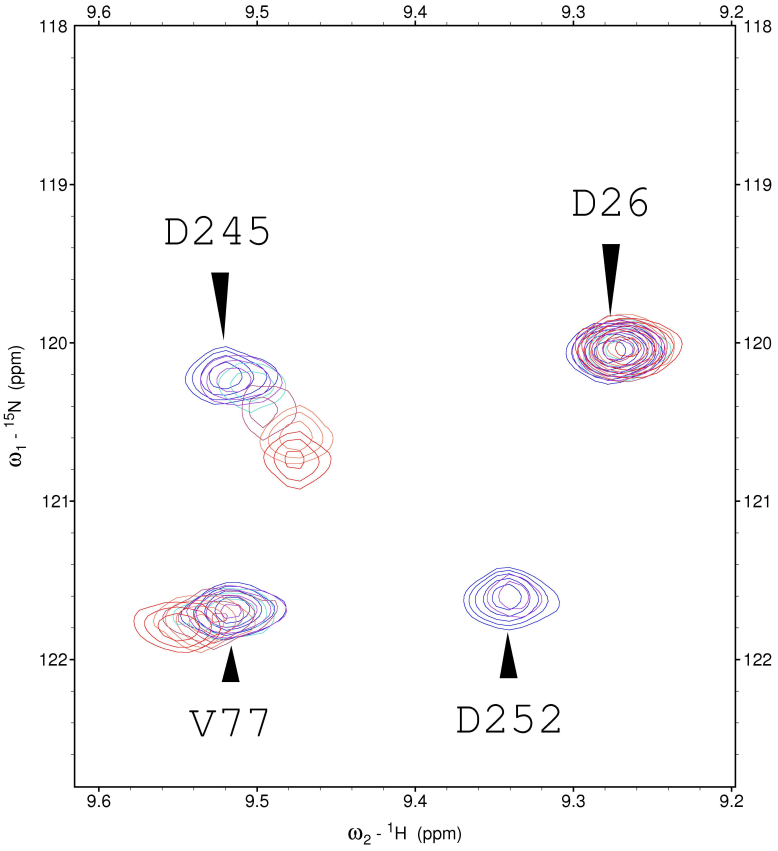

Figure 5.6: Example of a subset of residues of CvPheH showing different responses to phenylalanine titration. At a constant CvPheH concentration of 380 µM, spectra were recorded at 0 µM (blue), 25 µM (purple), 50 µM (turquoise), 100 µM (maroon), 200 µM (orange), and 600 µM (red) phenylalanine.

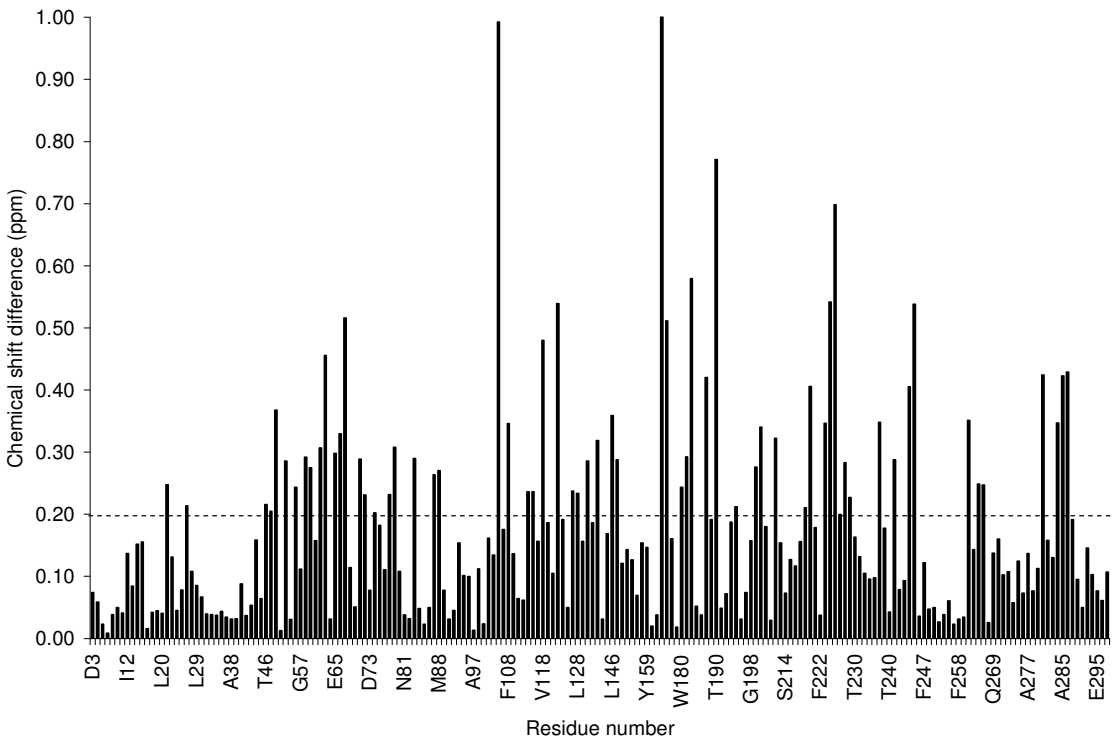

Figure 5.7: Normalized chemical shift perturbation of ^{1}H and ^{15}N chemical shifts of CvPheH as a function of residue number upon tritration with phenylalanine (1200 μM).

Titrations of CvPheH with 6-methyl-5-deazatetrahydropterin. The amino acid residues of CvPheH showing chemical shift perturbations upon tetrahydropterin binding were identified by titrating the enzyme with the redox-inactive analog 6-methyl-5-deazatetrahydropterin. The perturbations of the protein backbone amide nitrogen and amide hydrogen chemical shifts were monitored for each of the ligand concentrations used. We observed that upon binding of 6-methyl-5-deazatetrahydropterin multiple residues located throughout the protein showed significant chemical shift changes. In addition, we observed the total disappearance of the signals for multiple residues. The residue displaying maximal perturbation was Val106 and its chemical shift perturbation value was used to normalize the perturbations of the rest of the amino acids. The normalized weighted chemical shift average Δ_{avg} is plotted as a function of assigned residue number in Figure 5.8.

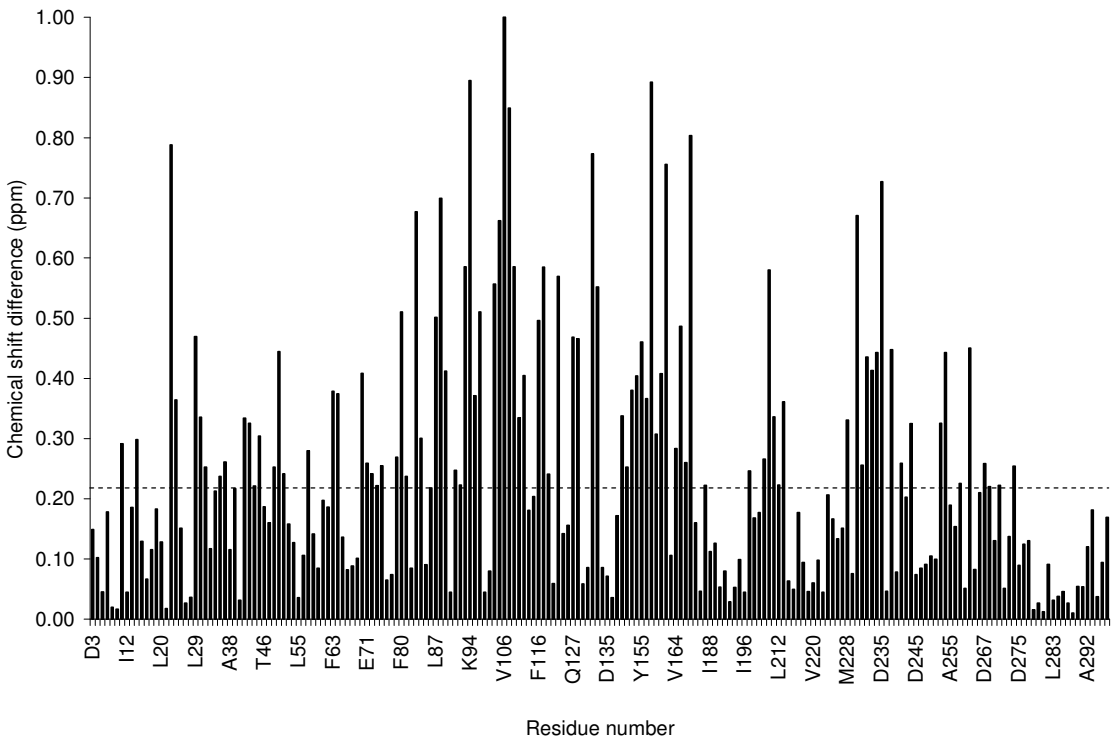

Figure 5.8: Normalized chemical shift perturbation of ^{1}H and ^{15}N chemical shifts of CvPheH as a function of residue number upon titration with 6-methyl-5-deazatetrahydropterin (1200 μM).

DISCUSSION

To analyze the consequences of ligand binding to CvPheH we assigned the ^{1}H, ^{13}C, and ^{15}N resonances of the free enzyme. Despite the size of CvPheH (32 kDa) The HSQC spectrum of the ^{1}H-^{15}N labeled enzyme (Figure 5.1) shows a combination of well dispersed peaks in addition to regions of overlapping peaks. The crowded regions most likely come from amino acids at the core of the protein and around the iron binding pocket. There are three main regions of the protein where no assignments could be made (Figure 5.9). Two of the unassigned protein regions comprise the segments of residues His138 to Val144, and Gly200 to Ser208. The first contains the iron ligands His138 and His143, and the second is close to the iron center in the tertiary structure. The presence of paramagnetic metals in the iron pocket could be the reason for the lack of NMR signals from those residues (*106, 107*). This hypothesis is supported by the ability of CvPheH to bind copper and iron (*36, 38*) and the fact that when assayed without extra added Fe(II) the apo-CvPheH shows up to 5% the activity of iron containing enzyme. The third unassigned region is an α-helix comprising residues Lys165 to Leu178 that is not close to the iron center; there is no obvious reason for the lack of signals from these residues.

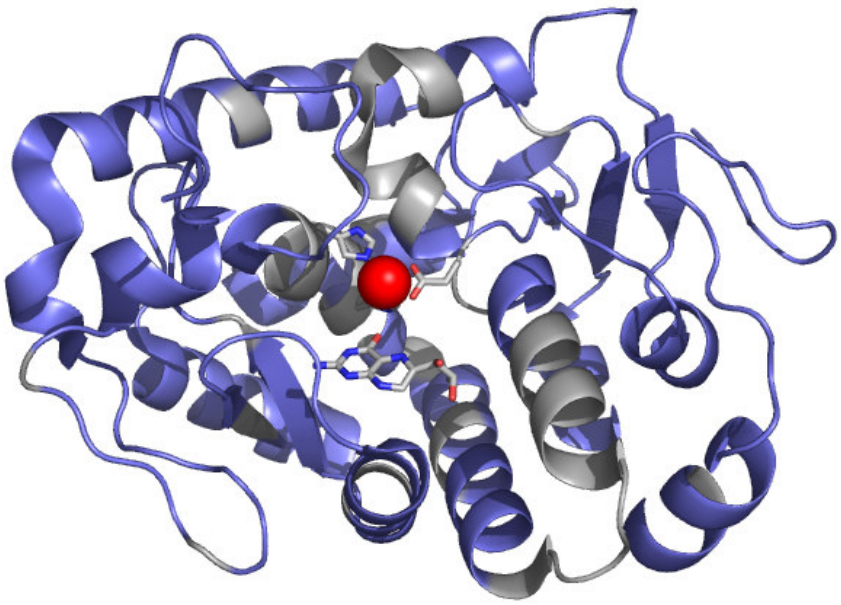

Figure 5.9: Crystal structure of CvPheH (PDB 1LTZ). The unassigned residues of the protein are shown in gray. The Fe(II) is represented as a red sphere and the iron ligands are shown as sticks.

The ^{1}H, ^{15}N correlation spectrum of a protein can be regarded as a fingerprint of its structure. The HSQC signals of individual nuclei report on the electronic and/or conformational environment of specific amino acids. Mapping the perturbations of the chemical shifts of a protein upon complexation with a ligand allows the identification of residues involved in binding sites and/or identifying conformational rearrangements triggered by ligand binding. However, there is no quantitative correlation between the size of the perturbation and the strength of the binding or the conformational rearrangement. In addition, complete disappearance of signals can occur upon complexation, but this information has to be taken into consideration when analyzing the data. A comparison of the chemical shifts of all the cross-peaks in the presence and absence of the ligand is required to define the area of the protein directly involved in binding in addition to those residues that are indirectly affected as a result of conformational rearrangements.

Crystal structures of the catalytic domains of both CvPheH and human PheH are available (*39*). Both enzymes have a similar fold in the catalytic domain and the structures can be superimposed with 1.2 Å RMSD. The residues of CvPheH that interact with phenylalanine can be inferred from the structure of the complex of the phenylalanine analog 3-(2-thienyl)-L-alanine and human PheH (*48*). Based on that structure, the corresponding residues in CvPheH that interact with phenylalanine through electrostatic forces are Arg123 and the backbone of Leu131. Interestingly, this last residue is a threonine in the human enzyme and the side chain hydroxyl group hydrogen bonds with the amino group of the substrate. Additionally, a conserved hydrophobic

cage is made up by Trp180, Phe185, and Pro134. As expected from the crystal structure, we observed significant chemical shift changes in these residues. However, the effect of phenylalanine binding expands beyond these few amino acids (Figure 5.7). Upon binding of phenylalanine residues throughout the protein show chemical shift changes in addition to the total disappearance of multiple signals. In Figure 5.10 the residues affected by phenylalanine binding are mapped onto the structure of CvPheH (PDB 1LTZ). In this figure the residues are color-coded according to their chemical shift perturbations. Residues with chemical shift perturbations below the overall average (0.17) were considered not significantly shifted and are colored blue. Residues with perturbations between 0.17 and 0.60 were considered moderately shifted and are colored orange. Finally, residues with chemical shift perturbations above 0.60 were considered highly shifted and are colored red. We included the residues whose signals disappeared during the titration in the analysis since they represent strong direct interactions or conformational rearrangements. Those residues are also colored red in Figure 5.10.

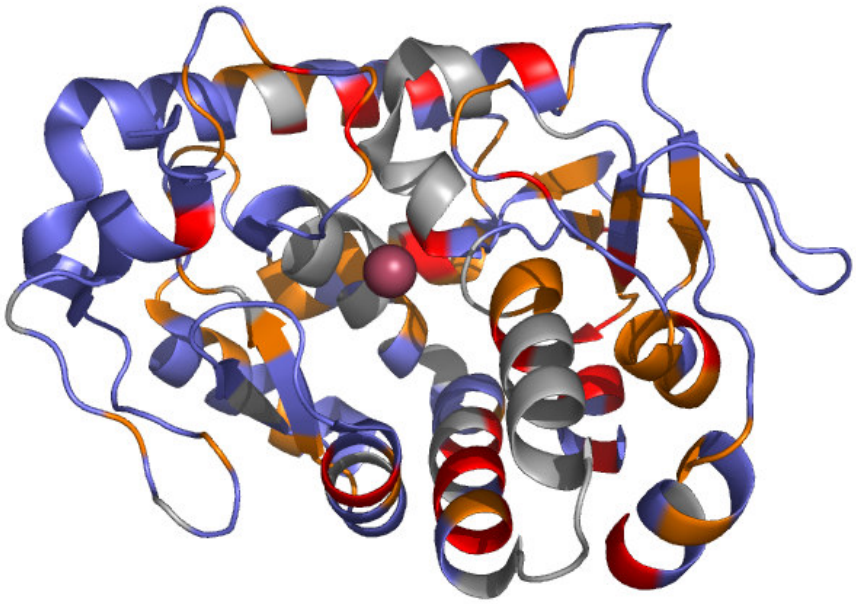

Figure 5.10: Chemical shift perturbations of the amide signals in CvPheH upon titration with phenylalanine. The chemical shift differences between free CvPheH and in the presence of 1200 µM phenylalanine were mapped onto the structure of CvPheH (PDB 1LTZ). The residues are colored according to the following scheme: unassigned residues are shown in gray; residues with a chemical shift perturbation (Δ_{avg}) smaller than the average (0.17) are colored blue. Residues with an Δ_{avg} between 0.17 and 0.6 are colored orange. Residues displaying an Δ_{avg} above 0.6 are colored red. Also, residues whose amide signals disappeared during the titration are colored red. The iron is shown as a purple sphere.

The binding of phenylalanine to CvPheH affects multiple residues located throughout the enzyme. The structure of CvPheH is characterized by three protein loops that cover the entrance to the iron center. When viewed as represented in Figure 5.10, two loops formed by residues Thr119 to Asp135 and Gln229 to Thr240 lie above the iron center. The corresponding loops in the human enzyme close upon binding of the amino acid; consistent with a similar phenylalanine binding site in CvPheH we observed significant chemical shift perturbations in some of the residues that form those loops. Binding of the amino acid to human PheH causes the enzyme to become more compact (*48*) and probably some of the perturbations that we observed on surface residues are product of a similar conformational rearrangement in CvPheH. However, we also observed significant chemical shift perturbations on specific residues located at the core of the protein and on secondary structure elements that form the frame of the enzyme. Some of these residues, although not in the active site, might be important for catalysis. The perturbation map generated upon phenylalanine binding sets the basis for site-directed mutagenesis studies aimed at identifying those residues away from the active site that are important for catalysis in CvPheH.

The crystal structure of CvPheH with BH_2 shows the residues that directly interact with the pterin (*39*). The main interactions occur with the protein back bone of a loop comprising residues Pro99 to Pro103. Also, the side chain of Phe107 π-stacks with the pterin. We used the redox-inactive analog 6-methyl-5-deazatetrahydropterin to map the residues that are affected by the binding of the pterin to CvPheH. Consistent with the crystallographic information, we observed complete disappearance of the signals of Gly100, Leu101, and Ile102. However, as in the case of phenylalanine, the effect of pterin biding is not localized to the binding site but it is spread throughout the enzyme (Figure 5.8). With this substrate, the overall average chemical shift perturbation was 0.24 and perturbations below that threshold were considered not significant. In Figure 5.11 the residues affected by 6-methyl-5-deazatetrahydropterin binding are mapped onto the structure of CvPheH (PDB 1LTZ). In this figure, residues with chemical shift perturbations below 0.24 are colored blue, residues with perturbations between 0.24 and 0.60 are colored orange and residues with perturbations above 0.60 are colored red. Also, the residues with signals that disappeared during the titration are colored red.

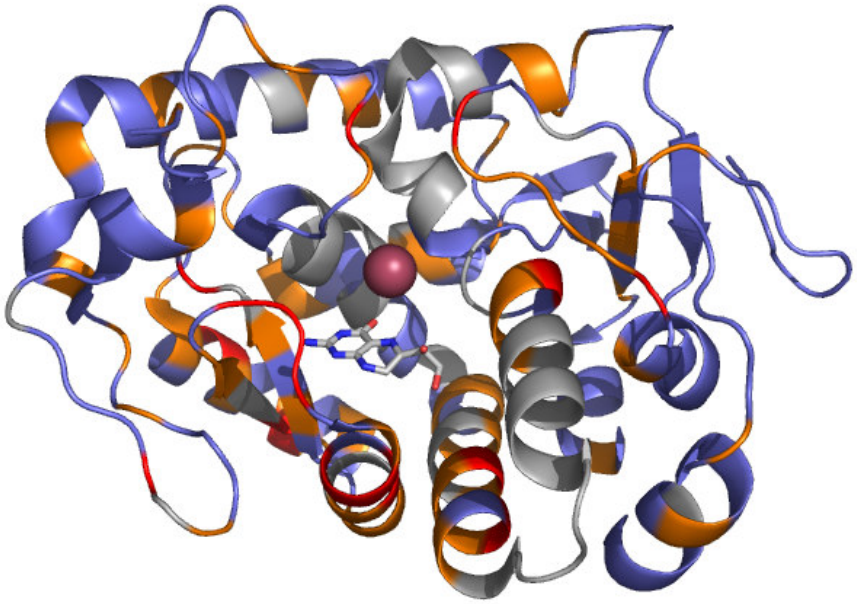

Figure 5.11: Chemical shift perturbations of the amide signals in CvPheH upon titration with 6-methyl-5-deazatetrahydropterin. The chemical shift differences between free CvPheH and in the presence of 1200 μM 6-methyl-5-deazatetrahydropterin were mapped onto the structure of CvPheH (PDB 1LTZ). The residues are colored according to the following scheme: unassigned residues are shown in gray; residues with a chemical shift perturbation (Δ_{avg}) smaller than the average (0.24) are colored blue. Residues with an Δ_{avg} between 0.24 and 0.6 are colored orange. Residues displaying an Δ_{avg} above 0.6 are colored red. Also, residues whose amide signals disappeared during the titration are colored red. The iron is shown as a purple sphere.

6-Methyl-5-deazatetrahydropterin is a competitive inhibitor for tetrahydrobiopterin (K_i = 30 μM) and we observed significant chemical shift perturbation of the residues that form the pterin biding site. However, Figure 5.11 shows that upon binding of the pterin multiple residues of CvPheH show significant chemical shift perturbations. Interestingly, binding of the pterin affects the two protein loops that interact with phenylalanine whereas binding of the latter does not affect the pterin binding loop, suggesting a specific synergism between the two substrates. Despite having different binding sites, comparison of Figures 5.10 and 5.11 shows that the pattern of perturbations generated upon binding of the amino acid or the pterin are very similar. The fact that similar residues, located throughout the enzyme, are affected by the binding of either substrate suggests that some of those residues might belong to networks that orchestrate catalysis.

The assignment of the NMR backbone resonance signals from CvPheH and the ligand binding studies presented here set the basis for site directed mutagenesis studies aimed at discerning the role of specific residues in catalysis in addition to relaxation studies that could correlate protein dynamics with the catalytic process. The similar tertiary structure and catalytic properties of bacterial and eukaryotic aromatic amino acid hydroxylases validate the extrapolation of the results from those studies to the other members of the family of aromatic amino acid hydroxylases.

CHAPTER VI

SUMMARY

The purpose of this study was to characterize the phenylalanine hydroxylase from *Chromobacterium violaceum* (CvPheH) mechanistically and structurally. The results from this study place the enzyme in context of the better understood eukaryotic aromatic amino acid hydroxylases. Chapter II described the use of kinetic isotope effects (KIEs) to study the mechanisms of hydroxylation of phenylalanine and 4-methylphenylalanine by CvPheH. The temperature dependence of the KIE and the iron requirement for catalysis of tetrahydropterin oxidation by CvPheH both demonstrate that the reactivity of the hydroxylating intermediate in this bacterial amino acid hydroxylase is indistinguishable from that of the eukaryotic enzymes. Thus, for mechanistic, if not regulatory studies, the bacterial enzyme is a valid model for the eukaryotic enzymes.

Chapter III described the use of KIEs effects as a probe of the chemical mechanism of aliphatic hydroxylation by CvPheH. The results are consistent with hydrogen atom abstraction as the mechanism. The magnitude of the isotope effect on aliphatic hydroxylation reported here is comparable to that found for benzylic hydroxylation by CvPheH and all the eukaryotic enzymes (*40, 41, 74*). Thus, for both reactions a similar mechanism of hydrogen atom abstraction followed by radical rebound can be proposed.

Chapter IV describes spectroscopic evidence for an Fe(IV) intermediate in the catalytic cycle of CvPheH. The intermediate is similar to those observed in other

enzymes using a 2-his 1-carboxylate triad motif (*27, 28, 81*). Rapid quench experiments and stopped-flow spectroscopy established the kinetic competency of the Fe(IV) species as the hydroxylating intermediate for phenylalanine hydroxylase.

Chapter V described the assignment of the NMR backbone resonance signals of CvPheH. The amide signals in the HSCQ spectrum of CvPheH were assigned using a suite of TROSY-based three-dimensional triple resonance experiments. From the 278 assignable residues in CvPheH we were able to assign 224. This constitutes 81 % of the assignable protein sequence. Unassigned residues were due mainly to heavy overlap or the lack of signals from the carbon atoms. The assignment of the backbone signals from CvPheH sets the basis for ligand binding studies as well as relaxation dynamics on this enzyme. The similar tertiary structure and catalytic properties of bacterial and eukaryotic aromatic amino acid hydroxylases validate the extrapolation of the results from those studies to the other members of the family.

REFERENCES

1. Eisensmith, R. C., and Woo, S. L. C. (1991) Phenylketonuria and the phenylalanine hydroxylase gene, *Mol. Biol. Med. 8*, 3-18.
2. Scriver, C. R., Waters, P. J., Sarkissian, C., Ryan, S., Prevost, L., Côté, D., Novak, J., Teebis, S., and Nowacki, P. M. (2000) PAHdb: A locus-specific knowledgebase, *Hum. Mutat. 15*, 99-104.
3. Guthrie, R., and Susi, A. (1963) A simple phenylalanine method for detecting phenylketonuria in large populations of newborn infants, *Pediatrics 32*, 338-343.
4. Fitzpatrick, P. F. (1999) Tetrahydropterin-dependent amino acid hydroxylases, *Annu. Rev. Biochem. 68*, 355-381.
5. Mallet, J. (1996) The TIPS/TINS lecture - Catecholamines - from gene regulation to neuropsychiatric disorders, *Trends Neurosci. 19*, 191-196.
6. Martinez, A., Knappskog, P. M., and Haavik, J. (2001) A structural approach into human tryptophan hydroxylase and its implications for the regulation of serotonin biosynthesis, *Curr. Med. Chem. 8*, 1077-1091.
7. Abu-Omar, M. M., Loaiza, A., and Hontzeas, N. (2005) Reaction mechanisms of mononuclear non-heme iron oxygenases, *Chem. Rev. 105*, 227-2252.
8. Bruijninex, P. C. A., van Koten, G., and Gebbinik, R. J. M. (2008) Mononuclear non-heme iron enzymes with the 2-His-1-carboxylate triad: Recent developments in enzymology and modeling studies, *Chem. Soc. Rev. 37*, 2716-2744.

9. Craine, J. E., Hall, E. S., and Kaufman, S. (1972) The isolation and characterization of dihydropteridine reductase from sheep liver, *J. Biol. Chem. 247*, 6082-6091.

10. Fitzpatrick, P. F. (1991) Steady-state kinetic mechanism of rat tyrosine hydroxylase, *Biochemistry 30*, 3658-3662.

11. Pember, S. O., Johnson, K. A., Villafranca, J. J., and Benkovic, S. J. (1989) Mechanistic studies on phenylalanine hydroxylase from *Chromobacterium violaceum*. Evidence for the formation of an enzyme-oxygen complex, *Biochemistry 28*, 2124-2130.

12. Volner, A., Zoidakis, J., and Abu-Omar, M. M. (2003) Order of substrate binding in bacterial phenylalanine hydroxylase and its mechanistic implication for pterin-dependent oxygenases, *J. Biol. Inorg. Chem. 8*, 121-128.

13. Kaufman, S., Bridgers, W. F., Eisenberg, F., and Friedman, S. (1962) The source of oxygen in the phenylalanine hydroxylase and the dopamine-β-hydroxylase catalyzed reactions, *Biochem. Biophys. Res. Commun. 9*, 497-502.

14. Dix, T. A., Bollag, G., Domanico, P. L., and Benkovic, S., J. (1985) Mechanism of "uncoupled" tetrahydropterin oxidation by phenylalanine hydroxylase, *Biochemistry 24*, 2955-2958.

15. Massey, V. (1994) Activation of molecular oxygen by flavins and flavoproteins, *J. Biol. Chem. 269*, 22459-22462.

16. Davis, M. D., and Kaufman, S. (1989) Evidence for the formation of the 4a-carbinolamine during the tyrosine-dependent oxidation of tetrahydrobiopterin by rat liver phenylalanine hydroxylase, *J. Biol. Chem. 264*, 8585-8596.

17. Massey, V., and Hemmerich, P. (1975) Flavin and pteridine monooxygenases, in *The Enzymes* (Boyer, P. D., Ed.) 3rd ed., pp 191-252, Academic Press, Inc., New York.

18. Carr, R. T., Balasubramanian, S., Hawkins, P. C. D., and Benkovic, S. J. (1995) Mechanism of metal-independent hydroxylation by *Chromobacterium violaceum* phenylalanine hydroxylase, *Biochemistry 34*, 7525-7532.

19. Fitzpatrick, P. F., Ralph, E. C., Ellis, H. R., Willmon, O. J., and Daubner, S. C. (2003) Characterization of metal ligand mutants of tyrosine hydroxylase: Insights into the plasticity of a 2-histidine-1-carboxylate triad, *Biochemistry 42*, 2081-2088.

20. Bassan, A., Blomberg, M. R. A., and Siegbahn, P. E. M. (2003) Mechanism of aromatic hydroxylation by an activated Fe^{IV}=O core in tetrahydrobiopterin-dependent hydroxylases, *Chem. Eur. J. 9*, 4055-4067.

21. Moran, G. R., Derecskei-Kovacs, A., Hillas, P. J., and Fitzpatrick, P. F. (2000) On the catalytic mechanism of tryptophan hydroxylase, *J. Am. Chem. Soc. 122*, 4537-4541.

22. Ellis, H. R., Daubner, S. C., and Fitzpatrick, P. F. (2000) Mutation of serine 395 of tyrosine hydroxylase decouples oxygen-oxygen bond cleavage and tyrosine hydroxylation, *Biochemistry 39*, 4174-4181.

23. Fitzpatrick, P. F. (2003) Mechanism of aromatic amino acid hydroxylation, *Biochemistry 42*, 14083-14091.

24. Costas, M., Mehn, M. P., Jenseng, M. P., and Que, L., Jr. (2004) Dioxygen activation at mononuclear nonheme iron active sites: Enzymes, models, and intermediates, *Chem. Rev. 104*, 939-986.

25. Que, L., Jr. (2007) The road to non-heme oxoferryls and beyond, *Acc. Chem. Res. 40*, 493-500.

26. Price, J. C., Barr, E. W., Glass, T. E., Krebs, C., and Bollinger, J. M., Jr. (2003) Evidence for hydrogen abstraction from C1 of taurine by the high-spin Fe(IV) intermediate detected during oxygen activation by taurine: α-ketoglutarate dioxygenase (TauD), *J. Am. Chem. Soc. 125*, 13008-13009.

27. Price, J. C., Barr, E. W., Tirupati, B., Bollinger, J. M., Jr., and Krebs, C. (2003) The first direct characterization of a high-valen iron intermediate in the reaction of an α-ketoglutarate-dependent dioxygenase: A high-spin Fe(IV) complex in taurine/α-ketoglutarate dioxygenase (TauD) from *Escherichia coli*, *Biochemistry 42*, 7497-7508.

28. Eser, B. E., Barr, E. W., Frantom, P. A., Saleh, L., Bollinger, J. M., Jr., Krebs, C., and Fitzpatrick, P. F. (2007) Direct spectroscopic evidence for a high-spin Fe(IV) intermediate in tyrosine hydroxylase, *J. Am. Chem. Soc. 129*, 11334-11335.

29. Eser, B. E., and Fitzpatrick, P. F. (2010) Measurement of intrinsic rate constants in the tyrosine hydroxylase reaction, *Biochemistry 49*, 645-652.

30. Pavon, J. A., and Fitzpatrick, P. F. (2006) Insights into the catalytic mechanisms of phenylalanine and tryptophan hydroxylase from kinetic isotope effects on aromatic hydroxylation, *Biochemistry 45*, 11030-11037.

31. Hillas, P. J., and Fitzpatrick, P. F. (1996) A mechanism for hydroxylation by tyrosine hydroxylase based on partitioning of substituted phenylalanines, *Biochemistry 35*, 6969-6975.

32. Frantom, P. A., and Fitzpatrick, P. F. (2003) Uncoupled forms of tyrosine hydroxylase unmask kinetic isotope effects on chemical steps, *J. Am. Chem. Soc. 125*, 16190-16191.

33. Guroff, G., Daly, J. W., Jerina, D. M., Renson, J., Witkop, B., and Udenfriend, S. (1967) Hydroxylation-induced migration: The NIH shift, *Science 157*, 1524-1530.

34. Guroff, G., Levitt, M., Daly, J. W., and Udenfriend, S. (1966) The production of meta-tritiotyrosine from p-tritiophenylalanine by phenylalanine hydroxylase, *Biochem. Biophys. Res. Commun. 25*, 253-259.

35. Guroff, G., Reifsnyder, C. A., and Daly, J. W. (1966) Retention of deuterium in p-tyrosine formed enzymatically from p-deuterophenylalanine, *Biochem. Biophys. Res. Commun. 24*, 720-724.

36. Chen, D., and Frey, P. A. (1998) Phenylalanine hydroxylase from *Chromobacterium violaceum* uncoupled oxidation of tetrahydropterin and the role of iron in hydroxylation, *J. Biol. Chem. 273*, 25594-25601.

37. Onishi, A., Liotta, L. J., and Benkovic, S. J. (1991) Cloning and expression of *Chromobacterium violaceum* phenylalanine hydroxylase in Escherichia coli and comparison of amino acid sequence with mammalian aromatic amino acid hydroxylases, *J. Biol. Chem. 266*, 18454-18459.

38. Carr, R. T., and Benkovic, S. J. (1993) An examination of the copper requirement of phenylalanine hydroxylase from *Chromobacterium violaceum*, *Biochemistry 32*, 14132-14138.

39. Erlandsen, H., Kim, J. Y., Patch, M. G., Han, A., Volner, A., Abu-Omar, M. M., and Stevens, R. C. (2002) Structural comparison of bacterial and human iron dependent phenylalanine hydroxylases: Similar fold, different stability and reaction rates, *J. Mol. Biol. 320*, 654-661.

40. Pavon, J. A., and Fitzpatrick, P. F. (2005) Intrinsic isotope effects on benzylic hydroxylation by the aromatic amino acid hydroxylases: evidence for hydrogen tunneling, coupled motion, and similar reactivities, *J. Am. Chem. Soc. 127*, 16414-16415.

41. Frantom, P. A., Rongson, P., Sulikowski, G. A., and Fitzpatrick, P. F. (2002) Intrinsic deuterium isotope effects on benzylic hydroxylation by tyrosine hydroxylase, *J. Am. Chem. Soc. 124*, 4202-4203.

42. Kobe, G., Jennings, I. G., House, C. M., Feil, S. C., Michell, B. J., Tiganis, T., Parker, M. W., Cotton, R. G. H., and Kemp, B. E. (1997) Regulation and crystallization of phosphorylated and dephosphorylated forms of truncated dimeric phenylalanine hydroxylase, *Protein Sci. 6*, 1352-1357.

43. Daubner, S. C., Hillas, P. J., and Fitzpatrick, P. F. (1997) Characterization of chimeric pterin dependent hydroxylases: Contributions of the regulatory domains of tyrosine and phenylalanine hydroxylase to substrate specificity, *Biochemistry 36*, 11574-11582.

44. Moran, G. R., Daubner, S. C., and Fitzpatrick, P. F. (1998) Expression and characterization of the catalytic core of tryptophan hydroxylase, *J. Biol. Chem. 273*, 12259-12266.

45. Daubner, S. C., Lohse, D. L., and Fitzpatrick, P. F. (1993) Expression and characterization of catalytic and regulatory domains of rat tyrosine hydroxylase, *Protein Sci. 2*, 1452-1460.

46. Ledley, F. D., DiLella, A. G., Kwok, S. C. M., and Woo, S. L. C. (1985) Homology between phenylalanine and tyrosine hydroxylases reveals common structural and functional domains, *Biochemistry 24*, 3389-3394.

47. Grenett, H. E., Ledley, F. D., Reed, L. L., and Woo, S. L. C. (1987) Full-length cDNA for rabbit tryptophan hydroxylase: Functional domains and evolution of aromatic amino acid hydroxylases, *Proc. Natl. Acad. Sci. U. S. A. 84*, 5530-5534.

48. Andersen, O. A., Flatmark, T., and Hough, E. (2002) Crystal structure of the ternary complex of the catalytic domain of human phenylalanine hydroxylase with tetrahydrobiopterin and 3-(2-thienyl)-L-alanine, and its implications for the mechanims of catalysis and substrate activation, *J. Mol. Biol. 320*, 1095-1108.

49. Wang, L., Erlandsen, H., Haavik, J., Knappskog, P. M., and Stevens, R. C. (2002) Three-dimensional structure of human tryptophan hydroxylase and its

implications for the biosynthesis of the neurotransmitters serotonin and melatonin, *Biochemistry 41*, 12569-12574.

50. Goodwill, K. E., Sabatier, C., Marks, C., Raag, R., Fitzpatrick, P. F., and Stevens, R. C. (1997) Crystal structure of tyrosine hydroxylase at 2.3 Å and its implications for inherited neurodegenerative diseases, *Nat. Struct. Biol. 4*, 578-585.

51. Chow, M. S., Eser, B. E., Wilson, S. A., Hodgson, K. O., Hedman, B., Fitzpatrick, P. F., and Solomon, E. I. (2009) Spectroscopy and kinetics of wild-type and mutant tyrosine hydroxylase: Mechanistic insight into O_2 activation, *J. Am. Chem. Soc. 131*, 7685-7698.

52. Sura, G. R., Lasagna, M., Gawandi, V., Reinhart, G. D., and Fitzpatrick, P. F. (2006) Effects of ligands on the mobility of an active-site loop in tyrosine hydroxylase as monitored by flourescence anisotropy, *Biochemistry 45*, 9632-9638.

53. Wang, S., Sura, G. R., Dangott, L. J., and Fitzpatrick, P. F. (2009) Identification by hydrogen/deuterium exchange of structural changes in tyrosine hydroxylase associated with regulation, *Biochemistry 48*, 4972-4979.

54. Li, J., Dangott, L. J., and Fitzpatrick, P. F. (2010) Regulation of phenylalanine hydroxylase: Conformational changes upon phenylalanine binding detected by hydrogen/deuterium exchange and mass spectrometry, *Biochemistry 49*, 3327-3335.

55. Kaufman, S. (1971) The phenylalanine hydroxylating system from mammalian liver, *Adv. Enzymol. Relat. Areas. Mol. Biol. 35*, 245-319.

56. Carr, R. T., and Benkovic, S. J. (1993) A re-examination of the metal requirement of *Chromobacterium violaceum* phenylalanine hydroxylase, *Adv. Exp. Med. Biol. 338*, 63-66.

57. Gottschall, D. W., Dietrich, R. F., and Benkovic, S. J. (1982) Phenylalanine hydroxylase. Correlation of the iron content with activity and the preparation and reconstitution of the apoenzyme, *J. Biol. Chem. 257*, 854-849.

58. Siegmund, H. U., and Kaufman, S. (1991) Hydroxylation of 4-methylphenylalanine by rat liver phenylalanine hydroxylase, *J. Biol. Chem. 266*, 2903-2910.

59. Fitzpatrick, P. F. (1994) Kinetic isotope effects on hydroxylation of ring-deuterated phenylalanines by tyrosine hydroxylase provide evidence against partitioning of an arene oxide intermediate, *J. Am. Chem. Soc. 116*, 1133-1134.

60. Ramsey, A. J., Hillas, P. J., and Fitzpatrick, P. F. (1996) Characterization of the active site iron in tyrosine hydroxylase. Redox states of the iron, *J. Biol. Chem. 271*, 24395-24400.

61. Shiman, R., Jones, S. H., and Gray, D. W. (1990) Mechanism of phenylalanine regulation of phenylalanine hydroxylase, *J. Biol. Chem. 265*, 11633-11642.

62. Daubner, S. C., Hillas, P. J., and Fitzpatrick, P. F. (1997) Characterization of chimeric pterin-dependent hydroxylases: contributions of the regulatory domains

of tyrosine and phenylalanine hydroxylase to substrate specificity, *Biochemistry 36*, 11574-11582.

63. Fujisawa, H., and Nakata, H. (1987) Phenylalanine 4-monooxygenase from *Chromobacterium violaceum*, *Methods Enzymol. 142*, 44-49.

64. Abita, J.-P., Parniak, M., and Kaufman, S. (1984) The activation of rat liver phenylalanine hydroxylase by limited proteolysis, lysolecithin, and tocopherol phosphate. Changes in conformation and catalytic properties, *J. Biol. Chem. 259*, 14560-14566.

65. Fitzpatrick, P. F. (2005) Isotope effects from partitioning of intermediates in enzyme-catalyzed hydroxylation reactions in *Isotope effects in Chemistry and Biology* (Kohen, A., and Limbach, H., Ed.), pp 861-873, Marcel Dekker, Inc., New York.

66. Bahnson, B. J., and Klinman, J. P. (1995) Hydrogen tunneling in enzyme catalysis, *Method. Enzymol. 249*, 373-397.

67. Kohen, A., and Klinman, J. P. (1999) Hydrogen tunneling in biology, *Chemistry & Biology 6*, 191-198.

68. Brown, E. R., Coker, G. T., and O'Malley, K. L. (1987) Organization and evolution of the rat tyrosine hydroxylase gene, *Biochemistry 26*, 5208-5212.

69. Erlandsen, H., Fusetti, F., Martinez, A., Hough, E., Flatmark, T., and Stevens, R. C. (1997) Crystal structure of the catalytic domain of human phenylalanine hydroxylase reveals the structural basis for phenylketonuria, *Nature Struct.Biol. 4*, 995-1000.

70. Bell, R. P. (1974) Recent advances in the study of kinetic hydrogen isotope effects, *Chem. Soc. Rev. 3*, 513-544.

71. Klinman, J. P. (2006) Linking protein structure and dynamics to catalysis: The role of hydrogen tunneling, *Phil. Trans. R. Soc. B 361*, 1323-1331.

72. Limbach, H.-H., Lopez, J. M., and Kohen, A. (2006) Arrhenius curves of hydrogen transfers: Tunnel effects, isotope effects and effects of pre-equilibria, *Phil. Trans. R. Soc. B 361*, 1399-1415.

73. Ellis, H. R., McCusker, K. P., and Fitzpatrick, P. (2002) Use of a tyrosine hydroxylase mutant enzyme with reduced metal affinity allows detection of activity with cobalt in place of iron, *Arch. Biochem. Biophys. 408*, 305-307.

74. Panay, A. J., and Fitzpatrick, P. F. (2008) Kinetic isotope effects on aromatic and benzylic hydroxylation by *Chromobacterium violaceum* phenylalanine hydroxylase as probes of chemical mechanism and reactivity, *Biochemistry 47*, 11118-11124.

75. Fitzpatrick, P. F. (2000) The aromatic amino acid hydroxylases, *Advan. Enzymol. Relat. Areas. Mol. Biol. 74*, 235-294.

76. Wasinger, E. C., Mitic, N., Hedman, B., Caradonna, J. P., Solomon, E. I., and Hodgson, K. O. (2002) X-ray absorption spectroscopy investigation of the resting ferrous and cosubstrate-bound active sites of phenylalanine hydroxylase, *Biochemistry 41*, 6211-6217.

77. Miwa, G. T., Garland, W. A., Hodshon, B. J., Lu, A. Y. H., and Northrop, D. B. (1980) Kinetic isotope effects in cytochrome P-450-catalyzed oxidation

reactions. Intermolecular and intramolecular deuterium isotope effects during the *N*-demethylation of *N,N*-dimethylphentermine, *J. Biol. Chem. 255*, 6049-6054.

78. Groves, J. T., McClusky, G. A., White, R. E., and Coon, M. J. (1978) Aliphatic hydroxylation by highly purified liver microsomal cytochrome P450. Evidence for a carbon radical intermediate, *Biochem. Biophys. Res. Commun. 81*, 154-160.

79. Jones, J. P., Rettie, A. E., and Trager, W. (1990) Intrinsic isotope effects suggest that the reaction coordinate symmetry for the cytochrome P-450 catalyzed hydroxylation of octane is isozyme independent, *J. Med. Chem. 33*.

80. Ravi, N., Bollinger, J. M., Jr., Huynh, B. H., Stubbe, J., and Edmonson, D. E. (1994) Mechanism of assembly of the tyrosyl radical-diiron (III) cofactor *E. coli* ribonucleotide reductase: 1. Mössbauer characterization of the diferric radical precursor, *J. Am. Chem. Soc. 116*, 8007-8014.

81. Hoffart, L. M., Barr, E. W., Guyer, R. B., Bollinger, J. M., Jr., and Krebs, C. (2006) Direct spectroscopic detection of a C-H-cleaving high-spin Fe(IV) complex in a prolyl-4-hydroxylase, *Proc. Natl. Acad. Sci. USA 103*, 14738-14743.

82. Kaufman, S. (1993) The phenylalanine hydroxylating system, *Advan. Enzymol. Relat. Areas. Mol. Biol. 67*, 77-264.

83. Eisensmith, R. C., and Woo, S. L. (1991) Phenylketonuria and the phenylalanine hydroxylase gene, *Mol. Biol. Med. 8*, 3-18.

84. Baldwin, J., Krebs, C., Ley, B. A., Edmonson, D. E., Huynh, B. H., and Bollinger, J. M., Jr. (2000) Mechanism of rapid electron transfer during oxygen

activation in the R2 subunit of *Escherichia coli* ribonucleotide reductase. 1. Evidence for a transient tryptophan radical, *J. Am. Chem. Soc. 122*, 12195-12206.

85. Johnson, K. A., Simpson, Z. B., and Blom, T. (2009) Global kinetic explorer: A new computer program for dynamic simulation and fitting of kinetic data, *Anal. Biochem. 387*, 20-29.

86. Johnson, K. A., Simpson, Z. B., and Blom, T. (2009) FitSpace Explorer: An algorithm to evaluate multidimensional parameter space in fitting kinetic data, *Anal. Biochem. 387*, 30-41.

87. Fitzpatrick, P. F. (1989) The metal requirement of rat tyrosine hydroxylase, *Biochem. Biophys. Res. Commun. 161*, 211-125.

88. Ramsey, A. J., and Fitzpatrick, P. F. (1998) Effects of phosphorylation of serine 40 of tyrosine hydroxylase on binding of catecholamines: Evidence for a novel regulatory mechanism, *Biochemistry 37*, 8980-8986.

89. Xia, T., Gray, D. W., and Shiman, R. (1994) Regulation of rat liver phenylalanine hydroxylase, *J. Biol. Chem. 269*, 24657-24665.

90. Benkovic, S. J., and Hammes-Schiffer, S. (2003) A perspective on enzyme catalysis, *Science 301*, 1196-1202.

91. Hammes, G. G. (2002) Multiple conformational changes in enzyme catalysis, *Biochemistry 41*, 8221-8228.

92. Tousignant, A., and Pelletier, J. N. (2004) Protein motions promote catalysis, *Chemistry & Biology 11*, 1037-1042.

93. Boehr, D. D., Dyson, H. J., and Wright, P. E. (2006) An NMR perspective on enzyme dynamics, *Chem. Rev. 106*, 3055-3079.

94. Mittermaier, A., and Kay, L. E. (2006) New tools provide new insights in NMR studies of protein dynamics, *Science 312*, 224-228.

95. Moad, G., Luthy, C. L., Benkovic, P. A., and Benkovic, S. J. (1979) Studies on 6-methyl-5-deazatetrahydropterin and its 4a adducts *J. Am. Chem. Soc. 101*, 6068-6076.

96. Marley, J., Lu, M., and Bracken, C. (2001) A method for efficient isotopic labeling of recombinant proteins, *Journal of Biomolecular NMR 20*, 71-75.

97. Davis, R. W., Botstein, D., and Roth, J. R. (1980) *Advanced Bacterial Genetics: A Manual for Genetic Engineering*, Cold Spring Harbor Laboratory, Cold Spring Harbor, NY.

98. Baynes, B. M., Wang, D. I. C., and Trout, B. L. (2005) Role of arginine in the stabilization of proteins against aggregation, *Biochemistry 44*, 4919-4925.

99. Golovanov, A. P., Hautbergue, G., M, Wilson, S., A., and Lian, L.-Y. (2004) A simple method for improving protein solubility and long-term stability, *J. Am. Chem. Soc. 126*, 8933-8939.

100. Mori, S., Abeygunawardana, C., Johnson, M. O., and van Zijl, P. C. (1995) Improved sensitiviy of HSQC spectra of exchanging protons at short interscan delays using a new fast HSQC (FHSQC) detection scheme that avoids water saturation, *J. Mag. Reson. B 108*, 94-98.

101. Grzesiek, S., Anglister, J., and Bax, A. (1993) Correlation of backbone amide and aliphatic side-chain resonances in C-13/N-15 enriched proteins by isotropic mixing of C-13 magnetization, *J. Mag. Reson. B 101*, 114-119.

102. Salzmann, M., Pervushin, K., Wider, G., Senn, H., and Wuthrich, K. (1998) TROSY in triple resonance experiments: New perspectives for sequential assingment of large proteins, *Proc. Natl. Acad. Sci. U. S. A. 95*, 13585-13590.

103. Delaglio, F., Grzesiek, S., Vuister, G. W., Zhu, G., Pfeifer, J., and Bax, A. (1995) NMRPipe: A multidimensional spectral processing system based on UNIX pipes, *J. Biomol. NMR 6*, 277-293.

104. Goddard, T. D., and Kneller, D. G. SPARKY 3. University of California, San Francisco.

105. Grzesiek, S., Bax, A., Clore, G. M., Gronenborn, A. M., Hu, J. S., Kaufman, J., Palmer, I., Stahl, S. J., and Wingfield, P. T. (1996) The solution structure of HIV-1 Nef reveals an unexpected fold and permits delineation of the binding surface for the SH3 domain of Hck tyrosine protein kinase, *Nat. Struct. Biol. 3*, 340-345.

106. Redfield, A. G., and Gupta, R. K. (1972) Pulsed NMR study of the structure of cytochrome c, *Cold Spring Harbor Symp. Quant. Biol. 36*, 405-411.

107. Sorkin, D. L., and Miller, A. F. (2000) Amino acid-specific isotopic labeling and active site NMR studies of iron (II)- and iron(III)-superoxide dismutase from *Escherichia coli*, *J. Biomol. NMR 17*, 311-322.

APPENDIX A

Table A-1: Amino acid sequence of *C. violaceum* phenylalanine hydroxylase. The nitrogen and hydrogen resonances for the assigned residues are listed.

Residue	N (ppm)	H (ppm)	Residue	N (ppm)	H (ppm)
M1	–	–	G19	–	–
N2	–	–	L20	121.45	8.08
D3	121.375	8.386	S21	119.026	8.158
R4	121.422	8.191	H22	116.88	7.677
A5	125.691	8.298	D23	124.047	9.406
D6	119.026	8.158	A24	–	–
F7	120.732	7.836	N25	113.167	8.513
V8	124.616	7.872	D26	120.057	9.277
V9	127.249	8.216	F27	113.842	7.925
P10	–	–	T28	106.611	8.214
D11	121.45	8.08	L29	118.559	8.204
I12	123.035	8.735	P30	–	–
T13	119.794	7.795	Q31	126.089	8.815
T14	119.949	7.839	P32	–	–
R15	121.035	8.051	L33	124.991	7.688
K16	117.114	8.391	D34	114.626	8.562
N17	113.127	7.146	R35	117.671	7.732
V18	121.787	6.977	Y36	118.786	6.741

Table A-1: Continued

Residue	N (ppm)	H (ppm)	Residue	N (ppm)	H (ppm)
S37	123.144	9.375	L55	117.369	7.615
A38	122.828	8.931	P56	–	–
E39	119.222	8.309	G57	114.47	9.153
D40	122.143	7.798	R58	116.384	8.225
H41	119.247	7.546	A59	121.498	8.682
A42	121.436	7.71	C60	117.171	8.281
T43	122.498	8.874	D61	126.145	10.177
W44	123.035	8.735	E62	119.728	10.344
A45	120.499	8.312	F63	122.637	7.823
T46	117.226	8.229	L64	–	–
L47	–	–	E65	120.694	8.536
Y48	120.977	8.851	G66	109.094	7.695
Q49	118.274	8.39	L67	121.714	7.482
R50	119.949	7.839	E68	118.01	7.075
Q51	116.409	7.985	R69	119.938	8.567
C52	117.561	8.51	L70	115.736	7.8
K53	117.566	7.34	E71	113.829	7.369
L54	118.509	7.083	V72	118.509	7.083

Table A-1: Continued

Residue	N (ppm)	H (ppm)	Residue	N (ppm)	H (ppm)
D73	127.607	8.653	T91	103.857	7.864
A74	122.458	8.168	G92	111.83	8.061
D75	113.436	8.227	W93	121.692	6.865
R76	116.229	7.011	K94	111.375	7.806
V77	121.688	9.516	I95	–	–
P78	–	–	V96	–	–
D79	121.222	8.283	A97	127.365	9.183
F80	129.384	9.79	V98	112.148	8.169
N81	117.01	8.539	P99	–	–
K82	121.975	7.593	G100	101.930	6.649
L83	120.965	7.549	L101	125.235	8.157
N84	118.772	8.601	I102	118.664	7.88
E85	119.968	7.408	P103	–	–
K86	117.399	6.996	D104	123.757	8.507
L87	123.044	8.436	D105	114.851	8.688
M88	119.872	8.87	V106	121.843	6.861
A89	119.809	6.665	F107	122.971	7.853
A90	118.942	7.459	F108	115.461	8.503

Table A-1: Continued

Residue	N (ppm)	H (ppm)	Residue	N (ppm)	H (ppm)
E109	118.216	7.349	Q127	122.155	7.695
H110	–	–	L128	118.858	7.066
L111	–	–	D129	114.452	8.283
A112	118.324	8.625	Y130	119.738	7.377
N113	116.19	7.536	L131	127.436	7.716
R114	114.128	7.587	Q132	124.207	8.49
R115	118.966	7.718	E133	121.444	8.31
F116	124.802	9.512	P134	–	–
P117	–	–	D135	119.241	6.852
V118	115.023	7.081	V136	118.324	8.625
T119	–	–	F137	121.337	6.994
W120	120.239	7.576	H138	–	–
W121	120.463	5.699	D139	–	–
L122	122.164	8.679	L140	–	–
R123	124.772	9.402	F141	–	–
E124	119.839	8.234	G142	–	–
P125	–	–	H143	–	–
H126	112.273	7.836	V144	–	–

Table A-1: Continued

Residue	N (ppm)	H (ppm)	Residue	N (ppm)	H (ppm)
P145	–	–	G163	112.565	7.96
L146	120.048	8.276	V164	122.161	7.636
L147	120.602	8.119	K165	–	–
I148	–	–	A166	–	–
N149	–	–	K167	–	–
P150	–	–	A168	–	–
V151	117.317	6.85	L169	–	–
F152	122.81	8.165	G170	–	–
A153	120.524	8.366	A171	–	–
D154	117.730	7.711	L172	–	–
Y155	124.767	8.381	P173	–	–
L156	–	–	M174	–	–
E157	–	–	L175	–	–
A158	122.384	8.053	A176	–	–
Y159	122.438	9.057	R177	–	–
G160	107.941	8.491	L178	–	–
K161	121.44	8.579	Y179	122.739	8.21
G162	108.261	8.055	W180	120.578	8.719

Table A-1: Continued

Residue	N (ppm)	H (ppm)	Residue	N (ppm)	H (ppm)
Y181	112.498	8.453	A199	130.070	8.495
T182	112.538	7.558	G200	–	–
V183	–	–	I201	–	–
E184	–	–	L202	–	–
F185	114.018	7.482	S203	–	–
G186	110.049	7.623	S204	–	–
L187	121.711	7.653	K205	–	–
I188	119.433	9.121	S206	–	–
N189	127.748	8.723	E207	–	–
T190	114.756	7.208	S208	–	–
P191	–	–	I209	119.229	6.48
A192	117.909	7.353	Y210	120.571	6.625
G193	107.994	7.639	C211	111.219	8.13
M194	123.063	8.693	L212	120.729	6.448
R195	125.794	9.309	D213	117.819	7.598
I196	119.993	8.527	S214	113.443	7.529
Y197	122.613	7.761	A215	130.092	8.911
G198	108.776	7.639	S216	121.039	8.942

Table A-1: Continued

Residue	N (ppm)	H (ppm)	Residue	N (ppm)	H (ppm)
P217	–	–	T236	109.741	7.145
N218	116.629	9.488	F237	117.819	7.598
R219	120.386	8.898	Q238	–	–
V220	124.044	8.783	K239	118.710	7.349
G221	111.901	9.446	T240	115.094	7.139
F222	122.579	8.291	Y241	117.334	7.774
D223	–	–	F242	121.389	10.358
L224	129.347	8.516	V243	125.784	9.112
M225	116.846	7.902	I244	124.664	8.843
R226	120.813	7.777	D245	120.206	9.52
I227	122.971	7.853	S246	108.373	7.14
M228	114.203	7.743	F247	121.204	8.628
N229	116.142	7.356	K248	124.664	8.843
T230	118.431	7.758	Q249	119.776	7.656
R231	122.069	7.96	L250	117.351	6.611
Y232	115.913	8.125	F251	119.370	7.672
R233	115.274	7.764	D252	121.155	9.359
I234	115.454	8.451	A253	121.711	7.653
D235	120.255	8.401	T254	103.935	7.424

Table A-1: Continued

Residue	N (ppm)	H (ppm)	Residue	N (ppm)	H (ppm)
A255	125.79	7.105	G274	134.368	8.505
P256	–	–	D275	122.915	7.081
D257	119.058	7.925	I276	118.664	7.88
F258	126.714	8.578	A277	102.987	8.437
A259	124.381	8.377	P278	–	–
P260	–	–	D279	113.979	7.832
L261	–	–	D280	120.947	7.213
Y262	117.730	7.711	L281	124.476	8.713
L263	117.123	7.349	V282	129.057	8.712
Q264	118.942	7.459	L283	132.28	8.555
L265	117.730	7.711	N284	114.455	8.21
A266	123.826	7.495	A285	130.871	8.839
D267	114.934	7.799	G286	115.883	9.402
A268	124.026	7.227	D287	124.574	8.808
Q269	122.584	8.319	R288	111.56	7.699
P270	–	–	Q289	123.25	8.391
W271	124.477	9.052	G290	–	–
G272	110.804	9.116	W291	121.975	7.593
A273	124.92	8.847	A292	126.016	8.498

Table A-1: Continued

Residue	N (ppm)	H (ppm)	Residue	N (ppm)	H (ppm)
D293	119.938	8.567			
T294	109.383	6.93			
E295	123.641	8.755			
D296	122.177	8.276			
V297	124.204	8.285			

Table A-2: Amino acids in *C. violaceum* phenylalanine hydroxylase showing significant chemical shift perturbations upon binding of phenylalanine.

Residue	Normalized weighted average Chemical shift Perturbation (ppm)		Signal disappearance
	$0.17 < \Delta_{avg} < 0.6$	$\Delta_{avg} > 0.6$	
T13	-	-	▲
H22	0.25		
F27	0.21		
T46	0.22		
Y48	-	-	▲
Q49	0.37		
Q51	-	-	▲
C52	0.29		
L54	-	-	▲
R58	0.29		
A59	0.27		
D61	0.31		
E62	0.46		
F63	-	-	▲
E65	0.30		
G66	0.33		

Table A-2: Continued.

Residue	Normalized weighted average Chemical shift Perturbation (ppm)		Signal disappearance
	$0.17 < \Delta_{avg} < 0.6$	$\Delta_{avg} > 0.6$	
L67	0.52		
L70	0.29		
E71	0.23		
A74	0.20		
D75	0.18		
V77	0.23		
D79	0.31		
L83	0.29		
L87	0.26		
M88	0.27		
D105		0.99	
V106	-	-	▲
F108	0.35		
R114	0.24		
R115	0.24		
V118	0.48		
W120	0.19		

Table A-2: Continued.

Residue	Normalized weighted average Chemical shift Perturbation (ppm)		Signal disappearance
	$0.17 < \Delta_{avg} < 0.6$	$\Delta_{avg} > 0.6$	
R123	0.54		
E124	0.19		
Q127	0.24		
L128	-	-	▲
Y130	0.29		
L131	-	-	▲
Q132	0.32		
L146	0.36		
V151	0.29		
D154	-	-	▲
Y155	-	-	▲
Y159	-	-	▲
G160	-	-	▲
K161	-	-	▲
G162		1.00	
G163	0.51		
Y179	-	-	▲

Table A-2: Continued.

Residue	Normalized weighted average Chemical shift Perturbation (ppm)		Signal disappearance
	$0.17 < \Delta_{avg} < 0.6$	$\Delta_{avg} > 0.6$	
W180	0.24		
Y181	0.29		
T182	0.58		
I188	0.42		
N189	0.19		
T190		0.77	
M194	0.19		
R195	0.21		
A199	-	-	▲
Y210	-	-	▲
L212	0.32		
R219	0.21		
V220	0.41		
G221	0.18		
L224	0.35		
M225	0.54		
R226		0.70	
I227	0.20		

Table A-2: Continued.

Residue	Normalized weighted average Chemical shift Perturbation (ppm)		Signal disappearance
	$0.17 < \Delta_{avg} < 0.6$	$\Delta_{avg} > 0.6$	
M228	0.28		
N229	0.23		
R233	-	-	▲
D235	0.35		
T236	0.18		
Y241	0.29		
V243	-	-	▲
I244	0.41		
D245	0.54		
S246	-	-	▲
F247	-	-	▲
Q249	-	-	▲
L250	-	-	▲
D252	-	-	▲
T254	-	-	▲
A255	-	-	▲
D257	-	-	▲
F258	-	-	▲

Table A-2: Continued.

Residue	Normalized weighted average Chemical shift Perturbation (ppm)		Signal disappearance
	$0.17 < \Delta_{avg} < 0.6$	$\Delta_{avg} > 0.6$	
A259	-	-	▲
L263	0.35		
A266	0.25		
D267	0.25		
L281	0.42		
N284	0.35		
A285	0.42		
G286	0.43		
D287	0.19		

Table A-3: Amino acids in *C. violaceum* phenylalanine hydroxylase showing significant chemical shift perturbations upon binding of 6-methyl-5-deazatetrahydropterin.

Residue	Normalized weighted average Chemical shift Perturbation (ppm)		Signal disappearance
	$0.24<\Delta_{avg}<0.6$	$\Delta_{avg} > 0.6$	
V9	0.29		
T14	0.30		
D23		0.79	
N25	0.36		
L29	0.47		
Q31	0.34		
L33	0.25		
S37	0.26		
H41	0.33		
A42	0.33		
Q49	0.25		
Q51	0.44		
C52	0.24		
R58	0.28		
F63	0.38		
E65	0.37		

Table A-3: Continued.

Residue	Normalized weighted average Chemical shift Perturbation (ppm)		Signal disappearance
	$0.24<\Delta_{avg}<0.6$	$\Delta_{avg} > 0.6$	
L70	0.41		
E71	0.26		
D73	0.24		
D75	0.25		
D79	0.27		
F80	0.51		
L83		0.68	
N84	0.30		
L87	0.50		
M88		0.70	
A89	0.41		
T91	0.25		
W93	0.59		
K94		0.89	
A97	0.37		
V98	0.51		
G100	-	-	▲

Table A-3: Continued.

Residue	Normalized weighted average Chemical shift Perturbation (ppm)		Signal disappearance
	$0.24<\Delta_{avg}<0.6$	$\Delta_{avg} > 0.6$	
L101	-	-	▲
I102	-	-	▲
D104	0.56		
D105		0.66	
V106		1.00	
F108		0.85	
E109	0.59		
A112	0.33		
N113	0.40		
F116	0.50		
V118	0.58		
W120	-	-	▲
R123	0.57		
Q127	0.47		
L128	0.47		
L131		0.77	
Q132	0.55		

Table A-3: Continued.

Residue	Normalized weighted average Chemical shift Perturbation (ppm)		Signal disappearance
	$0.24<\Delta_{avg}<0.6$	$\Delta_{avg} > 0.6$	
V151	0.34		
F152	0.25		
A153	0.38		
D154	0.40		
Y155	0.46		
A158	0.37		
Y159		0.89	
G160	0.31		
K161	0.41		
G162		0.76	
V164	0.28		
Y179	0.49		
W180	0.26		
Y181		0.80	
Y197	0.25		
I209	0.27		
Y210	0.58		

Table A-3: Continued.

Residue	Normalized weighted average Chemical shift Perturbation (ppm)		Signal disappearance
	$0.24<\Delta_{avg}<0.6$	$\Delta_{avg} > 0.6$	
C211	0.34		
D213	0.36		
M228	0.33		
T230		0.67	
R231	0.26		
Y232	0.44		
R233	0.41		
I234	0.44		
D235		0.73	
T240	0.45		
F242	0.26		
I244	0.33		
D252	0.33		
T254	0.44		
L263	0.45		
D267	0.26		
G274	0.25		

VITA

Aram Joel Panay Escobar received his Bachelor of Science degree in chemistry from Universidad del Valle, Cali, Colombia in 2004. He entered the Biochemistry and Biophysics graduate program at Texas A&M University in August 2004 and received his Ph.D degree in August 2010. His research interests include enzyme mechanisms, enzyme dynamics, and protein engineering.

Mr. Panay can be reached at:

TAMU Dept of Biochemistry
103 Biochemistry Bldg
2128 TAMU
College Station, TX 77843-2128
joelpanay@tamu.edu

Relevant publications:

Panay, A. J., Fitzpatrick P.F. (2008). Kinetic Isotope Effects on Aromatic and Benzylic Hydroxylation by *Chromobacterium violaceum* Phenylalanine Hydroxylase as Probes of Chemical Mechanism and Reactivity, *Biochemistry* 47, 11118-11124.

Panay, A. J., Fitzpatrick, P. F. (2010) Measurement of the Intramolecular Isotope Effect on Aliphatic Hydroxylation by *Chromobacterium violaceum* Phenylalanine Hydroxylase, *J. Am. Chem. Soc.* 132, 5584-5585.

Panay, A. J., Fitzpatrick, P. F. (2009) Mechanistic Studies of Aliphatic Hydroxylation by Phenylalanine Hydroxylase. 21st Enzyme Mechanisms Conference. Tucson, AZ, USA.